THE INTERACTION OF FAST NEUTRAL ATOMS WITH METAL SURFACES

by

MOHD NOR BIN MD YUSUF M. Sc.

A Thesis submitted to the
University of Warwick in United Kingdom
for the Degree of
Doctor of Philosophy

This thesis is based on work conducted by the author in the Department of Physics, University of Warwick, United Kingdom in the period October 1985 to December 1988

Submitted in December 1989

TABLE OF CONTENTS

LIST OF TABLES AND ILLUSTRATIONS

Plate

Table

ACKNOWLEDGEMENTS

I would like to thank Dr.T. A. Delchar, my research supervisor, for introducing me to the field of Surface Physics in general and to fast neutral atoms in particular, and for many very interesting discussions and also for his continuous help and encouragement throughout the course of this work.

I take great pleasure in thanking all those individuals in the Department of Physics who have helped me with this work, and particularly to Rob, the Surface Physics technician for technical support, Roger, Adrian and Pete of the Electronics Workshop for their help in building the computer-controlled ramp generator and the bolometer.

I would like to thank my employer, Universiti Teknologi Malaysia, for the provision of Study Leave and Scholarship, and Jabatan Perkhidmatan Awam Malaysia, for the Federal Scholarship, during the past three and a half years of my study leave here.

Finally, I would like to thank my wife, Rafinah, and my children, Sazli, Azlan and Norhafizah, for their constant encouragement, patience and understanding.

DECLARATION

The work reported in this Thesis was performed by myself, except where specifically acknowledged as otherwise in the text, in the Department of Physics, University of Warwick, United Kingdom.

For convenience, the references cited in the text are listed at the end of the chapter where the citations have been made.

Parts of Chapter Five have been published in Surf. Sci. **182** (1987) 231. The absolute bolometer is to be submitted for publication in J. Phys. E.

MOHD NOR BIN MD YUSUF

ABSTRACT

The interactions of fast neutral atoms (H_2, He, Ne, N_2 and Ar) in the energy range of 200 eV to 7 keV on polycrystalline gold and lithium surfaces have been studied under UHV conditions. It was found that the majority of the secondary electrons formed in the interactions have low energy (1-3 eV), and the spectra have structure which shows no evidence of any significant effect of beam type and target temperature. The electrons are ejected into a solid angle around the surface normal in a "near cosine" angular distribution. With the aid of a thermistor-based absolute bolometer of new design, the secondary electron yield coefficient was found to increase linearly with the fast atom energy, and dependent on the projectile's atomic number the larger the value. The variation of the yield with angle of incidence (θ_i) deviates slightly from the sec θ_i law, which suggests that the majority of the electrons are formed deep under the surface.

In the step of collision with the gold surface, a small fraction of the fast neutral atoms are ionised, for which it is believed to be a result of an electron promotion mechanism. It is found that for the ionisation to occur the fast neutrals must have energy larger than a threshold of about 350 eV. In the case of the lithium surface, the fast atoms also cause ejection of neutral Li atoms and slow Li^+ ions ($\approx$ 10 eV).

A series of computer simulations of rainbow peak scattering of fast He atoms from a two atom unreconstructed clean Cu{111} surface has been carried out using a Born-Mayer repulsive potential $V(r) = A \exp(-br)$; a good fit with the experimental data can be achieved with $A = 1805$ eV and $b = 4.14$ $Å^{-1}$.

CHAPTER ONE

INTRODUCTION

1.1 Overview

In the context of this thesis, fast neutral atoms are considered to be ground state neutral atoms which have kinetic energies of 100 eV or higher. Conceptually, they might be thought of as thermal gas atoms which have undergone acceleration, but in practice, by virtue of their method of production fast neutral atoms form a class of their own.

Since its first inception in 1930 until the mid 1960s, fast neutral atom beams were not being used in many experiments. The reason for this early lack of interest towards them lies in their neutrality which leads to difficulties in several experimental aspects, particularly in beam production, focusing and detection. Early experiments which involved the use of fast neutral atoms, were centred around the quest for finding ways to measure and detect them,i.e, experiments to measure the yield of secondary electrons [1,2].

The early 1960s saw the beginning of rapid development in surface science due to the commercial availability of Ultra High Vacuum (UHV) components. The old surface techniques, such as Low Energy Electron Diffraction (LEED) and Field Emission Microscopy (FEM) were perfected, and at the same time new methods were developed. Of the new

techniques developed since then, two have helped indirectly revitalise interest in fast neutral atom beams, namely, Low Energy Ion Scattering (LEIS) and Secondary Ion Mass Spectroscopy (SIMS). Both LEIS and SIMS uses intense and energetic ion beams to analyse surface compositions; LEIS in particular is used for analysis of surface structure while SIMS for depth profiling. An entirely new technique for surface composition analysis, which uses fast neutral atom beam was developed by White and co-workers [3]; it works on the basis of identification and analysis of optical lines and bands that are produced in the collision process, and thus called Surface Composition by Analysis of Neutral and Ion Impact Radiation (SCANIIR).

LEIS works well with metal surfaces; although it must be noted here that ions undergo efficient neutralisation at the surfaces [4]. In that case the backscattered signal has most of its ions removed and vital information associated with them is lost. To use fast neutral atoms as the projectiles for the scattering experiments essentially eliminates the neutralisation problems and further enhances the results. This was shown by Souda et. al. [5] who performed scattering experiments using beams of argon ions and neutrals on a TaC(001) surface, and found that the results obtained with the neutral beams consistently showed more marked shadowing and focusing effects than those obtained with the ion beams.

With insulator and semiconductor surfaces, an additional problem arises due to the transfer of charges from the ions to the surfaces in a process known as surface

charging [6]. Because of the surfaces's low conductivity, the charges accumulate and a potential develops across the insulator between the front surface and the substrate, with the surface positive. The macroscopic field defocuses the ion beam and decreases its energy, apart from causing ion migration in the subsurface region [7]. Electron flooding to the surface, among other techniques [8], helps reduce but not eliminate the macroscopic field. This is where fast neutral atoms have an advantage over the ions; they do not cause surface charge-up problems, although it must be noted here that space charge problem in the order of few volts due to electron loss and or secondary electrons still exists irrespective of the beam type. White et. al. [9] investigated the ion migration problems using beams of N_2^+ and N_2^* on SiO_2 surface and found that the use of N_2^* reduced the migration activity by four orders of magnitude.

The problems of surface charge-up and its associated macroscopic field as discussed earlier also appear in SIMS. Here, its presence particularly distorts the secondary ion signal for it can destabilise or capture the slow secondary ions. Naturally, the use of molecular beams in SIMS-like experiments was pursued, and towards the late 1960s it was established that molecular beams could be used as probes for surface analysis on insulators. Following that, after nearly a decade in the doldrums, fast neutral atom beams found its use in depth profiling for glass (Iino et. al., 1981) and for mass spectrometry (FABMS by Vickerman et. al., 1981/82) on glass and organic materials [10]. Despite all that, ion beams are still the choice for SIMS simply because ion guns

which are capable of producing energetic and intense ion beams are commercially available. However, recently Eccles et. al. [11] reported a newly constructed raster-scanned microfocused (FWHM = 5 μm) neutral beam gun for use in SIMS imaging of insulator surfaces.

1.2 Review of the interaction of fast neutral atoms with surfaces

The basic question pertinent to the interaction of atoms with surfaces is how the atoms lose their energy. As for the question theoreticians are divided into two lines of thought, that is, it occurs through the excitation of phonons or electron-hole pairs [12]. In this section, the experiments which involve the interaction of fast neutral atoms with surfaces are reviewed briefly. The author tries to present them in their chronological order, and wherever possible the reasons why the experimenters turned to fast neutral atoms are also discussed.

When a beam of fast neutral atoms collides with a solid surface, the following observable processes may take place, individually or simultaneously:

(i) ejection of secondary electrons

(ii) production of visible, ultra-violet and infrared radiations

(iii) sputtering of the surface atoms

(iv) elastic and inelastic scattering of the fast atoms

(v) absorption of the fast atoms into the subsurface region followed by desorption

(vi) ionisation of the fast atoms

Due to their small de Broglie wavelength, compared to the spatial periodicity of the surface atoms, and their ability to penetrate deep into the subsurface regions, as expected, fast atom diffraction from surfaces is not observed.

The phenomenon of secondary electron ejection from a surface under fast atom bombardment was first systematically observed by Rostagni in 1934 (He on Cu; 50 - 400 eV) [1]. The experiment was made possible following the discovery of charge exchange mechanism for the generation of fast neutral atoms by Kallman and Rosen in 1930. It was found that the number of the ejected electrons was proportional to the number of the fast neutrals. In the experiment the number of the fast neutrals was estimated by measuring the slow positive ion current produced in the charge exchange process. It then became a fashion to use the ejected electron current as a means of detecting and measuring the flux of fast neutral atom beam.

Subsequent experiments on ejected electron current were aimed mainly at refining the value of the secondary electron yield coefficient; a quantity defined as the average number of secondary electrons emitted from the surface per incoming neutral atom, and normally denoted by $\gamma^{\bullet}$ [*]. Secondary electron yield coefficient data between fast neutral atoms with metal surfaces are very scarce - the list for such

---

[*] In the literature, γ is usually used to denote secondary electron yield coefficient obtained with electron beam, γ^{+} for ion-induced potential emission, and γ^{+}_{kin} for ion-induced kinetic electron emission (KEE).

experiments is quickly exhausted. Among other reported works are those of Arifov et. al. (Ar on Mo in energy range 200 to 2000 eV) [13], Berry (He, N_2 and Ar on Ta; 0.5-2.5 keV) [2], Haugsjaa et. al. (Ar and H_2 on gold; 50-1000 eV) [14], Medved et. al. (Ar on Mo; 200-2500 eV) [15], Morita et. al. (H_2 on several metals; 10-40 keV) [16], and Utterback et. al. (He and N_2 on gold; 50-1000 eV) [17]. Except the degassed Mo surfaces used by Arifov et. al. and Medved et. al., the others were "laboratory surfaces", i.e., without surface cleaning procedures [18,19] and in a background pressure of $\approx 10^{-7}$ torr or higher. Generally, these experiments reported of increase in the yield of secondary electrons with beam energy. Several significant conclusions were drawn from these experiments [18]:

(i) There exists a threshold energy, E_{th}, for the fast neutral below which no secondary electron will appear. The value of E_{th} varies from as low as 50 eV [1,2,14,17] to about 700 eV [13,15,20].

(ii) A mass effect exists, i.e., γ^* is generally greater at a given energy for light neutrals than for the heavy ones.

(iii) γ^* rises rapidly and monotonically with the fast neutral energy to a value in the order of unity at 1 keV. This feature is generally insensitive to the actual surface chosen for the experiment.

Secondary electron yields obtained using primary electrons [21] and slow ions [22] show marked dependency on the degree of surface coverage. The same is also true for the secondary electron yield obtained with fast neutrals.

Since most of the fast neutral experiments cited above were carried out in poor vacuum conditions, and thus have no well defined surfaces, it is therefore not surprising to observe the insensitivities of the secondary electron yield with surface type [18].

Molecular beam SIMS, SCANIIR and FABMS work on the basis that bombardment of a surface with a fast atom beam will sputter the surface atoms. The sputtering occurs because the energetic atoms impart energy to the surface atoms in excess of their local binding energies. In molecular beam SIMS and FABMS, the sputtered particles are mass analysed so that the surface species can be identified. A significant portion of the sputtered fragments leave the surface in excited electronic states, and on de-excitation, optical radiations can be observed. In SCANIIR the surface constituents are determined by analysing the spectral distribution of the radiations and identifying the prominent optical lines and bands.

The success in using Auger electrons as a means to identify surface composition [23] reactivated the studies to use slow positive ions and metastables [24] as complementary probes in surface study. The works of Hagstrum [25] with very low energy ion beams gave birth to another surface technique called Ion Neutralisation Spectroscopy (INS). INS features the ejected electrons energy distribution curves which have a bearing on the ionisation potential of the collider ions and the surface work function. One interesting feature of the ejected electrons is that within the range of the INS energies the electron energy distribution curve

remains unchanged. However, when the energy of the ion beam is increased into the region of several hundreds eV, the yield of the ejected electrons increases dramatically. This observation led experimenters to conclude that there were two types of secondary electron ejection mechanisms, namely, potential ejection which dominates in the low energy range, and kinetic ejection for high energy range [26]. In this latter range, especially with the fast neutral atoms, theoretical and experimental studies alike are very rare.

The use of fast ion beams led to the development of the LEIS technique, which was discussed in an earlier section. To the best of the author's knowledge there is no report involving the use of fast neutral atom beam in a strictly LEIS procedure, i.e., using fast neutrals as the projectiles followed by detection of the scattered fast neutrals. This can be understood in the light of the stringent condition required by LEIS, namely the need for a highly monoenergetic ion beam, a requirement which has yet to be fulfilled by todays fast atom sources. The use of time-of-flight technique in conjunction with fast atoms in a LEIS-like experiment is an area yet to be explored. The LEIS-like experiments of Souda et. al. [5] mentioned earlier in this chapter were a slight modification to the true LEIS; they used fast neutrals as the projectiles and measured the energy distribution of the scattered ions, and called the technique Neutral Beam Incident Ion Scattering Spectroscopy (NBISS).

Limited by the instrumental problem mentioned above, scattering experiments using fast neutral atoms took another

approach, namely measuring the in-plane scattered beam intensities with respect to the polar angle measured from the surface normal. Experiments of this type are called "angle-resolved fast atom scattering (ARFAS)" and were first reported by Nielsen and Delchar [27] who performed scattering experiments between a fast He atom beam and a W{100} surface. Results from such experiments confirmed the existence of "rainbow peaks" as predicted by Garrison [28] and Helbig [29]. The so-called rainbow peaks observed in fast atom scattering are different in origin, at least theoretically, from those observed in thermal atom scattering. The latter, as proposed by McClure [30], are due to the spatial periodicity of the atom-surface interaction field while the former is due to the presence of a second scattering centre, that is, an adjacent atom which places a lower limit on the deflection angle. ARFAS results showed that the fast atom rainbow peaks were nearly invariant with the fast atom energy, this eliminates the stringent need for a monoenergetic collider beam. Apart from that there were two additional peaks, which were thought to be due to the fast neutral atoms which had penetrated the surface and re-emerged after undergoing scattering from the subsurface layers, a view which was later confirmed theoretically by Chang et. al. [31]. Further discussion on fast atom scattering will be given in Chapter Five, in which computer simulations of fast atom scattering on a two atom surface are used to obtain a better interatomic potential for the fast atom/surface interaction.

In 1980, it was suggested by Luitjens et. al. [32] that not only neutralisation of the ions, but also the reionisation of the neutralised ions occur during ion scattering at solid surface. Following that, Souda and Aono made a close examination of the process, for which they performed LEIS experiments using He^+ ion beam on 29 target elements [33]. On approaching the surface, a portion of the He^+ ions were neutralised due to the Auger process and then reionised in the collision with the target atoms. For the reionisation to occur, it was observed that the primary He^+ ions must have energy above a threshold value (E_{th}), which generally increases with the number of the valence electrons of the target atoms.

The dependence of the threshold ionisation energy (E_{th}) on the density of the target atom's valence electrons led Souda and Aono to suggest a model for the reionisation process based on the electron promotion mechanism once proposed by Barat and Lichten [34] [Fig. 1.1]. Curve I represents the total energy of the neutral He^* atom and a neutral target atom M as a function of their separation with the former approaching, and curve II is the similar plot for the He^+ ion and the then negatively charged surface atom M^- as the former receeds. The dotted line is the critical distance corresponding to the threshold energy E_{th}. If the energy of the neutral He^* atom is higher than E_{th}, its distance of closest approach to the target atom is smaller than the critical distance. At that small distance and in a very brief time, if the curves intersect each other, a quasimolecule "HeM" is formed which then fragments into an

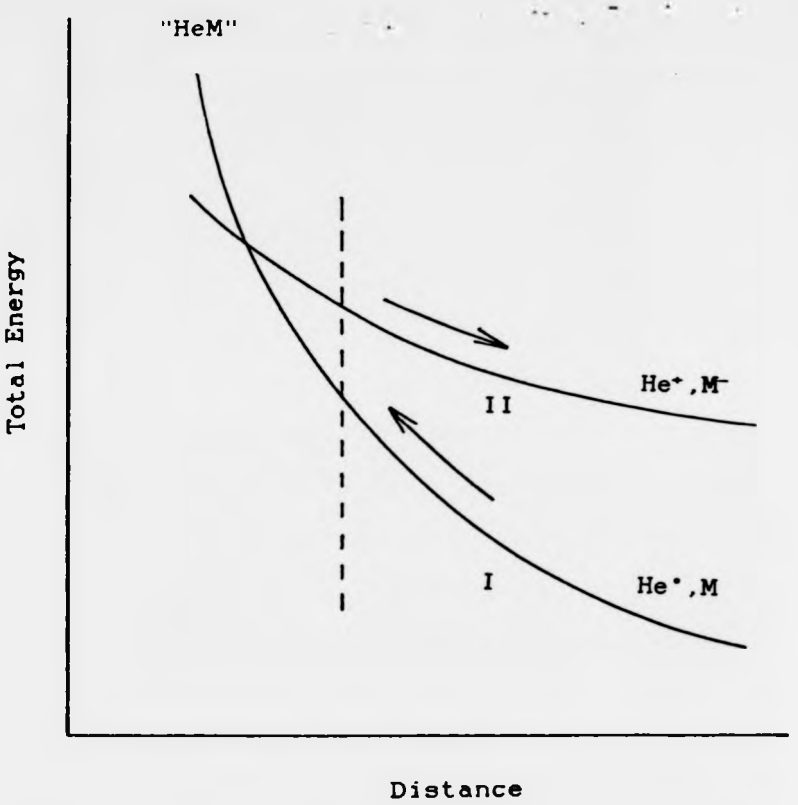

Fig. 1.1 : Schematic figure showing the ionisation of He* by the electron promotion mechanism (after Souda and Aono [33]).

He^+ ion and a negative M^- ion. This electron promotion mechanism is supported by the fact that as the number of the metal atom's valence electrons increases, electron transfer from He^* to M becomes more difficult, and that is manifested in the increased threshold energy E_{th} for the ionisation.

1.3 Review of the theoretical treatments

On the theoretical front, the pioneering and only study of gas-metal interactions at high energy was due to Kirson et. al. [35], who used the Sudden Collision Approximation to calculate the electron-hole pair excitation and its associated energy transfer probabilities for the collision of 272 eV H_2, He and Ar on lithium surface. To avoid the need for further substantial numerical calculation they ignored other important processes which have high probability of occurrence, such as sputtering, atom penetration and energy transfer to phonons, which they believed will not affect the results of their calculations on the electronic excitation.

In the following, the main idea of the calculation is described briefly; interested readers must refer to the original literature. The interaction is treated as a multiple scattering process and the calculation is performed in two representations, namely, coordinate representation $\{r\}$ and electronic state representation $\{\emptyset\}$, which are mutually transformable. α denotes the state of the internal electrons which is characterised by eigenfunction $\emptyset_\alpha$, energy ε_α, momentum k_α and another quantum number j_α. $S_{\alpha\beta}$ which is

the off-diagonal element of the scattering matrix S, associated with the transition of the electronic state from α to β. In Dirac notation, $S_{\alpha\beta}$ is given by

$$S_{\alpha\beta} = \langle \phi_\alpha \mid S \mid \phi_\beta \rangle$$

The transition amplitude for single electron excitation, which the authors expected to be the dominant process, is given by

$$T^{(1)}_{\alpha\beta} = \langle \phi_\alpha \mid 1-S \mid \phi_\beta \rangle = \delta_{\alpha\beta} - S^{(1)}_{\alpha\beta}$$

where 1 is the unity matrix, $\delta_{\alpha\beta}$ is the Kronecker δ. The transition probability from initial state α ($\varepsilon_\alpha < E_F$) to final state β ($\varepsilon_\beta > E_F$) is given by

$$P(\varepsilon_\alpha \rightarrow \varepsilon_\beta) = \sum_{j_\alpha, j_\beta} \int \mid T^{(1)}_{\alpha\beta} \mid^2 d\Omega_\alpha \, d\Omega_\beta$$

where the integration is over the angular directions of k_α, k_β and E_F is the Fermi energy. The probability for energy transfer δE in the transition is

$$P(\delta E) = \frac{\aleph^2}{(2\pi)^6} \left(\frac{2m}{\hbar^2}\right)^3 \int d\varepsilon_\alpha \sqrt{\varepsilon_\alpha} \sqrt{(\varepsilon_\alpha + \delta E)} \, P(\varepsilon_\alpha \rightarrow \varepsilon_\beta)$$

where $\aleph$ is the normalisation volume of the electrons. Results of the calculation with argon are reproduced in Fig. 1.2.

Several conclusions were drawn from the calculations:

(i) During the collision, energy is transferred from the fast neutral atoms to the metal electrons; maximum energy transfer probability lies in the energy range of 10–30 eV. This allows for energetic excitation of the metal electrons to the continuum.

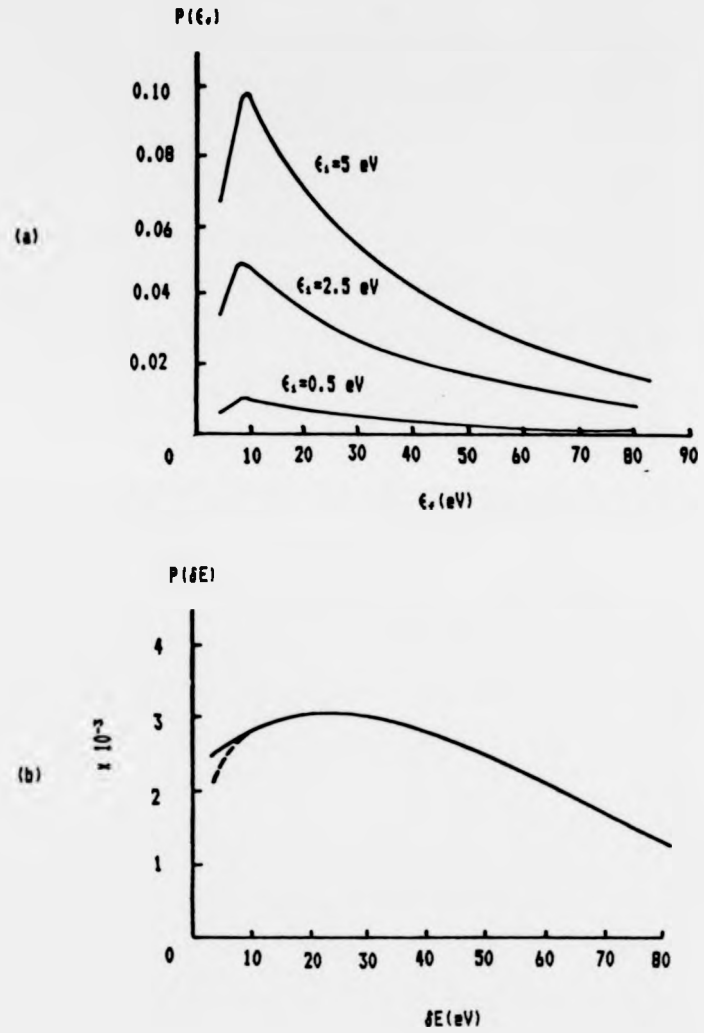

Fig. 1.2 : (a) Calculated probability for single electron-hole pair excitation for an Ar + Li(surface) collision, as a function of the electron final energy ϵ_f, for three values of the electron initial energy (after Kirson et. al. [35]).

(b) Calculated probability per unit energy, P(δE), of energy transfer δE for an Ar + Li(surface) collision. Dashed line is for probability of energy transfer δE resulting in electron excitation beyond the Li threshold [35].

(ii) The efficiency of the energy transfer depends on the species of the interacting systems; the order of transfer effectiveness for the three gases is H_2≫Ar≫He. The order suggests that energy transfer is strongly affected by the range and strength of the interaction potential between the fast atom and the metal electrons.

(iii) Ionisation of the metal electrons, i.e., excitation to final energy levels above the threshold of 8.5 eV for Li, is a likely process, in which event, low energy electrons are being ejected from the metal surface.

1.4 Objectives

The object of the work described in this thesis is to provide experimental data of interaction between fast neutral atoms with metal surfaces in a strictly UHV condition. Two polycrystalline metal surfaces are used, namely, lithium and gold surfaces, which represent a very light and a heavy target respectively. Five gases are used, they are H_2, He, Ne, N_2 and Ar; to represent quite a broad spectrum of projectiles, from very light atom to the heavy one, inert and non-inert. The experiments are confined mainly to the study of two phenomena, namely, the secondary electron ejection and the ionisation of the projectiles.

The general aim is to investigate the possibility of using fast neutral atoms as a surface probe in the manner similar to AES and INS. The energy distribution of the ejected electrons, especially from lithium surface, can be compared with the results from the calculations of Kirson

et. al.; and it is hoped that the experimental results will promote our understanding about the ejection of secondary electrons.

For the scattering of fast neutral atoms by surfaces, a simple two dimensional computer simulation model is developed. The aim is to use ARFAS data for He on a Cu(111) surface, kindly supplied to the author by Drs. H.B. Nielsen and T.A. Delchar, to obtain a better interatomic potential for the system; the first attempt of its kind.

1.5 References

[1] A. Rostagni, Nuovo Cimento **11** (1934) 99.

[2] H. W. Berry, Phys. Rev. **74** (1949) 848.

[3] C. W. White, D. L. Simms and N. H. Tolk, Science **177** (1972) 481.

[4] E. Taglauer, W. Englert, W. Heiland and D. P. Jackson, Phys. Rev. Letters **45** (1980) 740.

[5] R. Souda, M. Aono, C. Oshima, S. Otani and Y. Ishizawa, Surf. Sci. **179** (1987) 199.

[6] D. V. McCaughan and V. T. Murphy, J. Appl. Phys. **44** (1973) 3182.

[7] D. V. McCaughan and R. A. Kushner, in **Characterization of Solid Surfaces** (P. F. Kane and G. B. Larrabee, eds.) (Plenum, New York, 1974) Ch. 22.

[8] See for example, B. Van Zyl et. al., Rev. Sci. Instrum. **47** (1976) 814 and references cited therein.

[9] C. W. White, D. L. Simms and N. H. Tolk, in **Characterization of Solid Surfaces** (P. F. Kane and G. B. Larrabee, eds.) (Plenum, New York, 1974) Ch. 23.

[10] J. A. Van den Berg, Vacuum **36** (1986) 981.

[11] A. J. Eccles, J. A. Van den Berg, A. Brown and J. C. Vickerman, J. Vac. Sci. Technol. **A4** (1986) 1888.

[12] O. Gunnarson and K. Schönhammer, Phys. Rev. **B25** (1982) 2514.

[13] U. A. Arifov, R. R. Rakhimov and Kh. Dzhurakulov, Soviet Phys.-Doklady **7** (1962) 716.

[14] P. O. Haugsjaa, J. F. McIlwan and R. C. Amme, J. Chem. Phys. **48** (1968) 527.

[15] D. B. Medved, P. Mahadevan and J. K. Layton, Phys. Rev. **129** (1963) 2086.

[16] K. Morita, H. Akimune and T. Suita, Jpn. J. Appl. Phys. **5** (1966) 511.

[17] N. G. Utterback and G. H. Miller, Rev. Sci. Instrum. **32** (1961) 1101

[18] R. C. Amme, J. Chem. Phys., **50** (1969) 1891.

[19] H. D. Hagstrum, Rev. Sci. Instrum., **24** (1968) 1122. R. G. Musket, W McLean, C. A. Colmenares, D. M. Makowiecki and W. J. Siekhaus, Appl. Surf. Sci., **10** (1982) 143.

[20] E. S. Parilis and L. M. Kishinevskii, Soviet Phys.-Solid State **3** (1960) 885.

[21] H. Bruining, **Physics and Applications of Secondary Electron Emission** (Pergamon, London, 1954).

[22] J. H. Parker, Phys. Rev. **93** (1954) 1148.

[23] G. A. Harrower, Phys. Rev. **102** (1956) 340.

[24] P. D. Johnson, Ph. D. Thesis (University of Warwick, 1978) and references cited therein.

[25] H. D. Hagstrum, Phys. Rev. **96** (1954) 336.

[26] M. Kaminsky, **Atomic and Ionic Impact Phenomena on Metal Surfaces** (Springer-Verlag, Berlin, 1965) Ch. 14.

[27] H. B. Nielsen and T. A. Delchar, Surf. Sci. **141** (1984) 487.

[28] B. J. Garrison, Surf. Sci. **87** (1979) 683.

[29] H. F. Helbig, M. W. Linder, G. A. Morris and S. A. Steward, Surf. Sci. **114** (1982) 251.

[30] J. D. McClure, J. Chem. Phys. **52** (1970) 2712.

[31] C. C. Chang, B. J. Garrison, H. B. Nielsen and T. A. Delchar, Surf. Sci. **155** (1985) 327.

[32] S. B. Luitjens, A. J. Algra, E. P. Th. M. Suurmeijer and A. L. Boers, Surf. Sci. **99** (1980) 631.

[33] R. Souda and M. Aono, Nucl. Instr. Methods **B15** (1986) 138.

[34] M. Barat and W. Lichten, Phys. Rev. **A6** (1972) 211.

[35] Z. Kirson, R. B. Gerber and A. Nitzan, Surf. Sci. **124** (1983) 279.

CHAPTER TWO

A REVIEW ON ENERGY LOSS PROCESSES AND SECONDARY ELECTRON EMISSION FOR IONS AND NEUTRALS INTERACTING WITH SOLIDS

2.1 Introduction

All the phenomena mentioned earlier in Section 1.2 have one thing in common, that is, the fast neutral atoms lose their energy. In this chapter the energy loss processes for ions and neutrals interacting with solid will be selectively reviewed. The author has no intention to mention all the work done in this field (a very large body of data are given in Refs. [1,2,4,5,17]). Energy transfer is essential for fast atom induced kinetic electron emission, which is the central theme of this work; thus the inclusion of this topic in the thesis is indeed justified. Having mentioned the electron emission, towards the end of this chapter, details of the similarities and differences between ion and neutral induced electron emission will also be discussed.

2.2 Historical review

The concept of energy loss for particle projectile is relatively new; it first appeared early this century after the discovery of radioactivity by Marie Curie. However, the stopping of projectile in uniform homogeneous medium, a consequence of energy loss, has been of scientific interest since some 500 years ago [1]. It dated back to the era of

Leonardo da Vinci (1452 - 1519) who was commissioned to study the motion of large missiles thrown using ballistas. Unfortunately, due to the absence of proper understanding of mechanics, Leonardo was led to a scientifically wrong conclusion; he believed that the projectile range increases directly with the instantaneous applied force.

The concept of stopping power has never been considered until about 250 years ago when in 1740 Benjamin Robins predicted that the stopping of air on a projectile would be directly proportional to the projectile's velocity. This revolutionary idea would have been the inspiration for the establishment of Stoke's law and quite recently the calculation of stopping of ions in solids.

From early this century, stopping of projectile in matter continue to gain interest from both theorists and experimentalists. Until last decade, interest lies mainly in the high energy region (MeV), i.e., in the stopping of energetic nuclear reaction products. Now renewed interest is in ion implantation (5 - 500 keV). This technique proved to be technologically superior than the previously used diffusion method for use in the fabrication of VLSI chips [2].

The foundation of today's theory of stopping and range of particles in solids is due to many great scientists whose work had established the correct, or at least, the working model of the atom. Among the most important work are those of J. J. Thomson for discovering the electrons (1897), R. A. Millikan for the measurement of the electronic charge (1909), and E. R. Rutherford, Geiger and Marsden for the

concept of positively charged nucleus (1909 - 1911). Perhaps in the context of stopping theory the most enlightening contribution is due to N. Bohr who in 1913 successfully applied the then newly established quantum hypothesis (Planck (1900) and Einstein (1905)) to his model of nuclear atom: a heavy positively charged core surrounded by a cluster of orbiting electrons, each with specific discrete energy level [1,3]. In the analysis of the stopping of charged particles by matter, Bohr proposed a very important conclusion, that is, the energy loss of energetic ions could be divided into two components, namely, nuclear stopping (inelastic energy loss due to direct collision with the screened target nuclei) and electronic stopping (elastic energy loss due to excitation and ionisation of the target electrons). Based on recoil kinematics considering the relative masses and abundances of the target electrons and nuclei, he deduced that the electronic stopping would be far greater than in the nuclear stopping [1,4].

One serious problem faced by Bohr in the calculation of energy loss was the lack of knowledge of the charge state of the ion inside the matter, i.e., its effective charge while interacting with the target atoms. As a matter of fact, this problem is not fully answered until today. One of the ways out of the problem was by adopting the so-called "scaling law" which was actively used in the 1930s following the discovery of nuclear fission [5,6]. By assuming that protons and heavy ions react identically to the material, the scaling formula used was:

$$\frac{S_{HI}(v,Z_2)}{(Z_{HI}^{*}(v))^2} = \frac{S_p(v,Z_2)}{(Z_p^{*}(v))^2}$$

where $S_{HI}(v,Z_2)$ is the electronic stopping power of the heavy ion of atomic number Z_{HI} at some velocity v, in a target with atomic number Z_2, and effective charge at that velocity of Z_{HI}^{*}. S_p is the proton stopping power at the same velocity in the same material. The scaling law was not well justified theoretically and was severely criticised, but however, it remains to be useful simply because it is the most accurate way ever discovered [5,7].

Another solution to the effective charge problem was due to Bohr who in the early 1940s suggested that energetic ions could be assumed to be stripped of all electrons with velocities lower than the ion velocity. Using the Thomas-Fermi atom he could show that the ion effective charge, Z_1^{*}, is related to its velocity, v, as [1,8]:

$$Z_1^{*} = Z_1^{1/3}\left(\frac{v}{v_o}\right)$$

where v_o is the Bohr velocity ($\approx 2.2 \times 10^8$ cm/s). He also estimated a screening distance between two colliding atoms which limits the energy transfer between nuclei as:

$$a_{12} = \frac{a_o}{(Z_1^{2/3} + Z_2^{2/3})^{1/2}}$$

where a_o is the Bohr radius, 0.53 Å. These formulae serve as a model to most of the stopping theories developed until 1970s.

Another important contribution to the theory of ion stopping was that of Bethe and Bloch [1]. By assuming the target atoms behave like Thomas-Fermi atoms and treating the

target electrons as quantised plasma, they proposed a stopping formula which could predict accurately energy loss of high energy light positive ions, such as proton, H^+ and He^+, for different stopping materials. The general form of Bethe-Bloch formula is as follows [9]:

$$\varepsilon = \frac{4\pi Z_1^{\,2} Z_2 e^4}{mv^2}\left[\log\frac{2mv^2}{I} - \log\left(1-\frac{v^2}{c^2}\right) - \frac{v^2}{c^2} - \frac{C}{Z_2} - \frac{\delta}{2}\right] + \ldots$$

where I is the mean ionisation potential, C/Z_2 accounts for the shell correction and the term $\delta/2$ accounts for the density effect.

The Bohr and Bethe-Bloch stopping theories work reasonably well for high velocity ions; at low velocities large correction is needed. In this velocity region two important contributions came from Firsov (1957) [9,10] and Lindhard, Scharff and Schiøtt (abbreviated as LSS) (1963) [1,5,9,11]; both were based on Thomas-Fermi model of atom. Firsov's calculation of energy loss is through the momentum transfer of electrons from one atom to another. To calculate the energy loss to target nuclei he employed Bohr's model of screened collision, but used a different screening length parameter, which is

$$a = \frac{a_o}{(Z_1^{\,1/2} + Z_2^{\,1/2})^{2/3}}$$

The LSS theory of stopping and range of ions in matter is based on elastic scattering of free target electrons in the static field of screened point charge. It is reasonably accurate and applicable over the entire range of atomic species and energies. It have produced the most widely used

range estimates, and is considered as in the words of J. F. Ziegler [1] as "the peak and the last of comprehensive stopping and range theory based on statistical model of atom-atom collision".

Up to now we have come across several terms associated with energy loss. In the following section the terms used will be formally defined.

2.3 Definitions of terms associated with energy loss

In the literature, the term energy loss is meant for the average amount of energy lost by a collider particle per unit path length as it penetrates a medium [1,9]. Since the process is energy dependent, then mathematically energy loss is defined as

$$\frac{dE(E)}{dx} = \lim_{\delta x \longrightarrow 0} \frac{\delta E}{\delta x}$$

where E is the energy of the collider, δE is the amount of energy the collider lost as it penetrates a distance δx through the medium. Recalling the two major contributors towards the energy loss, i.e., nuclear and electronic, we may write a differential energy loss equation as

$$(dE/dx)_{tot} = (dE/dx)_n + (dE/dx)_e$$

In the case of an ion, an additional process has certain contribution towards the energy loss, although relatively small, namely, charge exchange process between the ion and the target atoms. Denoting this component of

energy loss as $(dE/dx)_{c.e.}$, the energy loss equation becomes [4]:

$$(dE/dx)_{tot} = (dE/dx)_n + (dE/dx)_e + (dE/dx)_{c.e.}$$

It must be noted here however, that most of the stopping and range calculations for ions discussed before ignored the last term.

Energy loss (dE/dx) is related to the stopping cross-section S(E) as follows [1,9]:

$$S(E) = (dE/dx)/N$$

where N is the atomic density of the medium. The electronic and nuclear stopping power are denoted by $S_e(E)$ and $S_n(E)$ respectively. The unit for stopping power commonly used in the literature is $eV\text{-}cm^2/atom$.

The total pathlength of the projectile in a medium is called range and usually denoted by R [1,2,4]. It may easily be obtained by integration of the deduced total stopping power, that is

$$R = \int_0^{E_o} - \frac{dE}{(dE/dx)_{tot}}$$

where E_o is the projectile's initial energy. Electronic losses dominate at high energies, but as the projectiles slow down, i.e., near the end of their path, elastic nuclear collisions take place, results in large angle scattering which cause range straggling, $R_\perp$, i.e., the lateral spread of the path of the projectile (Fig. 2.1).. Therefore it is important to know the projected range, R_p, which is the average depth to which a projectile will penetrate when the incident ion beam normal to the surface.

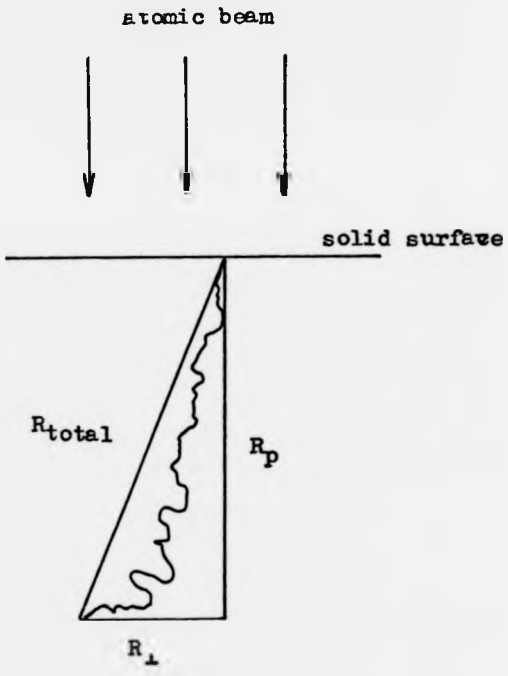

Fig. 2.1 : The path of an atomic particle entering a solid showing the total range, the projected range and the straggling (i.e., lateral spread)

2.4 The calculation of nuclear and electronic stopping power

The calculation of energy loss involves many assumptions and empirical correction factors, so it is best to proceed this section directly to the widely used LSS energy loss and range theory. Since both the nuclear and electronic energy loss are energy dependent [1,11], for simplicity they will be treated independently.

2.4.1 Nuclear energy loss

Nuclear energy loss is a result of elastic interactions between the projectile and a screened target nucleus; thus it is easier to treat this problem as a two body collision, for which the transferred energy (T) and its cross section ($d\sigma_n$) and the angle of scattering (Ø) is calculated. Fig. 2.2 shows trajectory of the colliding particles (M_p the projectile, M_t the target nucleus) before and after the collision in a laboratory coordinate system (Fig. 2.2a) and a centre of mass coordinate system (Fig. 2.2b). Using classical mechanics *, i.e., through the application of the laws of conservation of linear momentum and energy, it can be shown that the energy transferred from the projectile to the target atom is equal to the recoil energy of the latter, which is

---

* See Section 6.2 for further discussion on Bohr condition for the applicability of classical mechanics on high energy two body collision.

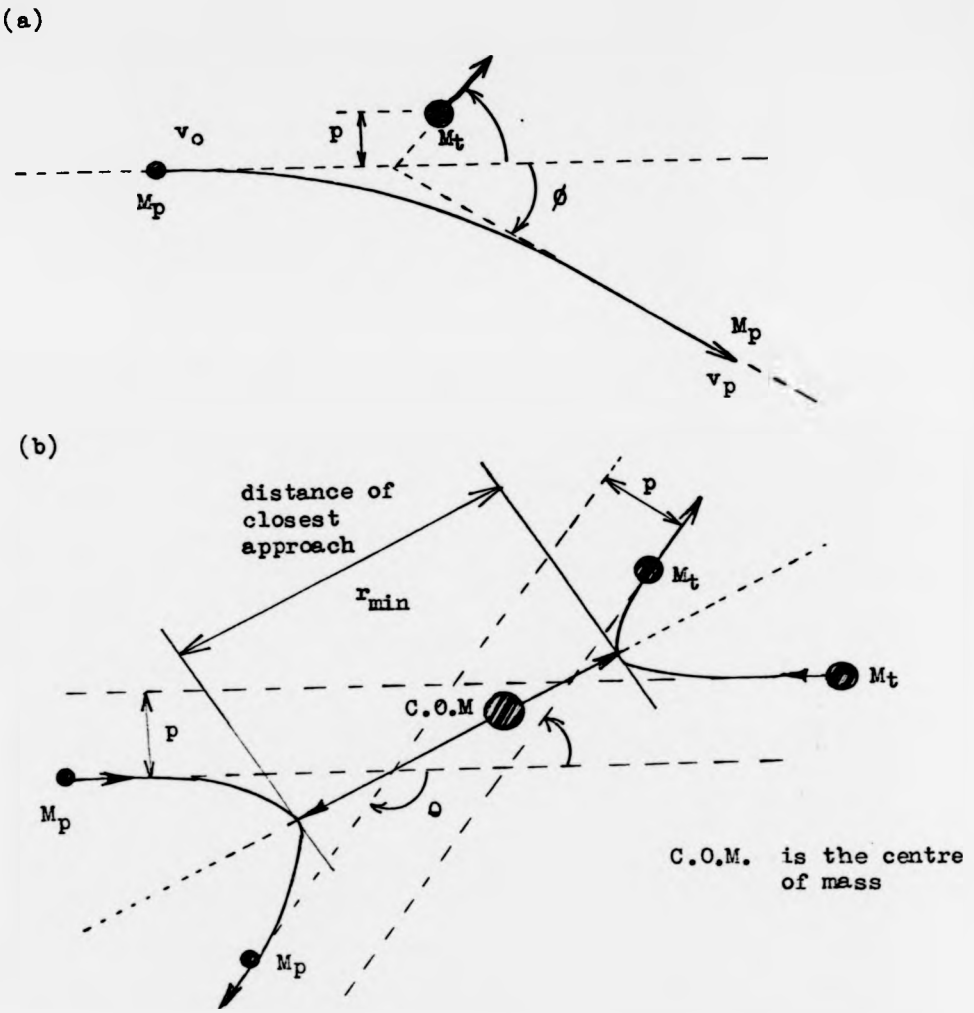

Fig. 2.2 : (a) The colliding atoms in a laboratory coordinate system

(b) The colliding atoms in a centre-of-mass coordinate system

$$T = \frac{4M_pM_tE_o}{(M_p+M_t)^2} \sin^2 \frac{\phi}{2}$$

where E_o is the collision energy of the projectile. The maximum energy transfer occurs in a head-on collision (i.e., ϕ=180°) is

$$T_{max} = \frac{4M_pM_tE_o}{(M_p+M_t)^2}$$

The next step in the calculation is to solve for the scattering angle, ϕ. To do this one needs to know the repulsive potential, V(r), between the colliding atoms. Unfortunately there is no definitive potential which is appropriate for all pairs of atoms and energies; the quite diverse choices of such potential is as shown in Fig. 2.3, and a good review of this field was given by Torrens [12]. In the LSS theory the potential they used takes the form

$$V(r) = \frac{Z_pZ_t}{r} e^2 \quad \phi_{TF}(r/a)$$

where $\phi_{TF}(r/a) = 1 - (r/a)[(r/a)^2 + 3]^{-\frac{1}{2}}$ is the Thomas-Fermi screening function, and

$$a = 0.885\ a_o/(Z_1^{2/3} + Z_2^{2/3})^{\frac{1}{2}}\ ,\ a_o = 0.53\ \text{Å}$$

is the reduced screening length parameter.

Inside the matter the collisions between the projectile and the target atoms are not limited to the head-on type only but the off-axis collisions as well. Therefore it is best to describe the collisions in term of an impact parameter, p [See Fig. 2.**2**]. If r is the pair separation,

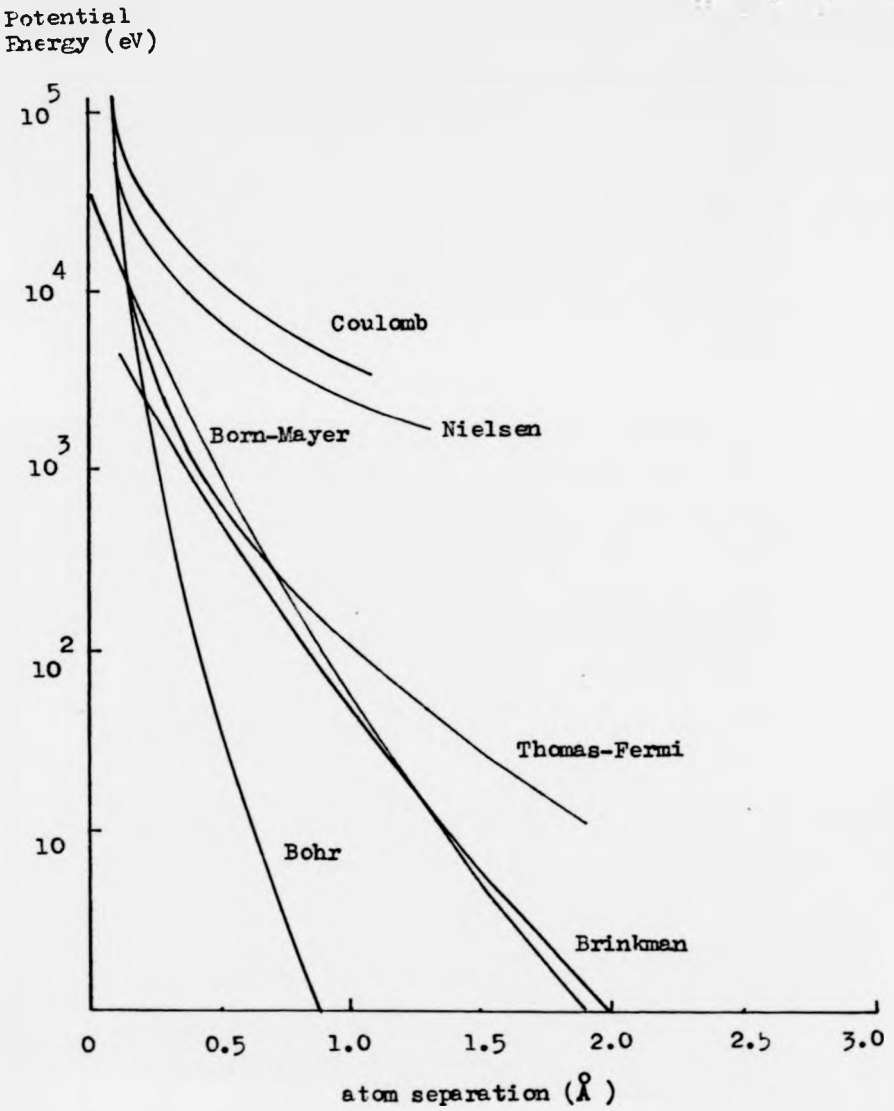

Fig. 2.3 : Plots of various interatomic potentials between a pair of Cu atoms. (Adapted from Ref. 4)

the centre-of-mass energy, i.e., the total energy of the system, E_c, is given by

$$E_c = \tfrac{1}{2}\,\mu\,\{\,(dr/t)^2 + r^2(d\emptyset/dt)^2\,\} + V(r)$$

where μ is the system reduced mass equals to $(M_t M_p)/(M_t+M_p)$. Applying law of conservation of angular momentum

$$J_c = \mu\, r^2\,(d\emptyset/dt) \;= \mu\, v_o\, p$$

where J_c is the central angular momentum, we obtain

$$v_o p = r^2\,(d\emptyset/dt).$$

Substitute this back into the energy equation, we obtain

$$(dr/dt) = v_o\,\{\,1 - V(r)/E_c - (p/r)^2\,\}^{\frac{1}{2}}$$

which is a radial equation of motion. Combining the last two equations, we obtain

$$(d\emptyset/dr) = (d\emptyset/dt)(\,dt/dr) = (d\emptyset/dt)/(dr/dt)$$

$$= \frac{p}{r^2\,\{\,1 - \dfrac{V(r)}{E_c} - \dfrac{p^2}{r^2}\,\}^{\frac{1}{2}}}$$

By taking π as the initial value of $\emptyset$, we may calculate $\emptyset$ as

$$\emptyset = \pi - \int_{-\infty}^{\infty} \frac{p\,dr}{r^2\,\{\,1 - \dfrac{V(r)}{E_c} - \dfrac{p^2}{r^2}\,\}^{\frac{1}{2}}}$$

To make comparison with the experimental results we need to use differential cross-section

$$d\sigma = 2\pi p dp$$

for which the total cross-section for energy transfer is

$$\sigma = \int_{T_{min}}^{T_{max}} (d\sigma/dT)\,dT$$

For a particular scattering angle, the probability that the energy transfer is T is related to σ by

$$p(T)dT = (1/\sigma)\ (d\sigma/dT)\ dT.$$

The nuclear stopping power, $S_n(E_o)$, is then calculated as follows:

$$S_n(E_o) = \int_0^\infty T\ d\sigma = \int_0^\infty T 2\pi p dp = 2\pi\mu E_o \int_0^{p_{max}} \sin^2(\emptyset/2)\ pdp$$

where p_{max} is the sum of the two atomic radii beyond which no energy is transferred in the collision.

To simplify the interpretation of the result, dimensionless reduced energy and range parameters were introduced in the LSS theory:

reduced energy, $\varepsilon \equiv E\ (aM_t)/\{Z_pZ_te^2(M_p+M_t)\}$

reduced range, $\rho \equiv RNM_t\ (4\pi a^2M_p)/(M_p+M_t)^2$

where R is the range, N is the target atomic density, and a is the Lindhard's reduced screening length parameter,

$$a = 0.885\ a_o\ /(Z_p^{2/3}+Z_t^{2/3})^{1/2}\ ,\ a_o = 0.53\ \text{A}.$$

In these reduced parameters, the nuclear energy loss is given by

$$(d\varepsilon/d\rho)_n = \sigma\ (M_p+M_t)\ /\ 4\pi e^2Z_pZ_tM_p$$

The differential cross-section for the energy transfer process is

$$d\sigma = \frac{\pi a^2}{2t^{3/2}}\ f(t^{1/2})\ dt$$

where t is the reduced transferred energy defined as

$$t = \varepsilon^2\ \sin^2\ (\emptyset/2) = \varepsilon^2\ (T/T_{max})$$

and $f(t^{1/2})$ is simply called " a function of t ". The reduced nuclear stopping is given by

$$S_n(\varepsilon) = \frac{1}{\varepsilon} \int_0^{\varepsilon} f(t^{1/2})\, d(t^{1/2})$$

The function $f(t^{1/2})$ has value which is dependent on one's choice of interatomic potential. For any arbitrary potential

$$f(x) = d/dx\ [x\ S_n(x)]$$

where x is a substitution for $t^{1/2}$. Evidently, like the interatomic potential, $f(t^{1/2})$ is also an empirical relation. Example given by Winterbon et. al. [4,13] has the form

$$f(t^{1/2}) = \lambda t^{(1/2-m)} \{1+(2\lambda t^{(1-m)} q\}^{-1/q}$$

where λ, m and q are empirical constants. Recently, Littmark and Ziegler [1,14] suggested a more complex form of f(x)

$$f(x) = \lambda_i x^{1-2m(x_i)} \qquad \text{for } x_i < x < x_{i+1}$$

$$\lambda_{i+1} = \lambda_i x_{i+1}^{2(m(x_i+1)-m(x_i))}$$

where $m(x) = 1 - \exp[-\exp \Sigma a_i (0.1 \ln x/x_1)^i]$

where a_i, λ_1 and x_1 are chosen constants.

2.4.2 Electronic energy loss

By assuming that the electronic energy loss is proportional to the projectile velocity (v_p), LSS formulation for the electronic energy loss takes the form

$$(dE/dx)_e = \xi \{8\pi e^2 N a_o Z_p Z_t / (Z_p^{2/3}+Z_t^{2/3})^{3/2}\} (v/v_o)$$

where $v_o = (Z_p e^2/h)$ is the Bohr velocity, and numerically $\xi \approx Z^{1/6}$. In terms of the reduced parameters the electronic energy loss is

$$d\varepsilon/d\rho = k\varepsilon^{1/2}$$

where

$$k \approx \frac{0.0793\, Z_p^{2/3}\, Z_t^{1/2}\, (M_p+M_t)^{3/2}}{(Z_p^{2/3} + Z_t^{2/3})^{3/4}\, M_p^{3/2}\, M_t^{1/2}}$$

2.5 Projectile range

LSS theory provided an approximate relation between R, $R_\perp$ and R_p as follows [11]:

$$R/R_p \approx 1 + M_t/3M_p$$

At low energies ($\varepsilon \leq 0.1$) the projectiles scarcely penetrate the atoms. By approximating the Thomas-Fermi function as $V(r) \approx r^{-3}$, Schiøtt [15] provided a range-energy relation

$$\rho \approx 3/2\ \varepsilon^{2/3}$$

and the projected range

$$\rho_p(\varepsilon) \approx 3/2\ C\ \varepsilon^{2/3}$$

or $$R_p \approx C\, M_t\, \{(Z_p^{1/3}+Z_t^{2/3})E\ /Z_pZ_t\}^{2/3}$$

where C is a correction factor.

Examples of the LSS range-energy curves in reduced units are shown in Fig. 2.4 .

Other calculations

The LSS energy loss and range theory is by no mean perfect. This can be understood in the light of the assumptions made for the interatomic potential used in their calculations. The present day interest in stopping and range theory lies in improving the Bohr, Firsov and LSS theories by utilising the power and speed of modern computers and

(a)

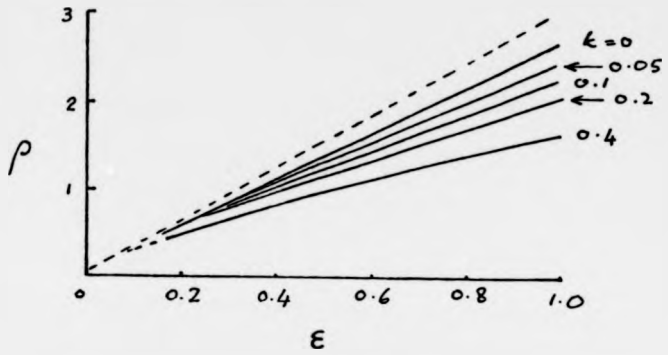

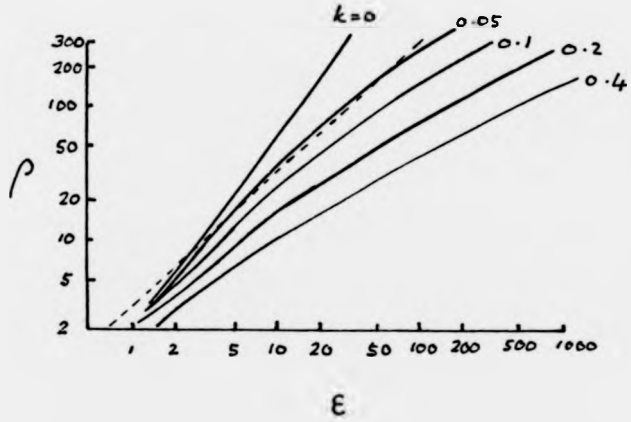

(b)

Fig. 2.4 : (a) The LSS energy -range curves in reduced units at low energies.
(b) The LSS energy-range curves in reduced units at high energies.

Dotted lines are for the range estimates when an inverse square potential between the nuclei is used.

(The curves are reproduced from Ref. 4)

employing the more realistic Hartree-Fock-Slater model of solid-state atom [1,9]. One example of such work is the Monte- Carlo program for calculating ion penetration in solid, codenamed MARLOWE [16]. Among the noted contributions are the work of Ziegler and co-workers, who among them have published a series of five books under the main title "The Stopping And Range Of Ions In Solids" % in which experimental and calculated values of stopping power of hydrogen [17], helium [5] and heavy ions in all elemental matter are tabulated.

2.6 The stopping of neutral atoms

The stopping theories developed so far were for ion-solid interactions, although it must be noted that much work have been carried out to study neutron scattering and stopping in solids. It was found that neutrons and protons in the 0 - 14 MeV energy region share the same pattern of angle-resolved differential scattering cross-section; although their absolute values differ by several orders of magnitude [18]. In the very low energy region ($\leq$ 20 keV), R. Blume et. al. [19,20] have reported that polycrystalline gold has similar stopping power for ions and neutrals of H, D and He. This behaviour is as expected; evidently from

---

% In the first volume of this series (Ref. [1]), the Fortran source code for all the programs and subroutines they used for the calculations of ion penetration in solids are listed, codenamed as STEST, STOPPING, STOP, RSTOP, TRIMS85, and PRAL.

Bohr's concept of effective charge (Z_p^*) of ions in solid [8,9]:

$$Z_p^* = Z_p^{1/3} (v/v_o) \quad , v_o \approx 2.2 \times 10^8 \text{ cm/s}$$

which is very small at very low velocities. In this energy region, the neutralisation probability becomes so large that the collision between the projectile and the target electrons is almost elastic. In other words, in the low energy region nuclear loss dominates, of which process ions and neutrals of same species share the same pattern of energy dependence.

The energy the projectile lost to the target may bring about several important and commercially useful changes in the latter. In ion implantation the concentration of the projectile atoms in the target changes the latter's conductivity. The sputtering of the target surface atoms can be used for coating of the target atoms onto other surface and the process itself becomes a standard routine in sample cleaning for surface analysis. The emission of secondary electrons not only useful for atomic particle detection but also for the understanding of surface electron wavefunction. In the following sections, the existing theories of ion and neutral induced secondary electron emission from solid will be briefly discussed.

2.7 Ion induced secondary electron emission

2.7.1 Introductory notes

Ion induced secondary electron emission from a solid surface can proceed by two qualitatively different ways, associated with two possible mechanisms of electron excitations. The two processes are usually taking place in different energy ranges of the ions and occurring to the detriment of either the potential energy or the kinetic energy of the interaction system. The processes are known as (i) potential electron emission (PEE), which can take place virtually at all ion energies, and (ii) kinetic electron emission (KEE), which have been observed to take place only when the ion velocity larger than 0.6×10^7 cm/s [21,22,23].

2.7.2 Potential electron emission (PEE)

In PEE, the potential energy released by the ion upon its neutralisation within the vicinity of the solid surface provides the energy required to free electrons from the latter. The condition for this process to occur was shown by Oliphant and Moon [22] to be that the ionisation potential of the ion (V_i) exceeds twice the work function of the solid ($\emptyset$), i.e., $V_i > 2\emptyset$.

PEE is an exothermic process, therefore it has no energy threshold, and being dependent on the ionisation potential alone it is rather independent of the ion energy. It has been observed experimentally that PEE yields are

fairly constant against ion velocity up to about 5×10^7 cm/s [22,24] and are expected to fall rapidly after that [25]. PEE yields are dependent on the state of the target cleanliness: low when the surface is clean, and increases when the surface is atomically dirty. In the same context, the energy distribution of the ejected electrons has more low energy electrons when the surface is dirty [21,22,23].

Based on the ideas of Oliphant and Moon, Massey (1930) treated the interaction problem using wave mechanics. However, rather wrongly, he assumed that the solid (metal) and the ion have equal energy levels. This, together with over simplified electron wavefunction, led him to predict a 100% electron yield, a value which is several times larger than one would obtain experimentally. Massey's theory was later improved by Shekter on one assumption, that is, the ion plays the part of a new energy level arising in the ion-metal system, lower than the occupied levels of the metal. This necessarily makes the combination an excited one; which on relaxation releases the energy of the neutralisation of the ion, which subsequently leads to emission of a metal electron through a two electron Auger type process. Shekter calculated the probability of occurrence of the process, and obtained a value about 10%, which is comparable to the experimental value [21,22].

Perhaps the most noted proponent of the theory of PEE was Hagstrum [25,26], who carefully performed the experiments using the first ever well defined metal surfaces. He further developed Shekter's theory by taking

into account several additional factors, namely, the displacement of the ion's energy levels near the metal surface, the finite lifetime of the initial state and the part played by resonance process in determining the relative probabilities of Auger neutralisation and Auger relaxation. Hagstrum's theory was so successful that it became the basis of a surface technique called "Ion Neutralisation Spectroscopy (INS)" [26,27]. The Auger electrons carry information on the density of states, thus useful for identification of the surface species. By virtue of the ion's low energy, given sufficient time, much of the Auger neutralisation takes place within about 3 A from the surface, thus makes INS information highly surface specific. In the following paragraphs, the PEE theories of Oliphant and Moon, and Shekter and Hagstrum are described briefly. Interested reader must refer to the original literature.

In summary, PEE is a result of ion neutralisation near the surface. The liberated ionisation (potential) energy brings about the emission of the surface electron through two possible transitions, namely, resonance neutralisation as proposed by Oliphant and Moon, and Auger neutralisation as suggested by Shekter and Hagstrum.

Oliphant and Moon proposed the tunneling of a metal electron through the surface barrier into an excited atomic level of the incoming ion without energy change; this process is clearly shown in Fig. 2.5a . This is a schematic diagram showing energy levels of a metallic surface (on the left) with its conduction band filled up to the Fermi level, and a localised potential well of an approaching ion (on the

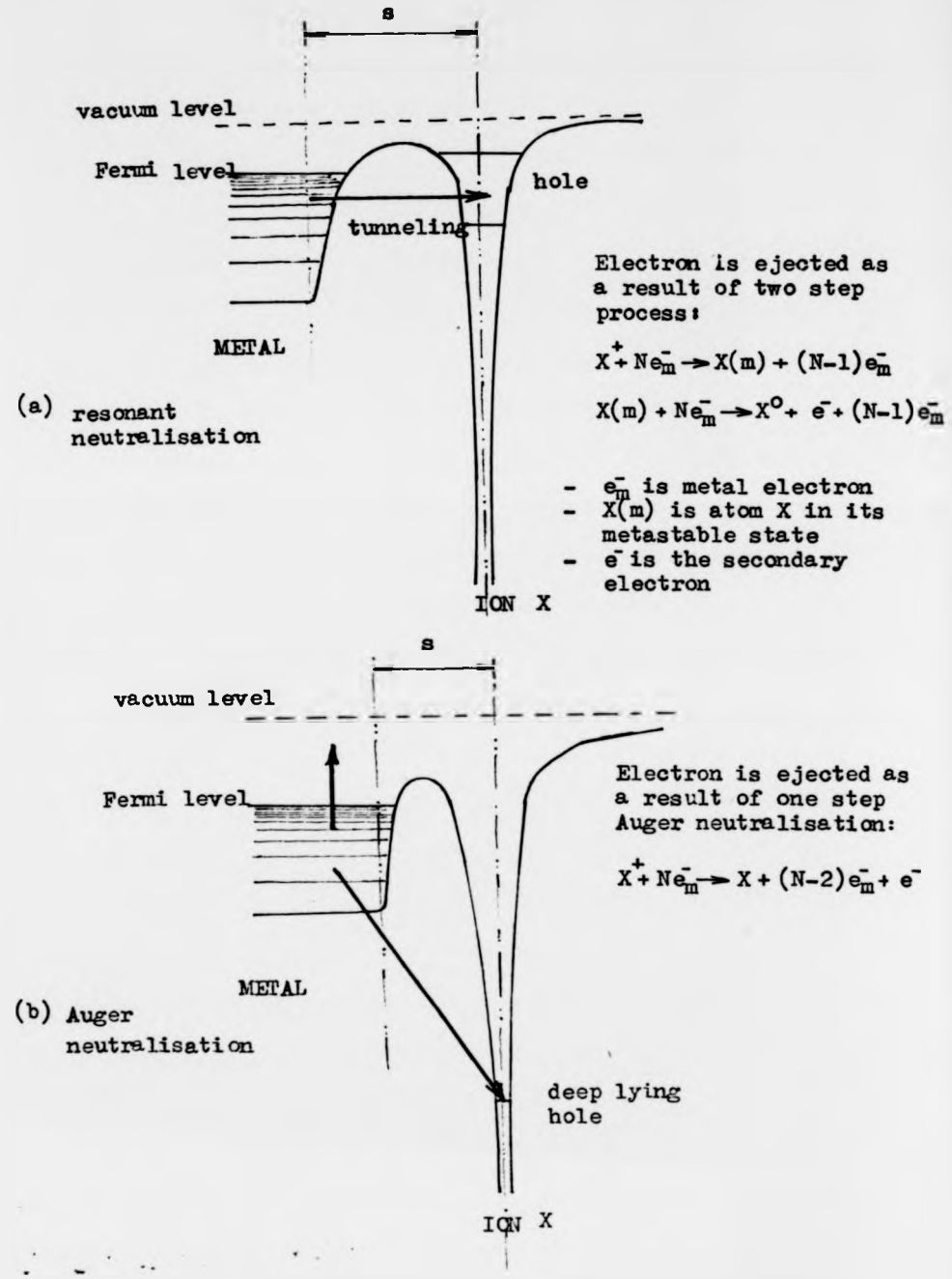

Fig. 2.5 : Schematic diagram showing (a) resonant neutralisation and (b) Auger neutralisation of an ion at a metal surface.

right) with its hole state forms a broadened energy level which straddles the Fermi level of the metal. In the case of an incoming metastable atom, the reverse transition may occur, and the process known as resonance ionisation.

Auger neutralisation involves transitions of two electrons almost simultaneously. An electron from the conduction band of the surface tunnels into a deeper lying hole at the bottom of the potential well of the approaching ion (Fig. 2.5b). In doing so the electron gives up its excess energy to another conduction electron, which is then emitted from the surface into the vacuum. In the case of a metastable atom, the excess energy goes to an electron in an excited state of the atom, which then leaves the atom carrying the excess energy into the vacuum. This process known as Auger de-excitation. Hagstrum was able to predict quite accurately the energy distribution of the ejected electrons. He did it by considering the transition rate of change of energy of the metal conduction electron as a function of the ion's approaching velocity and the liberated electrons escape probability.

Another widely quoted work on PEE is that of recent work of Kishinevskii (1973), who proposed a formula for calculating the yield coefficient (γ_p) [28]:

$$\gamma_p = 0.2\ (0.8E_i - 2\emptyset)\ /E_F$$

where E_i is the ionisation energy of the ion, E_F and $\emptyset$ the Fermi energy and work function of the metal respectively. However, when data of yield coefficients from clean metals become available, it have been shown recently that the

experimental values are somewhat lower, following a least square fit relation [29]

$$\gamma_p = 0.032\ (0.78E_i - 2\emptyset)$$

where E_i and $\emptyset$ are measured in eV.

2.7.3 Kinetic electron emission (KEE)

For kinetic electron emission, the source of energy for the emitted electron has never raised any doubts, namely, the kinetic energy of the ion. This is true whatever is the energy transfer mechanism, which has remained obscure until now. KEE is universal; it occurs when various solids are bombarded by particles of very different properties, and becomes important whenever $V_i < \emptyset$. Contrary to the PEE, which has been successfully treated theoretically by Shekter and Hagstrum, the phenomenon of KEE is not well understood. In a quite recent review on the subject, K. H. Krebs [30] concluded that the state of theoretical descriptions of KEE at present is insufficient, and added that "the development of a comprehensive theory is far away and may be impossible".

The kinetically ejected electrons have several interesting properties:

(a) The yield coefficient (γ_{kin}) is greatly influenced by the state of the target cleanliness [21,22,29]: like in the PEE, clean surface will produce lower yield than from a contaminated one.

(b) γ_{kin} varies with ion velocity (and hence, ion energy) typically as shown in Fig. 2.6. The graph shows that

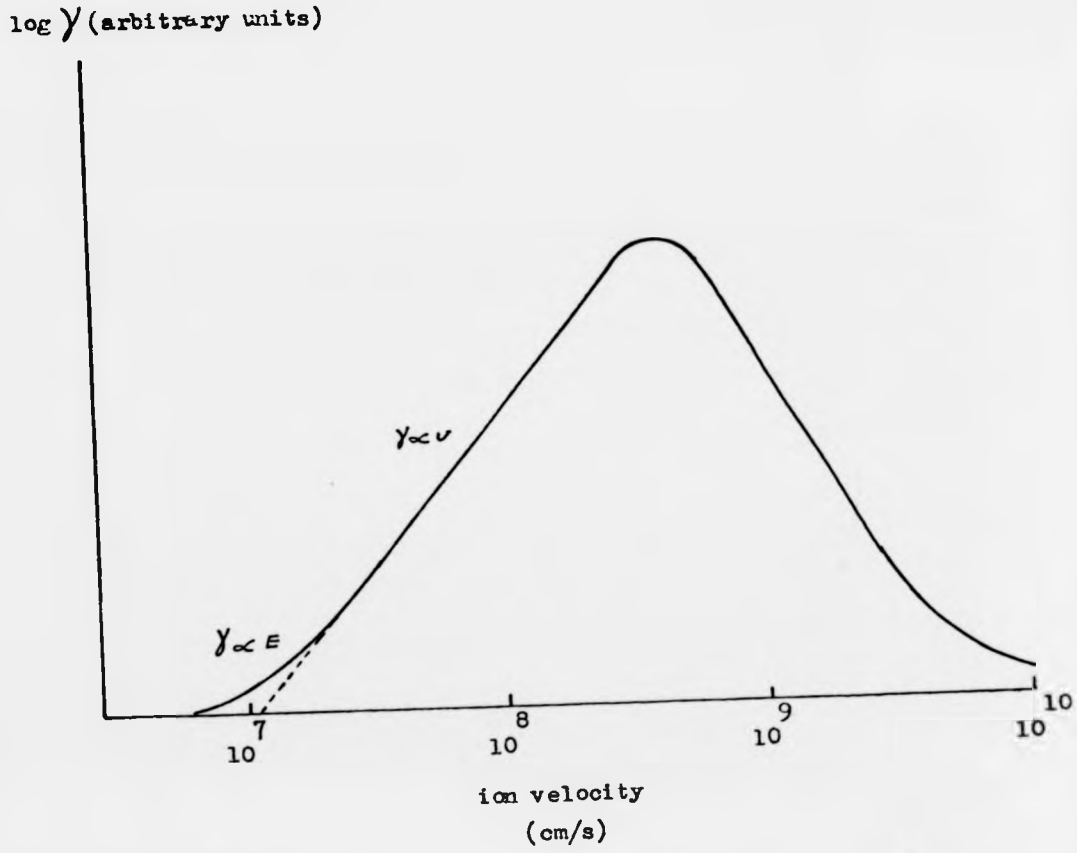

Fig. 2.6 : Schematic variation of KEE yield coefficient as a function of ion velocity.

for KEE to occur, the ion must possess velocity higher than a certain threshold of about 0.6×10^7 cm/s.

(c) For the same velocity of the ion, the yield coefficient has been found experimentally to be independent of the ion charge [21,22].

(d) The yield coefficient has an oscillating Z_i-dependence, where Z_i is the ion's atomic number [30], as shown in Fig. 2.7. This behaviour is related to the inelastic energy transfer, for which the electronic stopping power (S_e) is found to have oscillating Z_i-dependence as well [9].

(e) Given the same ion-target combination, surface orientation with greater transparency will produce lower yield coefficient [21,22].

(f) With a polycrystalline target, the yield coefficient (γ_{kin}) shows a sec θ_i- dependence on the angle of incidence (θ_i) measured with respect to the surface normal [21,33,34].

(g) The yield coefficient is found to be independent on the target temperature [21,35].

(h) The ejected electrons have energy distribution peaks at about 2 eV and a monotonically decreasing tail. The peak's FWHM is found to increase slowly with the ion's energy [22].

(i) The ejected electrons have spatial distribution which obeys the cosine law.

Several theories have been proposed for the mechanism of KEE. Among the old theories (presumably forgotten) are: the "thermal emission theory" of Kapitza (1923), the

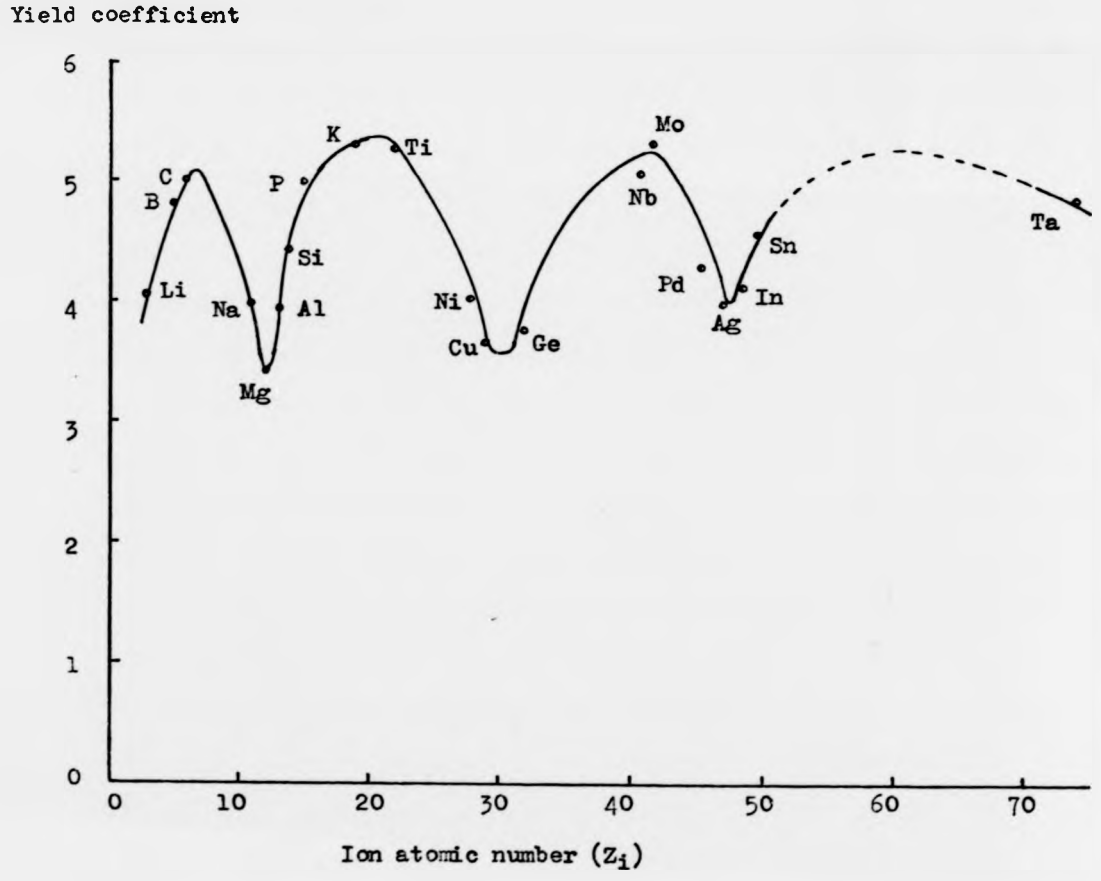

Fig. 2.7 : The variation of KEE yield coefficient from stainless steel with the ion atomic number at 26 keV . (After Krebs (Ref. 30))

"shaking theory" of Frenkel (1941) and the "radiation theory" of Izmailov (1955) [21,22].

Ploch laid the foundation of the so-called "standard" theories of KEE. Based on the close relationship between the energy dependence of the electron yield and the cross section for ionisation of an atom by ion impact (σ_i); he suggested that the electrons were formed by a process of ionisation of the lattice atom by the incident ion [21]. Three KEE theories which have been principally based on this assumption are those of von Roos and Parillis-Kishinevskii [36] for low velocity ions, and of Sternglass [37] for high velocity ions. In a recent review on this subject, N. Benazeth [38] pointed out three areas in which these theories may differ: (i) mechanism of calculating the energy transfer, which can be either through inelastic collision cross-section, or electronic stopping power, (ii) liberated electron slowing-down in the solid, which may be approached either by mean free path or by electronic stopping power, and (iii) inclusion or exclusion of electronic emission due to energetic recoil target atoms.

In von Roos's theory, the solid is treated as a free "gas of lattice atoms" which obeys the Boltzmann distribution function. Electrons are liberated by these "free" atoms during ionising collision with the incident ions; no contribution from the atoms recoil energies is taken into account. The number of electrons liberated in the collision is calculated using ionisation cross-section, σ_i; and the number of electrons finally escape from the solid is calculated using a simple velocity dependent escape

probability, ignoring the possibility that some of the electrons being absorbed by the lattice.

To calculate the number of electrons liberated in the collision, Sternglass used the concept of mean energy loss per secondary formed ($\underline{E}$) and total stopping power (dE/dx). Since dE/dx is a function of ion energy (E), and hence its distance from the surface (x), the number of electrons formed in the collision is also a function of E and x, i.e., $n(E,x)$. He rightly ignored the contribution from the recoil energies because at high velocities nuclear stopping power is negligible. The number of electrons eventually leave the surface is calculated by using an exponential escape probability

$$P(x) = P_1 A \exp(-x/L_s)$$

where L_s is the characteristic length of the attenuation process, x is the perpendicular distance of the electron from the surface, P_1 and A are constants. This means that the yield from a thin layer of thickness dx located at a depth x is given by

$$d\gamma = n(E,x)P(x)dx.$$

Parilis and Kishinevskii assumed that the collision between the incident ion and a lattice atom results in the ionisation of the latter with a hole in its filled band, and considered that the process has the same cross-section as for the formation of an electron-hole pair. As for the process of energy transfer, Parilis and Kishinevskii apply the Firsov's calculation of energy loss, which is based on a friction model. They then treated the ejection of electron from the surface as a result of an Auger recombination of a

conduction electron with the hole. To calculate the electron yield coefficient they used exponential escape probability, as follows:

$$\gamma = \sigma(u)\, w(\delta)\, N \exp(-x/\lambda)\, dx$$

where N is target atomic density, x_n the depth at which the ion still retain the ability to ionise, $\sigma(u)$ is the cross-section for the formation of an electron-hole pair, u the ion velocity, and $w(\delta)$ the probability of the Auger process for a hole and δ is its depth.

2.8 Neutral atom induced secondary electron emission

Strictly speaking, a neutral atom in its ground state can induce electron emission from a solid surface through kinetic process only. In the early experiments on interactions of neutral atoms with metal surfaces, the fact was obscured by the presence of metastable component of the atoms [39]. Metastable atoms can induce electron emission from metal surfaces through resonance ionisation or Auger de-excitation transitions [27].

As have been pointed out in Chapter One, experimental data on interactions of neutral atoms with solid is indeed very scarce. With very few exceptions, most of the reported experiments on interaction of fast neutral atom with solids (mostly, metals) were performed on atomically dirty surfaces, due to the absence of UHV facilities. However, from that limited pool of data, it have been observed that the ejected electrons from fast atom/metal surface interactions show striking similarities, both quantitatively

and qualitatively, with the ion-induced kinetic electrons emitted from solids. Nevertheless, this is not surprising if one thinks in the line that ions undergo efficient neutralisation at metal surfaces, and hence penetrate the metals as neutral atoms. A pair review of this aspect is given by Arifov [21], who also performed the experiments with clean metal surfaces. With the exception of the pioneering work of Kirson et. al [40], theory on fast atom/metal interaction is almost a non-existence. In the context of kinetic electron emission, bearing in mind the efficient ion neutralisation mentioned earlier, perhaps it is not far too wrong to assume that any theory on ion-induced KEE is also applicable to fast neutrals.

2.9 The similarities and differences between ion and neutral induced secondary emission

Discussions on this topic can be very long, but in the author's opinion, it is adequate if it be confined only to the central aspects. To do this, it is customary to represent the work of Arifov et. al. [21,41] and Medved et. al. [31] on the subject.

In the early 1960s, both Arifov et. al. and Medved et. al., in different laboratories, measured the yield coefficients of secondary electrons emitted from cleaned polyscrystalline molybdenum surface, which they bombarded with atoms and ions of argon in the energy range up to 5 keV. The results of their experiment are depicted in

Fig. 2.8. Their results show a very good qualitative agreement over several aspects:

(1) In the case of bombardment with neutral Ar, ejection of electrons occurs only above an energy threshold ≈ 600 eV. This necessarily confirms the absence of metastable components in their neutral beam.

(2) Above the threshold energy, the yield versus energy curve of ion-induced emission is identical to the curve of neutral-induced emission, except for a constant vertical displacement. It must be noted here that results obtained by Medved et. al. show a slightly higher gradient for the ion-induced than for the neutral-induced, while Arifov et. al. consistently show that the two curves have the same slope. In another experiment using ions and atoms of Na on clean Mo, Arifov observed the same behaviour (Fig. 2.9). He also confirmed the addivity of the KEE and PEE processes. From theoretical and experimental view alike, the vertical displacement between the two yield curves is none other than the yield coefficient of potentially ejected electrons. Theoretically, within the range of energy concerned the PEE yield coefficient is independent of the ion energy, a behaviour which has been repeatedly observed in several other experiments [21].

It is rather unnecessary to discuss the reasons to which the observed discrepancy between the two results should be attributed to. What is important is that both results demonstrate distinct features of ion and neutral induced electron emission, which can be summarised as follows:

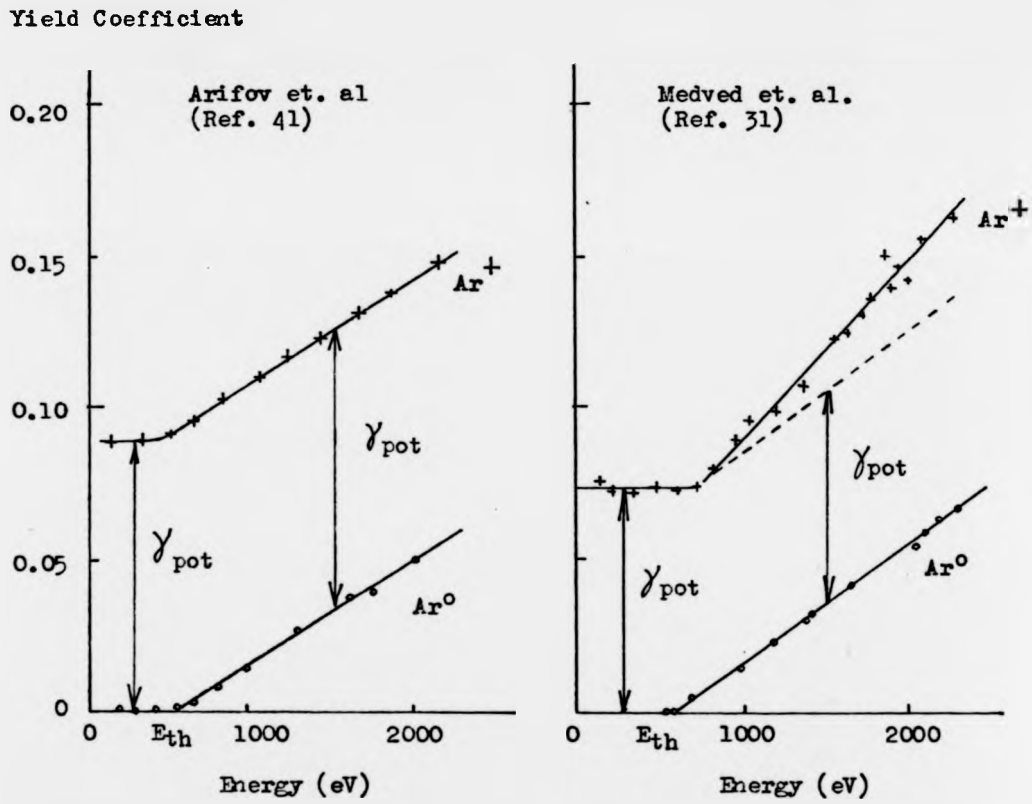

Fig. 2.8 : Graphs show variation of yield coefficient from cleaned Mo surfaces with the projectile energy; crosses are points obtained with Ar ions, circles are points obtained with neutral Ar atoms. (After Arifov et. al. (41) and Medved et. al. (31))

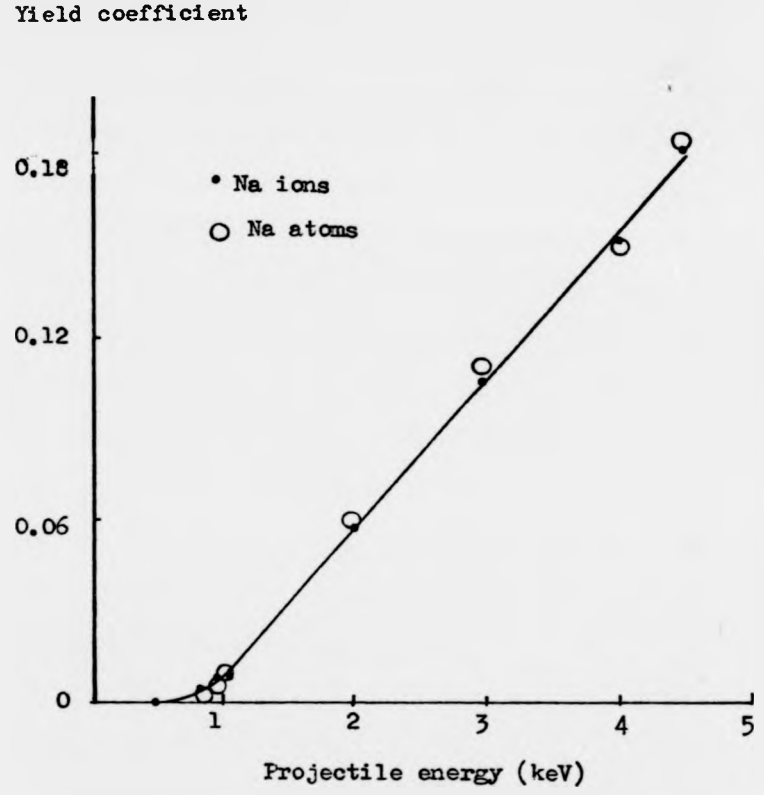

Fig. 2.9 : Coefficients of KEE as functions of the energy of the Na atoms and ions. (After Arifov (22))

(a) ion induced electron emission consists of two components, namely, PEE and KEE. PEE shows no energy dependent whilst is clearly that KEE is energy dependent.

(b) neutral induced electron emission has only one mechanism, namely, KEE, which is identical in nature with the ion induced KEE.

The kinetically ejected electrons, from both ion and neutral induced processes, have been observed to possess similar energy distribution curves, and similar yield dependence on projectile energy, angle of incidence and atom-target combination. It is the objective of this work, among others, to provide new data on fast neutral atom induced secondary electrons from clean metal surfaces.

2.10 References

[1] J. F. Zeigler, J. P. Biersack and U. Littmark, The Stopping and Range of Ions in Solids Vol. 1, (Pergamon Press, 1985).

[2] S. M. Sze (ed.), VLSI Technology, (McGraw Hill Int. edn., 1983).

[3] F. W. Sears, M. W. Zemansky and H. D. Young, University Physics , (Addison Wesley, 1987).

[4] P. D. Townsend, J. C. Kelly and N. E. W. Hartley, Ion Implantation, Sputtering and their Applications, (Academic Press, 1976).

[5] J. F. Zeigler, Helium Stopping Powers and Ranges in All Elements, (Pergamon, 1977).

[6] L. A. Turner, Rev. Mod. Phys. **12** (1940) 1.
N. Bohr, Phys. Rev. **59** (1941) 270.

[7] H. D. Betz, Rev. Mod. Phys. **44** (1972) 465.

[8] N. Bohr, Phys. Rev. **58** (1940) 654.

[9] W. K. Chu, in **Materials Characterisation using Ion Beams** (J. P. Thomas and A. Cachard. eds.) (Plenum, 1978) Ch. 1.

[10] O. B. Firsov, Sov. Phys. JETP **5** (1957) 1192.

[11] J. Lindhard and M. Scharff, Phys. Rev.**124** (1961) 128.

[12] I. M. Torrens, **Interatomic Potentials** (Academic Press, 1972).

[13] K. B. Winterbon, Rad. Eff. **13** (1972) 215.

[14] U. Littmark and J. F. Ziegler, Phys. Rev. **23A** (1981) 64.

[15] H. E. Schiøtt, Rad. Eff. **6** (1970) 107.

[16] M. T. Robinson and I. M. Torrens, Phys. Rev. B9 (1974) 5008.

[17] H. H. Andersen and J. F. Ziegler, **Hydrogen Stopping Powers and Ranges in All Elements** (Pergamon, 1977).

[18] H. Wagiran, Ph. D. Thesis, Aston University in Birmingham, U.K. (1987).

[19] R. Blume, W. Eckstein and H. Verbeek, Nucl. Instr. and Meth. **168** (1980) 57.

[20] R. Blume, W. Eckstein, H. Verbeek and K. Reichelt, Nucl. Instr. and Meth. **184** (1982) 67.

[21] M. Kaminsky, **Atomic and Ionic Impact Phenomena on Metal Surfaces** (Springer-Verlag, 1965).

[22] U. A. Arifov, **Interaction of Atomic Particles with a Solid Surface** (Consultants Bureau, 1969).

[23] G. Carter and J. S. Colligon, **Ion Bombardment of Solids** (Heinemann, 1968).

[24] M. Pedrix, S. Paletto, R. Goutte and C. Guilland, Phys. Lett **A28** (1969) 534.

[25] H. D. Hagstrum, Phys. Rev. **96** (1954) 325, 336.

[26] H. D. Hagstrum, Phys. Rev. **89** (1953) 244; **91** (1953) 543; **104** (1956) 317, 516, 672.

[27] D. P. Woodruff and T. A. Delchar, **Modern Techniques of Surface Science** (Cambridge Univ. Press, 1986).

[28] L. M. Kishinevskii, Rad. Eff. **19** (1973) 23.

[29] R. A. Baragiola, E. V. Alonso, J. Ferron and A. Oliva-Florio, Surf. Sci. **90** (1979) 240.

[30] K. H. Krebs, Vacuum **33** (1983) 555.

[31] D. B. Medved, P. Mahadevan and J. K. Layton, Phys. Rev. **129** (1963) 2086.

[32] G. D. Magnuson and C. E. Carlston, Phys. Rev. **129** (1963) 2409.

[33] R. A. Baragiola, E. V. Alonso and A. Oliva-Florio, Phys. Rev. **B19** (1979) 121.

[34] E. V. Alonso, R. A. Baragiola, J. Ferron, M. M. Jakas and A. Oliva-Florio, Phys. Rev. **B22** (1980) 80.

[35] P. Mahadevan, J. K. Layton and D. B. Medved, Phys. Rev. **129** (1963) 79.

[36] E. S. Parilis and L. M. Kishinevskii, Sov. Phys. Solid State **3** (1960) 885.

[37] E. J. Sternglass, Phys. Rev. **108** (1957) 1.

[38] N. Benazeth, Nucl. Instr. Meth. **194** (1982) 405.

[39] R. N. Vaney, Phys. Rev. **157** (1967) 113.

[40] Z. Kirson, R. B. Gerber and A. Nitzan, Surf. Sci. 124 (1983) 279.

[41] U. A. Arifov, R. R. Rakhimov and Kh. Dzhurakulov, Sov. Phys. Doklady 7 (1962) 716.

CHAPTER THREE

THE PRODUCTION AND DETECTION OF FAST NEUTRAL ATOM BEAMS

3.1 Mechanisms of beam production

In practical terms, a neutral atom beam is a well collimated stream of ground state atoms traversing a vacuum. Its production requires two levels of specifications; firstly on a macro level, one needs to have control of its intensity, energy profile and directionality and secondly, on a micro level, the beam's contents and their quantum states.

Beams of thermal energy neutral atoms have been produced chiefly by means of gas or vapour effusion. Effusive sources come in many designs, which range from the simple and inefficient thin-walled orifice oven sources to the more effective and sophisticated hydrodynamic, supersonic sources employing cascaded nozzles and skimmers [1,4]. Fast neutral atom beams are produced, as a rule, through the use of ion beams as intermediates. In most of the designs the ions are of the same species as the intended fast neutrals. The usual route for fast neutral atom production involves the utilisation of various ion neutralisation processes, although in the energy region of 1 to 50 eV there are some other possibilities, namely, gas dynamics, shock waves, laser radiation [1] and sputtering [2]. There are four main mechanisms in which ion neutralisation may take place, namely, charge exchange

process, recombination process, neutralisation at metal surfaces and photodetachment process [1].

(a) Charge exchange process

Phenomena of resonance charge exchange were first reported by Kallmann and Rosen in around 1930 [3]. In a symmetrical charge exchange, a positive ion travelling near to its neutral parent species can capture an electron from it and become neutralised without having a scattering collision at all. After neutralisation the original ion proceeds unaltered in speed and direction as a neutral particle while the product ion is scattered nearly perpendicular to its original path. The cross-section of this process, σ, will fall with increasing impact velocity, v_p, according to equation

$$\sigma^{\frac{1}{2}} = a - b \ln (v_p)$$

where a and b are constants [1]. At all times the cross-section for resonance charge transfer is much higher than that of momentum transfer. A typical example of the former process is as follows:

$$Ar^+(\text{fast}) + Ar^\bullet(\text{thermal}) \longrightarrow Ar^+(\text{thermal}) + Ar^\bullet(\text{fast})$$

$$\sigma = 2 \times 10^{-19}\ m^2$$

The repulsion due to their own space charge effect limits the ion beam intensity and hence the fast neutral atom beam intensity. Only relatively low intensities can be obtained particularly at the lower beam energies, i.e. $\leq$20 eV [4]. Nevertheless, it is worth noting here that since the early days of fast atom source designs, that is around 1930s, due to its simplicity, the charge transfer process has been the most widely employed method. The newly constructed neutral

gun of Eccles et. al. which was mentioned in Chapter One, works on the basis of neutralising through charge transfer a raster-scanned microfocused ion beam.

(b) Recombination process

This is a rather direct neutralisation process in which a low energy electron beam is introduced into the path of a well focused and accelerated positive ion beam. The fast neutral atom beam so produced retains the energy of the ion beam. The recombination process may occur in three different ways:

(i) radiative recombination

Typical example : $Ar^{+}(fast) + e^{-} \longrightarrow Ar^{\bullet}(fast) + h\nu$

$$\sigma \approx 10^{-24}\ m^{2}$$

(ii) dissociative recombination

Typical example : $Ar_{2}^{+}(fast) + e^{-} \longrightarrow 2Ar^{\bullet}(fast)$

$$\sigma \approx 10^{-18}\ m^{2}$$

Note that, although this process has a very high cross-section it needs a high pressure plasma (i.e., $\geq$0.1 torr) for it to occur.

(iii) three-body recombination

Typical example with argon:

$Ar^{+}(fast) + e^{-} + Ar^{\bullet}(thermal) \longrightarrow Ar^{\bullet}(fast) + Ar^{\bullet} + K.E.$

$$\sigma \approx 10^{-23}\ m^{2}$$

and $e^{-} + Ar^{+}(fast) + e^{-} \longrightarrow Ar^{\bullet}(fast) + e^{-} + K.E.$

$$\sigma \approx 10^{-19}\ m^{2}$$

In this process, the excess energy is taken up by a third particle, i.e., atom or electron.

(c) Neutralisation of an ion at a metal surface

In 1929, Oliphant suggested that fast neutral atoms may be produced by having a beam of fast ions collide with a metal surface at glancing incidence. The neutralisation of the ions was characterised by ejection of electrons from the surface, and was postulated by Hagstrum to occur by two different mechanisms [5]:

(i) resonance neutralisation of the ion

$$X^+ + ne^- \longrightarrow X^* \text{ (metastable)} + (n-1)e^-$$

followed by Auger deexcitation of the metastable X^*

$$X^* + (n-1)e^- \longrightarrow X^\circ + (n-2)e^- + e^-$$

(ii) Auger neutralisation

$$X^+ + ne^- \longrightarrow X^\circ + (n-2)e^- + e$$

where X^+ is the ion to be neutralised and ne^- are the total number of electron in the metal. Ross et. al. [6] generated a diffuse beam of 5 keV neutral Ar atoms by passing a beam of 5 keV Ar^+, initially produced by a commercial ion gun, through a grounded multi-holed metal neutraliser. An ion deflection grid was used to remove ions which escaped the neutralisation from the final central beam. Recently, Ohya et. al. [7] reported about production of fast atomic nitrogen beam by projecting a beam of nitrogen ions (92.5% N_2^+, 7.5% N^+) onto a Cu surface at 60° from the surface normal.

(d) Photodetachment process

Based on the idea of Branscomb (1963), van Zyl et. al. [8] succeeded in producing a fast hydrogen atom beam of energy between 100 eV and 30 keV and flux in the order of 10^{11} atoms sr^{-1} s^{-1} through a process known as photo-

detachment. In their work, an intense and well collimated beam of negatively charged H^- ions was made to intersect with a 30 W, yttrium aluminium garnet laser beam of wavelength 1060 nm, to produce fast neutral H atoms and electrons:

$$H^- + h\nu \longrightarrow H^\bullet + e^-$$

3.2 The designs of fast neutral atom guns

The designers of fast neutral atom gun have benefited from many advances already made in the field of fast ion beam production. This is necessarily true because any design for a fast neutral atom gun, must as a rule, include an ion source. The ions are then neutralised by any of the neutralisation processes discussed earlier, or a combination of them, to produce the fast neutral atoms. The success of the designs rely on one important property of the neutralisation process, that is, that the fast neutral atom beam so produced retains much of the directionality and energy profile of the ion beam.

Neutral gun designs can be divided into two categories according to where their neutralisation process takes place [9], that is :

(a) Guns which have a separate chamber for the neutralisation process, and

(b) Guns in which ions are formed and subsequently neutralised in the same chamber.

Historically, guns belonging to the first category were among the first to be developed. The extra chamber they

have, quite often necessitates an extra differential pumping stage in the vacuum system. However, they have the advantage of independent control over the beam intensity and energy. In contrast, guns in the second category generally are of compact construction because they use fewer stages of differential pumping. They have some drawbacks, namely, high gas load and strong dependence of beam intensity on energy. Most of the early fast neutral atom gun designs represented the first category very well. Designs of Ross et. al and of van Zyl et. al. which were discussed earlier belong to this category. In general, the guns were operated by first selecting the energy and the current of the ion beam. For guns which employ the charge transfer process, the intensity of the final neutral atom beam could be varied by controlling the pressure inside the charge transfer chamber since the probability P of a positive ion becoming neutralised by passing through a length L of its parent gas, at pressure p, is $P = \sigma_{ce} nLp$, where σ_{ce} is the cross-section for charge exchange and n is the atom density per unit volume per unit pressure. In the case of Ross's design, the choice of the type of the metal neutraliser and its transparency alters the cross-section of the neutralisation process, and hence the final neutral atom beam intensity.

Capillaritrons [10] and saddle field ion guns [11] are examples of guns which belong to the second category. Both are cold cathode devices and originally meant for the production of intense and energetic positive ion beams to be used for ion implantation, surface etching, mass analysis,

etc.. Ingenious modifications to the guns' geometry enable them to produce mainly fast neutral atom beams.

The capillaritron owns its name from its anode structure, which is a gas feeding tube ended by a fine bore capillary [Fig. 3.1]. When a positive high voltage is applied to the anode, an intense and symmetrical electric field appears between the capillary and the grounded cathode. This very intense field causes a micro discharge at the nozzle tip and positive gas ions are formed and accelerated into a relatively high pressure region at the vicinity of the tip where up to 50% of the ions are converted into fast neutrals. The remaining ions are removed from the final central beam by a pair of deflection plates.

The saddle field atom gun is one of two fast atom sources actually used by the author in this work. A more detail discussion on its design and working principle will be given in Chapter Four.

3.3 Detection and measurement of fast neutral atom beams

Due to the charges they carry, ion beams are easy to detect and their fluxes are relatively straightforward to measure. On the other hand, detection and measurement of non-charged atomic beams flux generally works on the basis of an indirect measurement.

For neutral atom beam of energy below 1 keV several methods of detection and measurement are available, such as, Pirani manometer, surface ionisation technique, condensation target method, chemical target method, and field ionisation

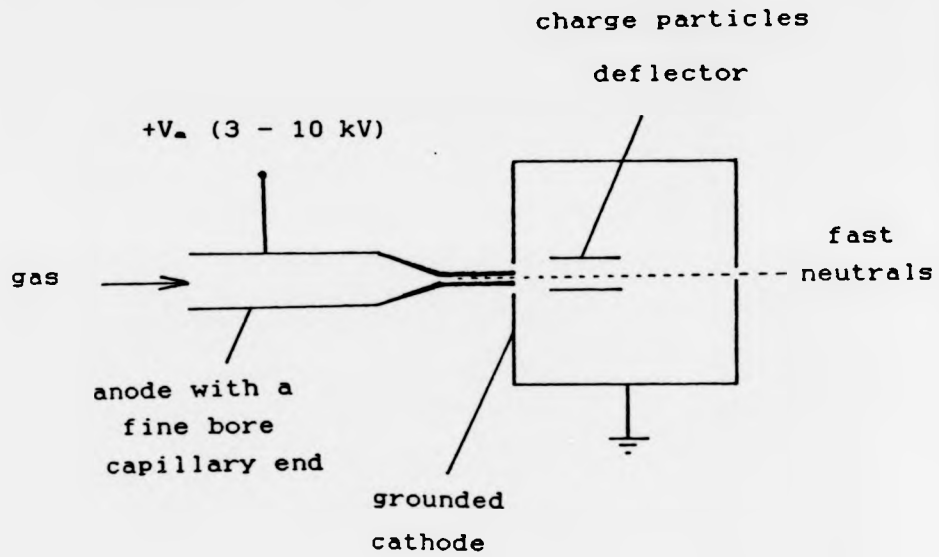

Fig. 3.1 : A schematic diagram showing the important components of a capillaritron.

detector [1,4]. The phenomenon of ejection of secondary electrons from a metal surface under the bombardment of fast neutral atom beam of energy 200 eV or higher, is widely used as mean of detection and flux measurement. For a neutral atom beam produced from a charge transfer chamber its intensity can be determined by measuring the slow ions produced in the charge exchange process. This technique needs correction for the scattered particles. Alternatively, if the differential charge exchange cross-section is known, the neutral beam's intensity can be calculated from the yield.

The commercially available detectors which work on the basis of electron ejection are channeltrons. They are curved or spiral small glass tubes with a semi insulating inner layer and behave like distributed dynode multipliers [12]. They may be used as neutral atom beam detectors. Generally, channeltrons are not used for absolute flux measurement and to do so one needs accurate information regarding the secondary electron ejection process.

For fast neutral atom beams of several keV, their detection and flux measurement are usually done by measuring the secondary electron emission on the one hand or by using bolometers on the other. As an example, Morita et. al. [13] described the principle of a "secondary emission detector (SED)" which works on the basis of angular dependence of secondary electron yield of fast neutral atoms on metal surface. Atomic beam bolometers are essentially the adaptations of those used for infrared detection, and have been used for relative [1,4,14] and absolute [13,15]

measurements. In Chapter Four, the working principle and performance of a newly designed thermistor-based absolute bolometer, which was actually used for measurements of yield coefficients, will be described.

3.4 References

[1] J. B. Hasted, Physics of Atomic Collisions (Butterworth, London, 1956).
H. Lew, in Methods of Experimental Physics Vol. 4A (eds. V. W. Hughes and H. L. Schultz) (Academic Press, New York, 1967) Ch. 1 and 2.
L. Vályi, Atom and Ion Sources (Wiley, London, 1977).

[2] J. Politiek, P. K. Kol, J. Los and P. G. Ikelaar, Rev. Sci. Instrum. 39 (1968) 1147.

[3] H. Kallmann and B. Rosen, Z. Physik 61 (1930) 61, 64 (1930) 806 as cited in R. N. Vaney, Phys. Rev. 157 (1967) 113.

[4] M. A. D. Fluendy and K. P. Lawley, Chemical Applications of Molecular Beam Scattering (Chapman and Hall, London, 1973).

[5] H. D. Hagstrum, Phys. Rev. 96 (1954) 336.

[6] M. M. Ross, R. J. Colton, S. L. Rose, J. R. Wyatt, J. J. DeCorpo and J. E. Campana, J. Vac. Sci. Technol. A2 (1984) 748.

[7] K. Ohya, K. Ishida and I. Mori, J. Phys. D: Appl. Phys. 19 (1986) 157.

[8] B. Van Zyl, N. G. Utterback and R. C. Amme, Rev. Sci. Instrum. 47 (1976) 814.

[9] J. A. Van den Berg, Vacuum 36 (1986) 981.

[10] J. F. Mahoney, Int. J. Mass Spectrom. Ion Phys. 48 (1985) 419.

[11] J. Franks, Vacuum 34 (1984) 259.

[12] J. Adams and B. W. Manley, Philips Tech. Rev. 28 (1967) 156.

[13] K. Morita, H. Akimune and T. Suita, Jpn. J. Appl. Phys. 5 (1966) 511.

[14] I. Amdur, in Methods of Experimental Physics Vol. 7A (eds, B. Bederson and W. L. Fite) (Academic Press, New York, 1968) Ch. 3.

[15] C. A. van de Runstraat, R. Wijnaendts van Resandt and J. Los, J. Phys. E: Sci. Instrum. 3 (1970) 575.

CHAPTER FOUR

THE EXPERIMENTAL HARDWARE

4.1 Introduction

The experiments were performed in a UHV chamber (or target chamber) which was equipped with a Bayard Alpert ionisation gauge, a Micromass Q7 quadrupole mass spectrometer, a retarding field analyser, a newly built atomic beam bolometer and a simple rotary sample manipulator. The UHV chamber was permanently joined to a beam formation chamber (or source chamber) which was equipped with a Bayard Alpert ionisation gauge and an eight inch Conflat flange which could be fitted with interchangeable fast atom guns. Connection between the two chambers was via a low conductance bevelled metal orifice of diameter 0.4 mm, which served both as a passage and a collimator for the fast atom beam [Fig. 4.1].

The mass spectrometer was added to the UHV chamber for two purposes:

(i) To monitor the UHV condition. Apart from monitoring partial pressure due to the fast atom beam; a quadrupole mass spectrometer when used with helium gas is a useful instrument for locating a leak.

(ii) To detect any material which is being sputtered away from the surface during the fast atom bombardment.

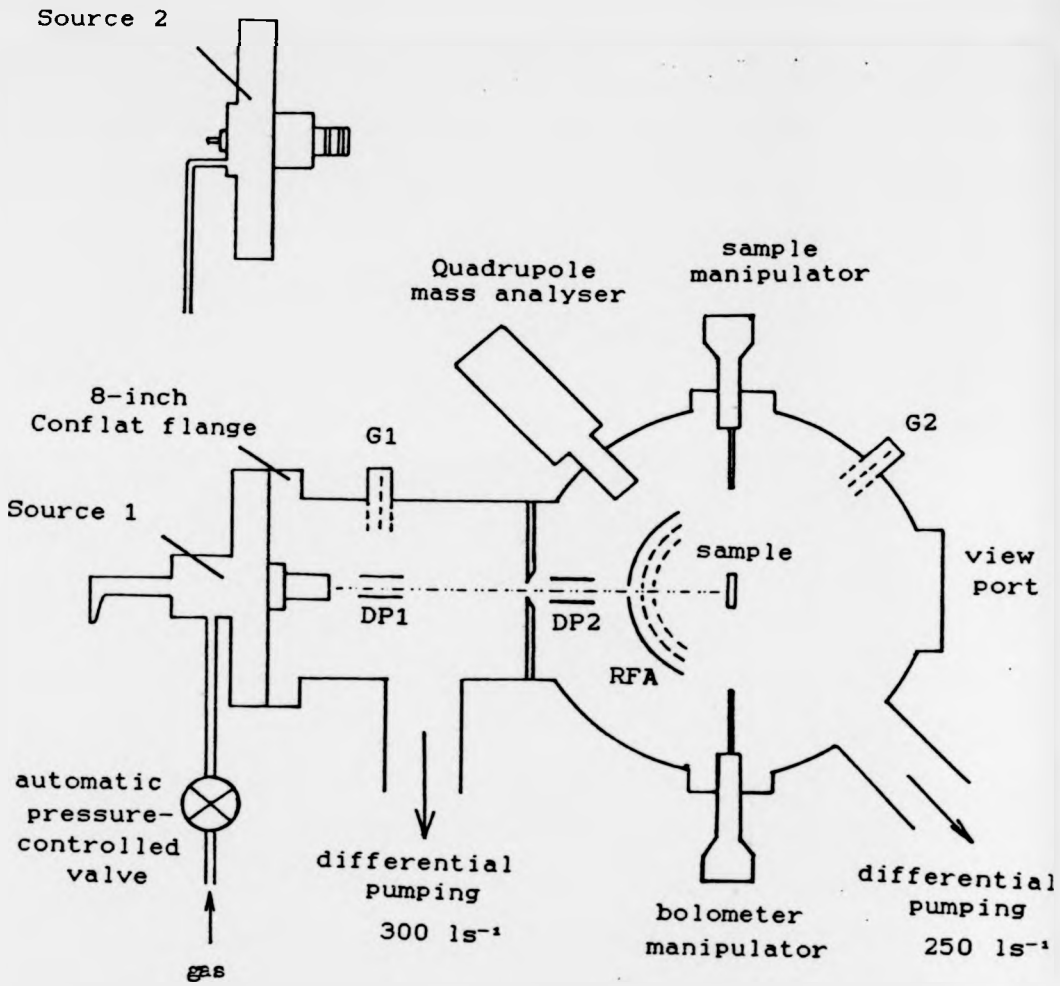

G1,G2	Bayard Alpert ionisation gauge
DP1,DP2	Deflecting plates
RFA	Retarding field analyser

Fig. 4.1 : Schematic diagram of the experimental apparatus

4.2 The UHV system

Both the UHV chamber and the beam formation chamber were fabricated from non-magnetic stainless steel type EN58B [1]. Each chamber was evacuated by an oil vapour diffusion pump backed by a rotary vacuum pump. The diffusion pumps used were the Edwards Model E04; which when used with oil (Santovac 5) have a pumping speed (for air) of 600 ls^{-1} and produce an ultimate vacuum of 10^{-10} torr. The backing pumps used were the Edwards single stage rotary pumps Model ES200 and ES330 for the beam formation chamber and the UHV chamber respectively. These two pumps combined gave effective pumping speeds of 300 ls^{-1} and 250 ls^{-1} for the source and target chambers respectively. Each pump combination had a molecular sieve sorb trap inserted between them, to prevent cracked oil products and water vapour from contaminating the vacuum system. The whole structure was mounted on an aluminium frame with the top of the chambers about 20 inches above a 5'x3'x1" hard asbestos table top [See Plate 1]. This strong table top was particularly useful for bakeout operation in which a simple but effective oven system was used. The oven was consisted of an asbestos padded aluminium walled enclosure of 2.5'x2.5'x2.75' and two 1 kW heaters. With both heaters switched on, the bakeout temperature would reach 210°C, but whenever the lithium sample was used, only one heater was switched on so that the bakeout temperature was reduced to 145°C, well below the lithium's melting point. All temperatures were read using a chromel-alumel thermocouple which was attached to the stainless steel wall

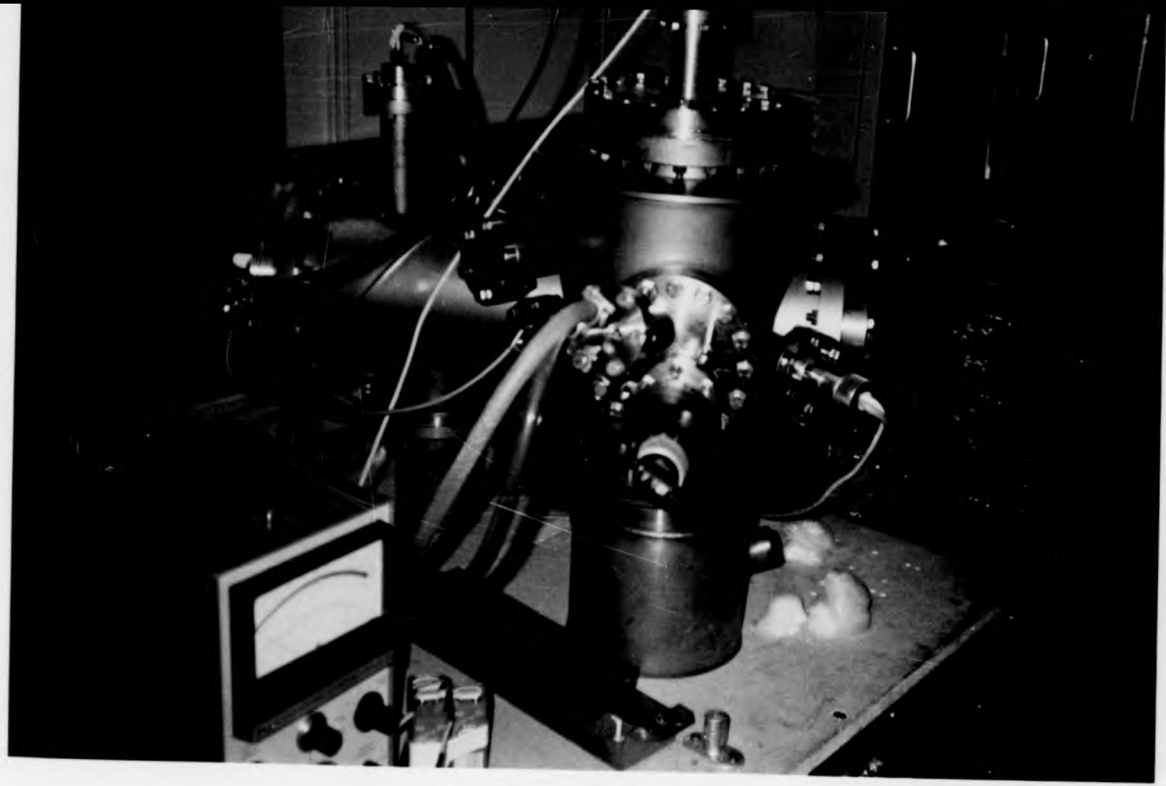

Plate 1

of the UHV chamber. Following the usual routine for obtaining UHV, ultimate vacua of 2×10^{-10} torr were obtained. A typical mass spectrum obtained from the UHV shows that the principal constituents in the system were water vapour, carbon dioxide and carbon monoxide [Fig. 4.2]

4.3 The measuring system

4.3.1 Computer-controlled ramp generator for the retarding field analyser

The measuring system used in the experiments made full use of the facilities provided by the "User Port" and the "ADVAL Port" of the BBC B microcomputer. An interface was specially designed to link the computer to the electrometer used in the experiments, a Keithley Model 602 (later called K602), to enable on-line data collection.

A conventional retarding field analyser, consisting of two hemispherical grids in front of a hemispherical collector, was used for the measurement of the secondary electron energy distributions [Fig. 4.3]. The specimen and the first grid were held at earth potential so that a field free region was created between them. The retarding grid was driven by a purpose built computer-controlled ramp generator [Fig. 4.4].

The BBC B User Port is part of the computer's Versatile Interface Adaptor (VIA), which is based on VIA chip 6522. A digital-to-analogue converter (DAC) was connected to the port to enable a dc voltage output to be programmed and

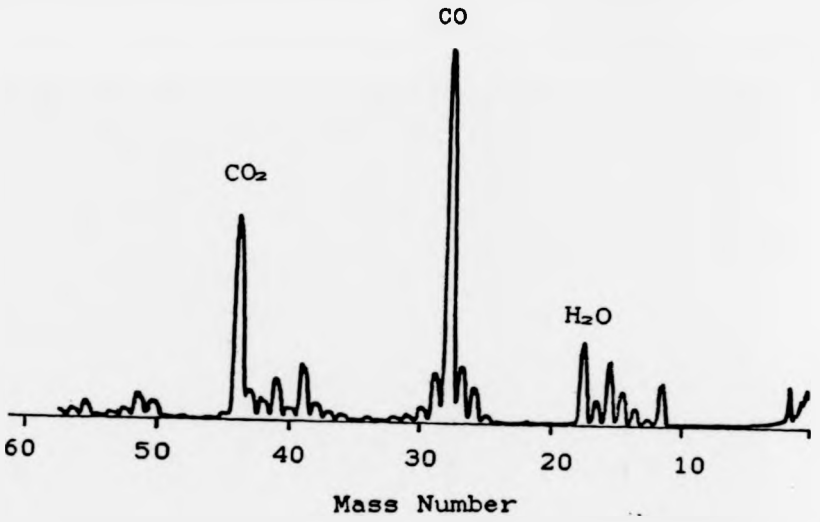

Fig. 4.2 : Mass spectrum of the UHV condition
(Background pressure: 3 x 10^{-9} torr)

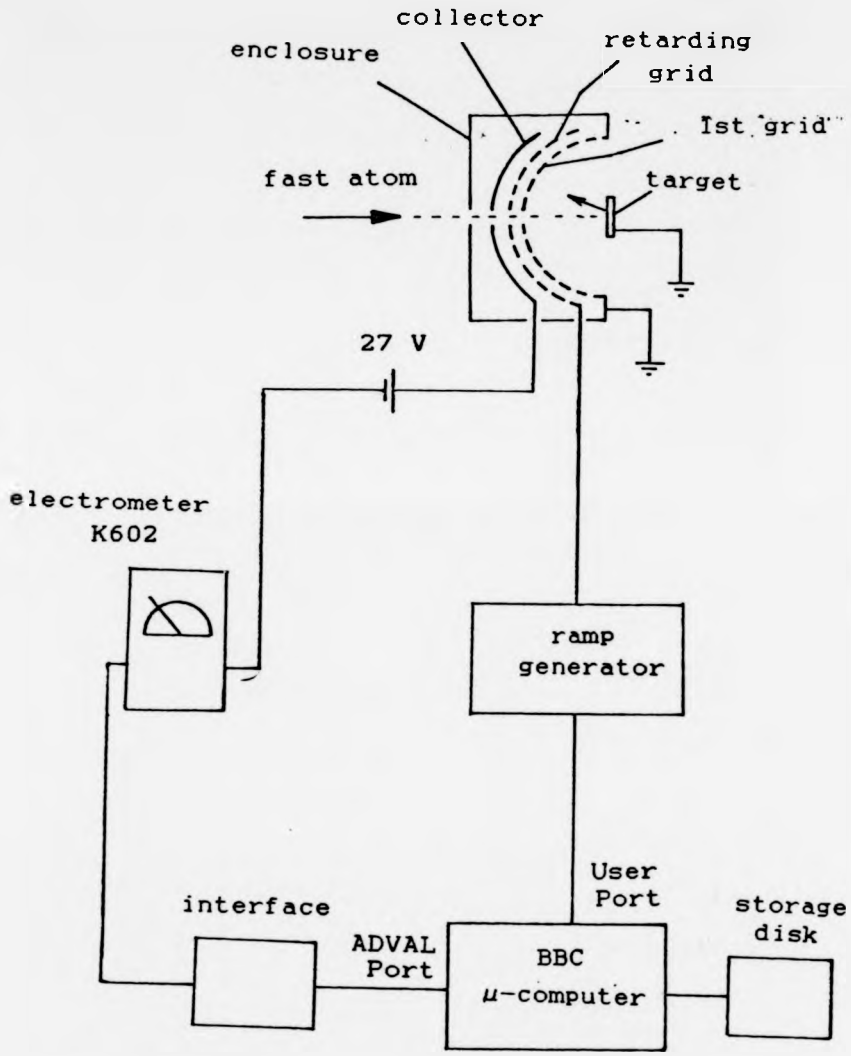

Fig. 4.3 : The retarding field analyser in an experimental set-up to determine the energy distribution of the ejected electrons.

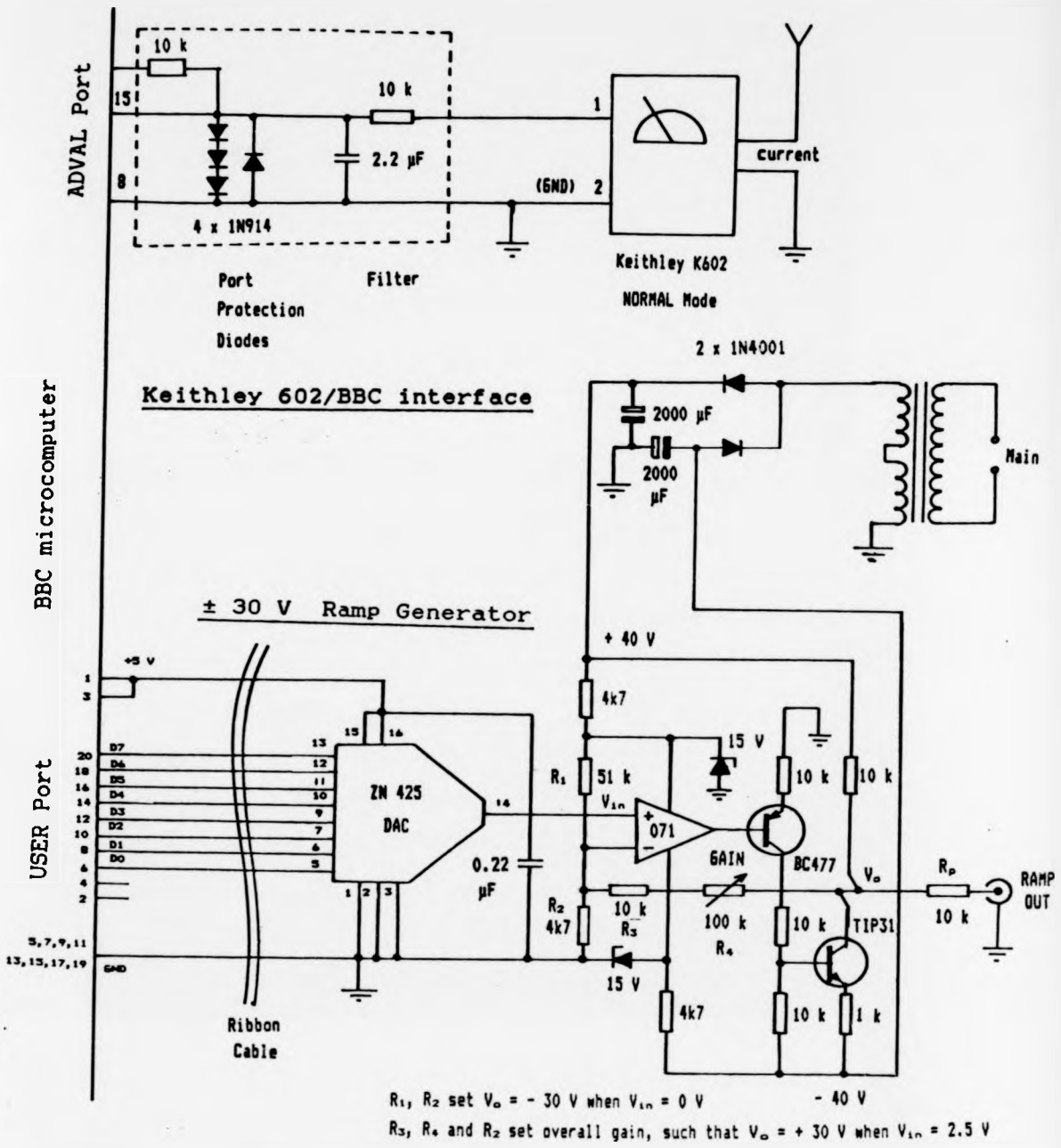

Fig. 4.4 : Circuit diagram for computer-controlled ramp generator and Keithley 602 interface

tapped. The routine used for controlling the output from DAC was written using assembly codes. [See Appendix 1(a)].

The high output impedance of the DAC necessitated that it be connected to the input of a FET operational amplifier which acted as a buffer. The final output stage was driven by an npn transistor amplifier which, for the chosen values of R_2, R_3 and R_4, was capable of generating a linear stepped-ramp from -30 V to +30 V.

One major advantage of the ramp generator was that it could easily be programmed to generate stepped-ramp voltages in either positive or negative going directions. Apart from that, the sweep time and the voltage range could also be programmed to suit the experimental requirements.

The K602 electrometer has an output jack which, when used in its voltage mode, will generate dc voltages from 0 to 1 V in inverse polarity to the input signal, but proportional to the current it is measuring in any single measurement range. The computer's ADVAL Port can accept only positive voltages from 0 to 1.8 V and will produce a corresponding number in the range 0 to 65520. An interface was designed such that K602's outputs of either polarity were converted into positive voltages before being fed into the ADVAL Port. With this feature, the retarding field analyser not only could be used to measure the energy distribution curve of secondary electrons up to 30 eV, but also of slow positive ions in the same energy range.

Like any other retarding field analyser this system also has the displacement current problem, resulting from the time varying field across the grid system (NB: the

capacitance between the retarding grid and the collector is about 35 pF). The contribution from the displacement current is indistinguishable from the current due to the secondary electrons; that is, as the ramp sweeps across its voltage range we can still get collector current even without the fast atom gun in operation. With this particular system, the problem worsens as the measurement range of the K602 is decreased; although the effect can be softened by making the duration of the step voltage longer. As a result, it is almost impossible to obtain a good retard potential data when the ejected electron current at the collector is smaller than 10^{-11} A. There are two ways in which the displacement current problem is eliminated:

(i) For ejected electron current in the order of 10^{-10} A or lower, the contribution from the displacement current accounts for as high as 35% of the total collector current recorded by K602. Nett retard potential data is obtained by subtracting the total collector current (i.e., secondary electron current + displacement current) with its corresponding background current (i.e., displacement current recorded without the fast atom gun in operation).

(ii) For ejected current in the order of 10^{-10} A or larger, the contribution from the displacement current is relatively negligible, and it can be cancelled by simply making the duration of each voltage step long enough for the displacement current to go to zero. It was found that a 3 second duration was adequate for this purpose, with the ADVAL number being recorded every 2.8 seconds. The computer routine used is set out in Appendix 1(b).

4.3.2 The thermistor-based absolute bolometer

The fast atom beam fluxes were measured using a thermistor-based absolute bolometer of a new design. The approach used by the author was based on that of Hemment [2] but modified to give an absolute bolometer of some simplicity, which needs no calibration. Its design is centred around a thermistor of negative temperature coefficient (n.t.c.) type, which is a semiconductor resistor whose resistance (R_{th}, in Ω) reduces with temperature (T, in K), as follows:

$$R_{th} = R_{20} \exp \left(\frac{B}{T} - \frac{B}{293} \right) \quad \Omega$$

where R_{20} is the thermistor's resistance at 20°C and B is the thermistor's characteristic temperature constant (in K).

The idea of the design is to elevate the thermistor's temperature well above that of the ambient by mean of Joule heating and maintain the isothermal (constant resistance) steady state by shielding and control of the ambient temperature. When a beam of fast neutrals strikes the thermistor such that all its kinetic energy is transformed into heating the latter, the Joule heating level must be reduced until the thermistor returns to the initial temperature and settles in a new steady state. In any isothermal steady state, the total power dissipated in the thermistor is the sum of the beam power and that of the Joule heating, that is:

$$P_{total} = P_{beam} + P_{Joule}$$

Provided that the ambient temperature is kept constant throughout the operation, a strictly crucial condition which can be realised practically, the fast atom beam's power is therefore essentially equal to the difference between the two Joule heating levels. In other words, this is a constant resistance mode of operation which enables one to obtain absolute flux measurement for fast atom beams by measuring the change in power supplied to the bridge.

The bolometer consists of two parts; the thermistor assembly and the Wheatstone bridge-FET Op Amp circuitry [Fig. 4.5]. The thermistor is the evacuated type RA53; it has a bead resistance of 5 KΩ at 20°C and B constant of 3250 K ± 5% (25 to 100°C). The thermistor's resistance-temperature curve is depicted in Fig. 3.6. The thermistor's dissipation constant, defined as the amount of power needed to elevate its temperature by one degree K above the ambient, is 12.5 μWK^{-1}. The thermistor glass envelope was carefully cut to expose the thermistor bead, on which a tiny speck of Araldite epoxy adhesive was used to attach a small square gold foil of 2.5x2.5x0.025 (mm) which served as the beam collector. Great care was taken not to short out the Pt alloy leads which supported the bead. The thermistor-collector assembly was mounted in a small aluminium enclosure with one lead kept very short and fastened to the mounting enclosure. To further minimise the effects of ambient fluctuations and surrounding heat sources, a single loop of water cooling coil was attached to the wall of the the aluminium enclosure [Fig. 4.7]. The water-cooled aluminium enclosure was mounted on a simple manipulator

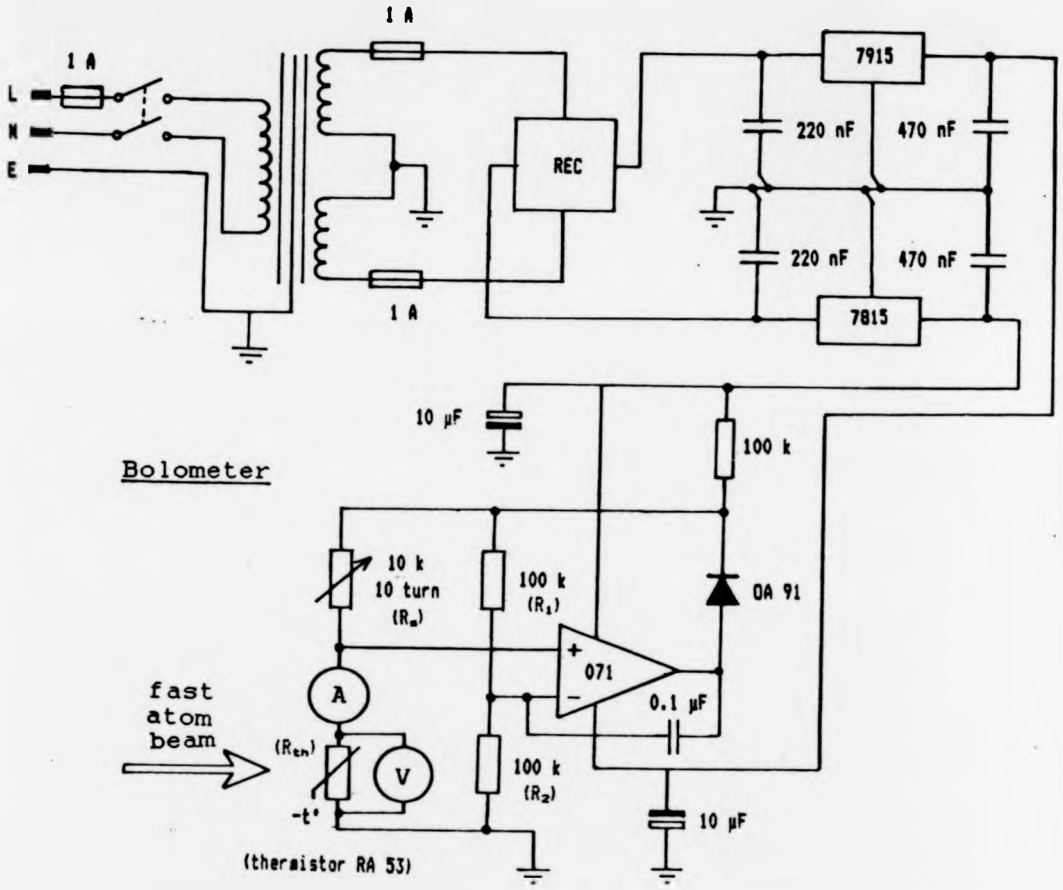

Fig. 4.5 : Circuit diagram for a thermistor-based absolute bolometer and its power supply.

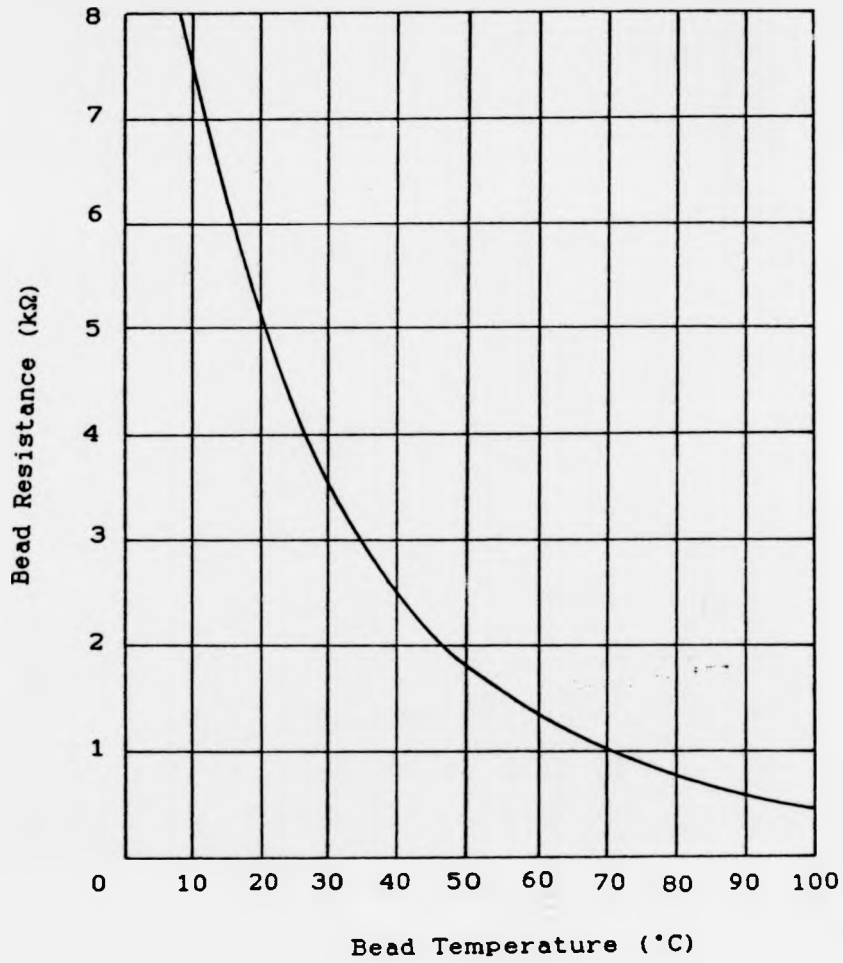

Fig. 4.6 : Graph of resistance versus temperature of thermistor RA53 at zero power.

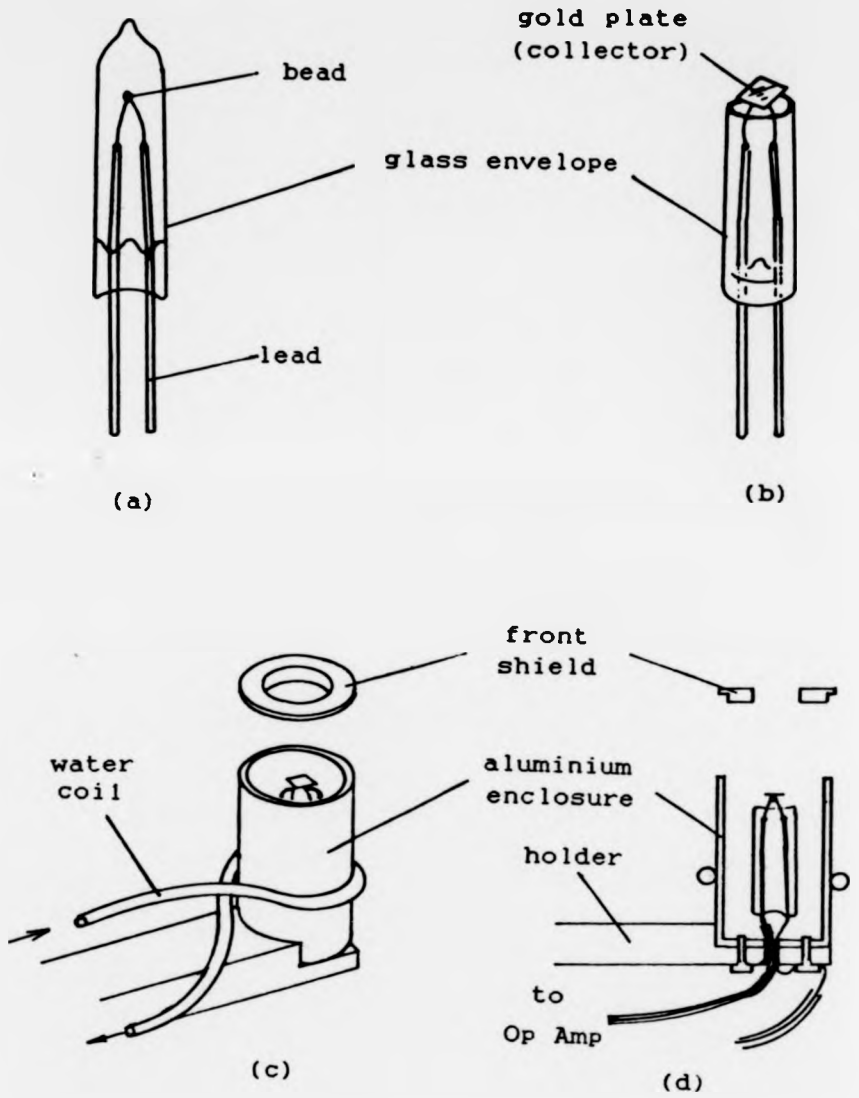

Fig. 4.7 : (a) Evacuated envelope thermistor type RA 53

(b) Thermistor RA 53 with top of its glass envelope cut to enable a thin gold foil being attached to the bead

(c),(d) The thermistor-collector assembly inside an aluminium enclosure which has a loop of water cooling coil attached to its wall.

which allowed lateral movement perpendicular to the path of the fast atom beam. The manipulator, in turn, was mounted on a three-post bellows which provided additional movement to the thermistor-collector assembly, so that it could be positioned exactly in the path of the beam [See Plate 2]. The power dissipation constant of the thermistor-collector assembly was measured in a vacuum of 10^{-9} torr and in two slightly different ambient temperatures, i.e., at 291 K (with the water cooling) and 303 K (with the water cooling shut). Within the limit of the experimental error, the dissipation constant was found to be (18.8 ± 0.1) μWK^{-1}, independent of the ambient temperature [Fig. 4.8].

The isothermal steady state (or constant resistance state) is maintained by controlling the voltage applied to the bridge via the FET Op Amp. When the bridge is balanced, the thermistor's resistance R_{th}, satisfies the following equation:

$$\frac{R_{th}}{R_s} = \frac{R_1}{R_2}$$

To simplify operations, the values of R_1 and R_2 were chosen to be equal so that any value set on the helipot (R_s) will also be the thermistor's resistance when the bridge is balanced. A bypass capacitor was put across the input-output of the FET Op-Amp to eliminate the effect of high frequency noise.

The out of balance voltage from the bridge was fed into the FET Op Amp inputs. Any power delivered to the thermistor by the fast atom beam will upset the bridge equilibrium

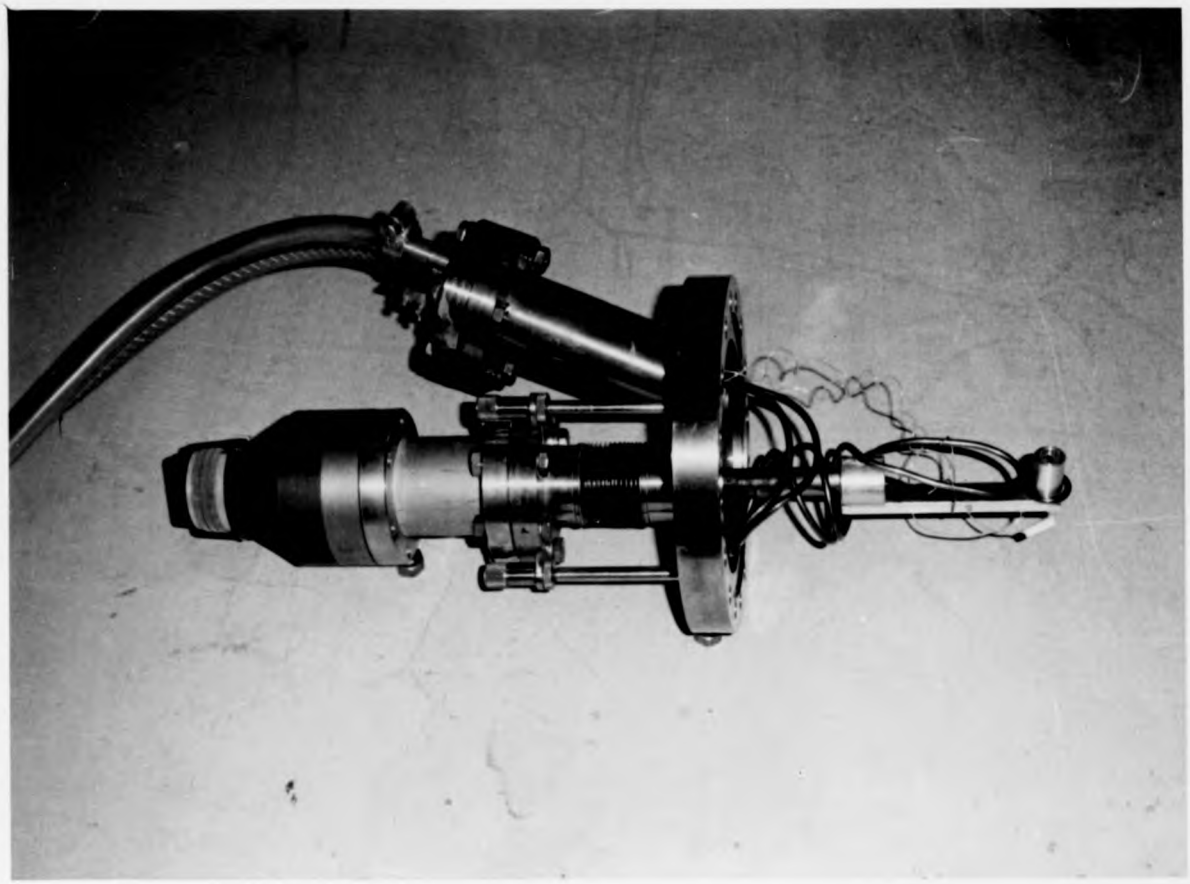

Plate 2

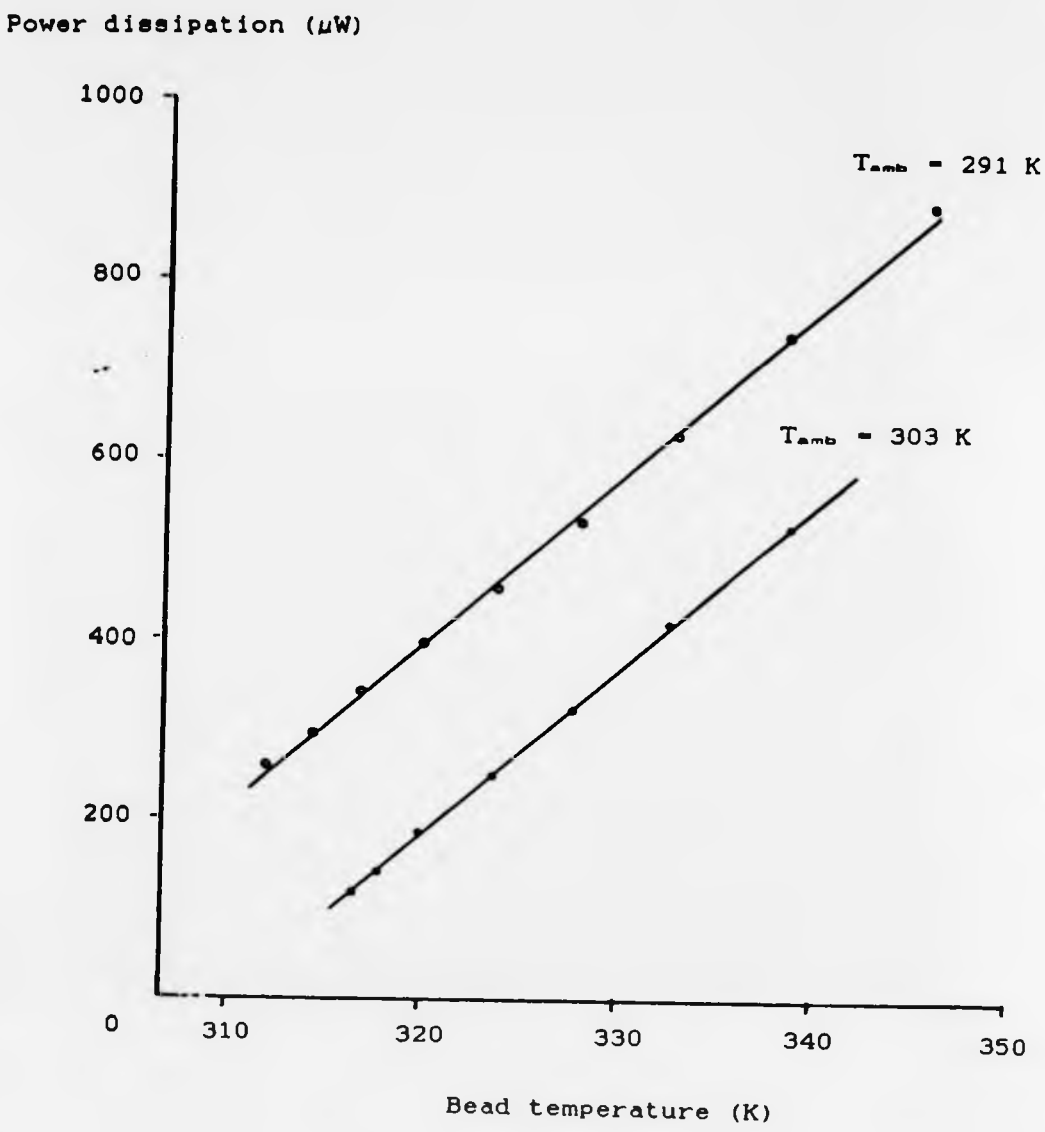

Fig. 4.8 : Graphs showing the power dissipation of thermistor RA53 versus temperature, at two different ambient temperatures.

condition, which is translated into a tiny voltage which appears across the Op Amp's inputs and is subsequently amplified. If the thermistor resistance goes down, the negative out of balance voltage is amplified and applied to the bridge. The reduced current through the thermistor, reduces the Joule heating and the thermistor resistance increases until the bridge balance condition is restored. The Joule heating level was evaluated by measuring the current and voltage to the thermistor using digital multimeters, which were set in the ranges that enable them to read down to 1 μA and 1 mV respectively. If E is the beam energy, V_i, I_i and V_f, I_f are voltage and current to the thermistor in the initial and the final steady states respectively; by assuming a total energy accommodation, an assumption which can often be realised practically [3], the number of the fast atoms per second (n) is given by

$$n = \frac{V_i I_i - V_f I_f}{E}$$

The sensitivity of the bolometer depends on the following factors:

(a) The preset value of R_s. By consulting the thermistor's resistance-temperature characteristic curve [Fig. 4.6], the best operating temperature can be pre-selected, but with one caution. Although the thermistor is more sensitive at lower temperature (i.e., the temperature coefficient at any temperature is given by $\alpha = -B/T^2$), it will take a longer time to reach the steady state, i.e., large response time [Fig. 4.9]. It was found that R_s= 3.25 KΩ gave the optimum operation condition in terms of sensitivity with a response

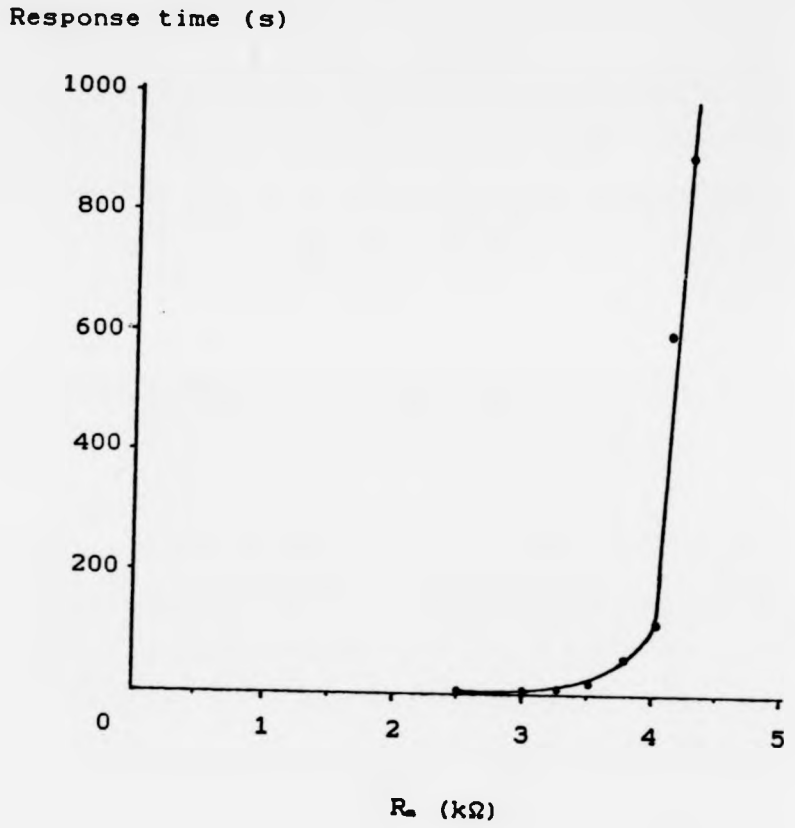

Fig. 4.9 : The response time of the bolometer against the helipot resistance (R_m).

time of less than 5s.

(b) The individual sensitivity of the digital ammeter and the digital voltmeter which were used to measure the Joule heating level in the thermistor. It must be emphasised here that error and sensitivity are two different quantities; but in practice, we can only have high confidence in the measured beam power if the latter has value much larger than the error value. This factor is best demonstrated by the following error calculations:

The beam power is $P = V_i I_i - V_f I_f$

Using calculus, the magnitude of error in P is

$$\delta P = V_i \delta I_i + I_i \delta V_i + V_f \delta I_f + I_f \delta V_f$$

where $\delta V_i = \delta V_f = 0.5$ mV and $\delta I_i = \delta I_f = 0.5$ μA.

Typical Joule heating levels with $R_s = 3.25$ kΩ are:

$V_i = 1028$ mV, $I_i = 316$ μA, $V_f = 940$ mV and $I_f = 289$ μA.

Inserting the values into the error equation, we obtain $\delta P = 1.29$ μW. For argument sake, suppose we use more sensitive meters, say $\delta Vi = \delta Vf = 0.05$ V, $\delta Ii = \delta If = 0.05$ μA; inserting back the values into the error equation gives $\delta P = 0.129$ μW.

Clearly, more sensitive meters can improve the confidence attached to the value of the beam power measured with the system. A practical approach to this matter is by incorporating additional Analogue-to-Digital Converters which can read the Joule heating level via a simple computer assembly. Further improvement in the value of δP, i.e., smaller value for δP, can also be achieved if the Joule heating level is made smaller by increasing the bridge equivalent resistance.

(c) The fluctuations in the ambient temperature. In the isothermal steady states, the total power dissipated in the thermistor must be kept at a level such that the temperature of the bead corresponds to the preset value of its resistance, i.e., $R_{th} = R_s$. In order to maintain the bead's resistance (R_{th}), its temperature (T_{th}) must be kept constant. The power levels and the bead temperature are related to the ambient temperature (T_{amb}) as follows:

$$P_{beam} + P_{Joule} = k\ (T_{th} - T_{amb})$$

where k is the thermistor power dissipation constant. Provided the beam power (P_{beam}) is constant, any change in the ambient temperature must be matched correspondingly by a change in the Joule heating power (P_{Joule}), in order to keep the bead temperature (T_{th}) and hence its resistance (R_{th}) constant. This change, in practice, is indistinguishable from the change which is caused by the beam power; therefore it contributes in setting the smallest detectable power of the bolometer. With $k = 18.8\ \mu WK^{-1}$, to limit this effect to within 0.1 μW, the ambient temperature fluctuations must not exceed 10^{-3} degrees K.

(d) Output drift of the operational amplifier is also a problem although by suitable choice of op amp this drift can be reduced to around 100 nV/$\sqrt{}$(month), which for practical purposes can be ignored.

(e) Stability of power supply.

By taking into account factor (b) and (c) above, the smallest detectable power for the bolometer is 1.5 μW. This is a value comparable to the power of most fast neutral atom beams in the energy regime of 1 keV or below !

4.4 The fast atom guns

Two types of fast neutral atom guns have been used by the author. The first gun worked on the basis of symmetrical charge transfer, and was capable of producing a neutral atom beam in the energy range of 200 eV to 1000 eV. It was designed by Johnson and Delchar [4] and built in the Physics Department Research Workshop. The second gun was a cold cathode saddle-field gun type FAB11NF manufactured by Ion Tech Ltd. It is claimed by the manufacturer that the gun is capable of producing a steady flux of truly fast neutral atom beam in the energy range of 2.5 keV to 8.5 keV. For convenience, the sources are called "Source 1" and "Source 2" respectively.

4.4.1 Source 1

This source comprised of three main components; a gas feedthrough, an electron gun and an electrostatic deflector. All these components are mounted on an 8-inch Conflat flange which has its own 8-way electrical feedthrough [Fig. 4.10a].

The gas supply system consists of an automatic pressure-controlled inlet valve and an array of seven stainless steel hypodermic needles. Each of these needles is of 5 mm length and has internal diameter of 0.2 mm. These long canal-like apertures enhance the thermal gas beam's forward directionality and at the same time provide sufficient flux of gas molecules to feed the electron gun.

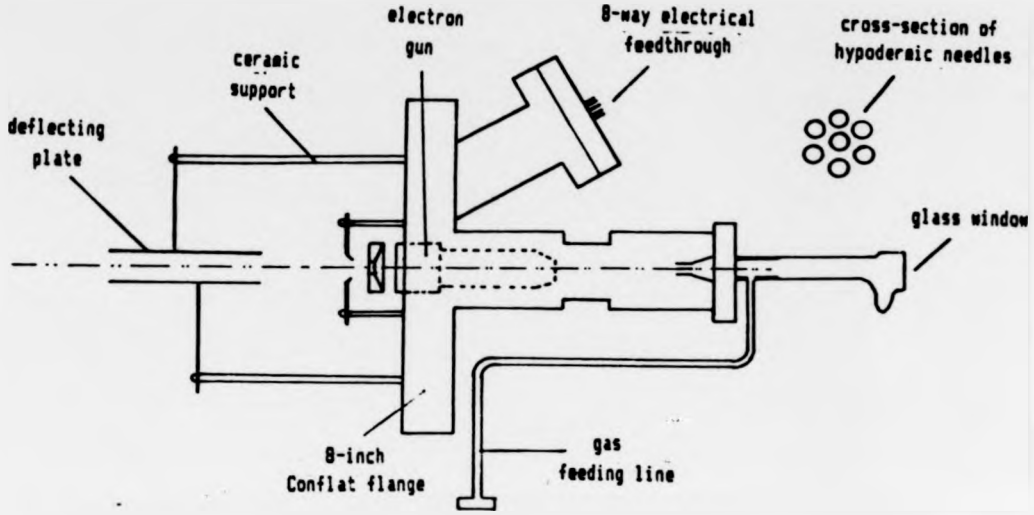

(a)

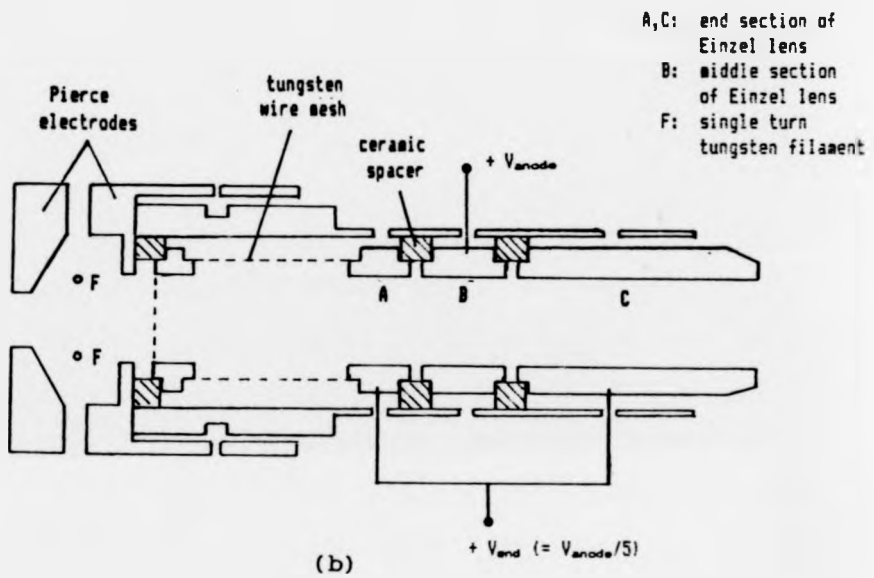

(b)

Fig. 4.10 : (a) Complete construction of Source 1

(b) The electron gun

The heart of this source is its electron gun [Fig. 4.10b]. It consists of a single turn tungsten filament embedded in a two piece Pierce electrode. Electrons from the incandescent tungsten filament are poorly focused into the incoming thermal gas beam by mean of a three piece Einzel lens. During its operation, the voltage ratio of the end and middle sections of the lens is maintained at 1 : 5.

It is thought that the generation of a fast neutral beam occurs inside the gun in a two step process. First, gas molecules are ionised by the electron beam, the ions then gain acceleration under the influence of the gun's focusing field and are subsequently neutralised in small angle charge transfer collisions with their thermal energy parent species. If this is the correct mechanism for fast atom production, i.e., a two step process in which each step is proportional to source pressure (p), then one would expect the number of fast neutrals to be a function of p^2.

The two step process was checked by the following means. Charged particles were removed from the central beam by mean of an electrostatic field deflector and the charge free beam was then collimated into the adjacent experiment chamber by the bevelled orifice. The beam intensity was monitored by measuring the current of ejected secondary electrons leaving the gold target; provided the filament current and the gun voltages are kept constant throughout the experiment, the beam intensity is directly proportional to the ejected electron current. To facilitate data processing, the output from electrometer K602 was linked to the BBC microcomputer via the interface while the source

pressure readings were fed into the computer via its keyboard. A program was written to enable the computer to display a logarithmic plot of the beam's intensity versus its pressure, and compute a best value for its slope. A typical graph showing the relation between the two quantities is depicted in Fig. 4.11. From several runs, its was found that in the pressure range between 6×10^{-6} torr to 1×10^{-4} torr, measured externally, the logarithmic plot of beam intensity as a function of its pressure had a slope of 1.9 ± 0.1, a value close enough to 2 to confirm the two step process.

One may expect that what emerges from the electron gun is a mixture of ground state neutrals, metastables, charged particles, Rydberg state atoms and photons. In a study using Time of Flight Technique (TOF) with the same source worked in a pulsating mode, Nielsen and Delchar [5] found that at a working beam pressure of about 10^{-4} torr, the content of metastables was negligible (less than 0.5 %). The study also showed that the fast neutrals are quite monoenergetic with the main beam having an energy equal to the potential applied to the central element of the Einzel lens.

The ultra-violet photon content of the beam, if any, is only attributable to radiative decay of one of the metastable states. In the case of He metastables, the UV photons are due to the decay of the 2^1P state, and were reported by Johnson and Delchar [4] to be less than 0.7%. Therefore it is safe to assume that at the working pressure of about 10^{-4} torr the beam is essentially free from UV

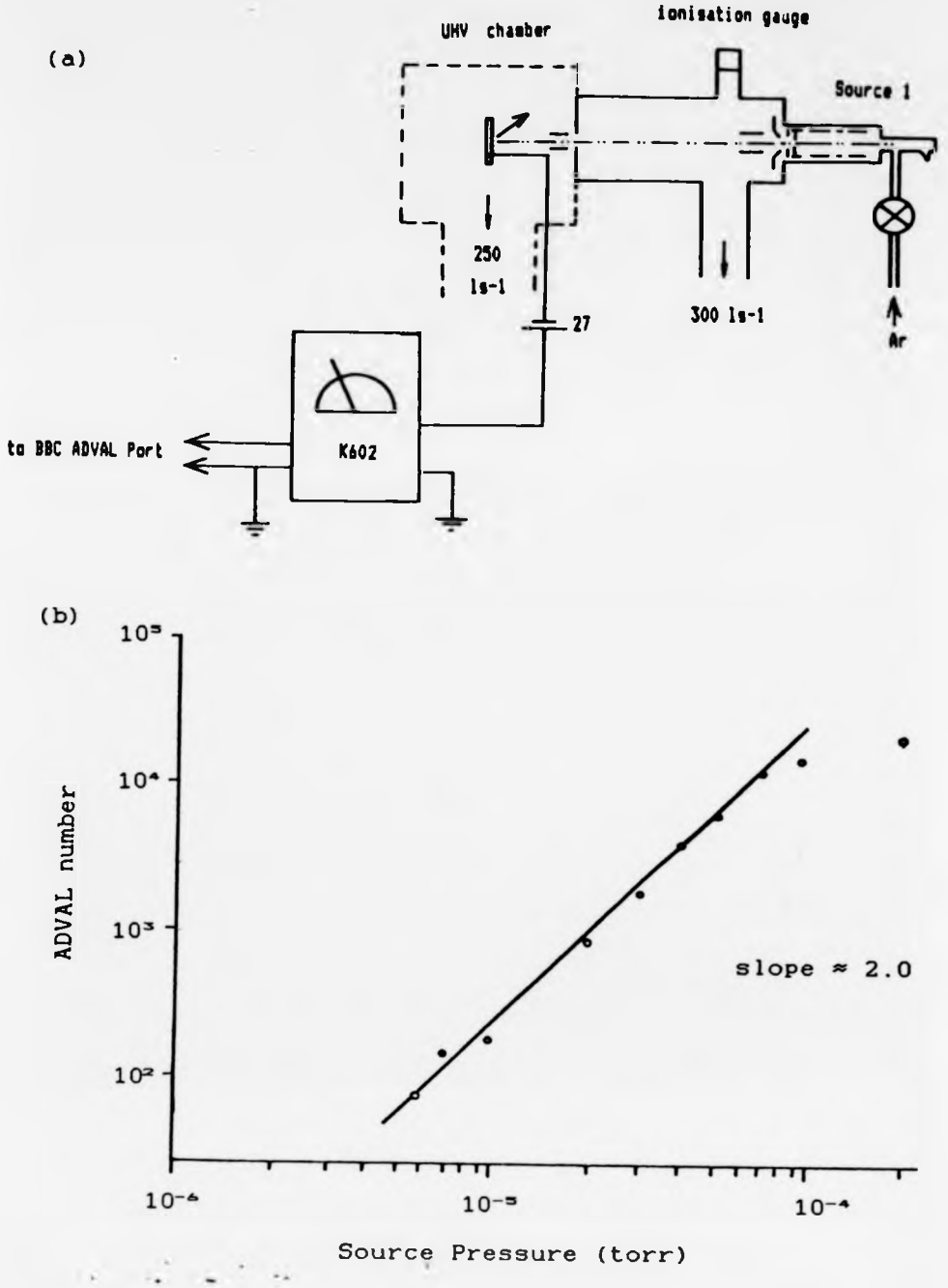

Fig. 4.11 : (a) Experimental set-up to verify for Source 1 that $I_- \alpha p^2$.

(b) Logarithmic plot of ADVAL number versus source pressure.

photons. Charged particles and Rydberg state atoms were removed by passing the beam between charged plates set either side of the beam, where the ions were deflected and Rydberg state atoms removed by the Stark effect in a high electric field.

Fig. 4.12 shows typical curves of normalised ejected electron current plotted against the beam energy at various source pressure. We can deduce two gun properties from the curves: (i) for a given energy, increasing the source pressure will increase the intensity of the fast atom beam, and (ii) for a given source pressure, there is a beam energy at which the intensity of the beam is maximum. This energy decreases with the source pressure.

4.4.2 Source 2

The heart of this source is an electrostatic saddle field which is capable of inducing electrons to describe long, stable, oscillatory paths without resort to the use of magnetic fields or a thermionic electron source. Its design was inspired by McIlraith's saddle field charge particle oscillator [6].

Basically, it is a cell which consists of a flat ring anode (also called annular anode, or simply, annulus), connected to a very high positive voltage, sandwiched in between two grounded top hat like metal cylinder cathodes [Fig. 4.13]. The saddle field configuration produced in this way has axial symmetry and performs better than that of a pair of parallel equally charged rods [7] which has planar

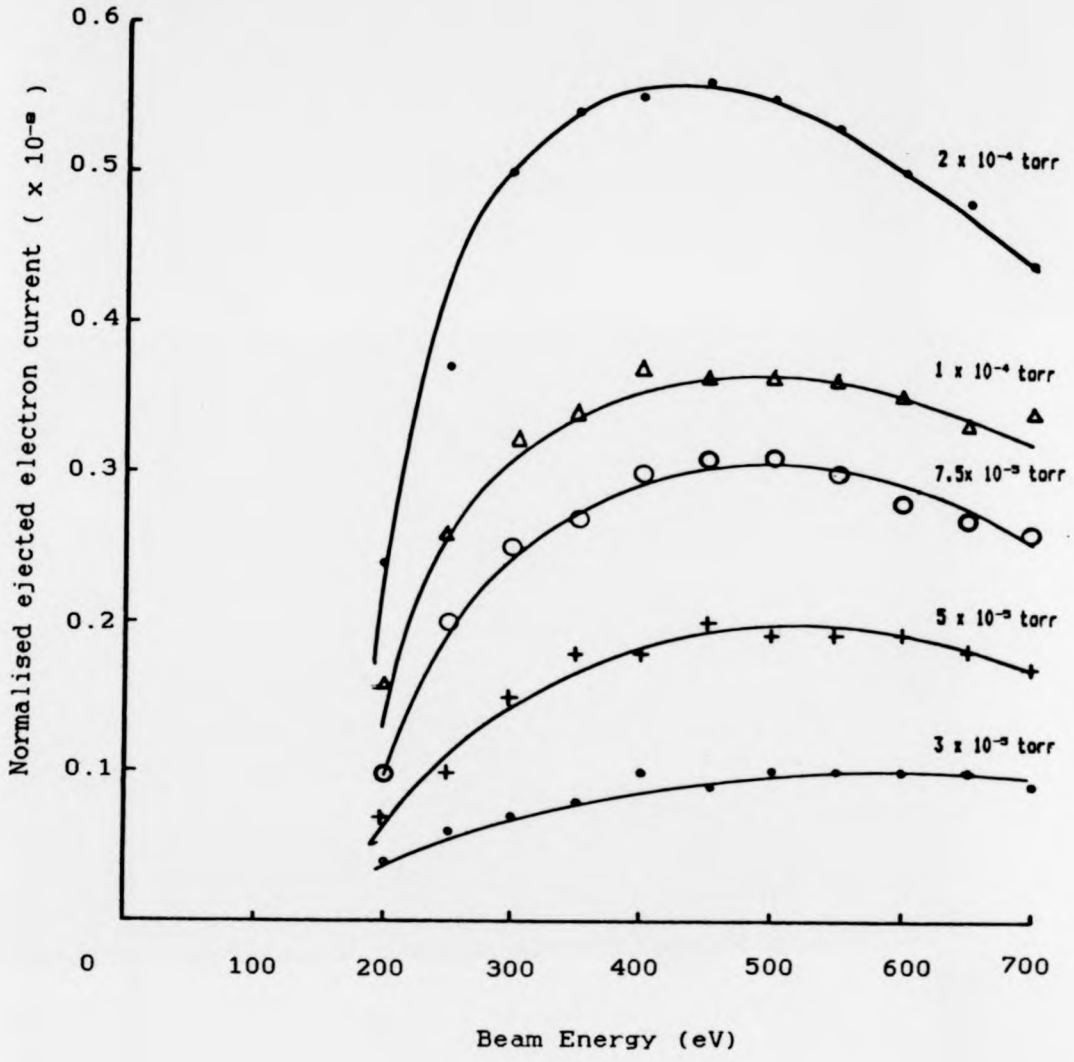

Fig. 4.12 : Curves of normalised ejected electron current versus fast atom energy of Source 1. The curves are for argon at source pressure as indicated.

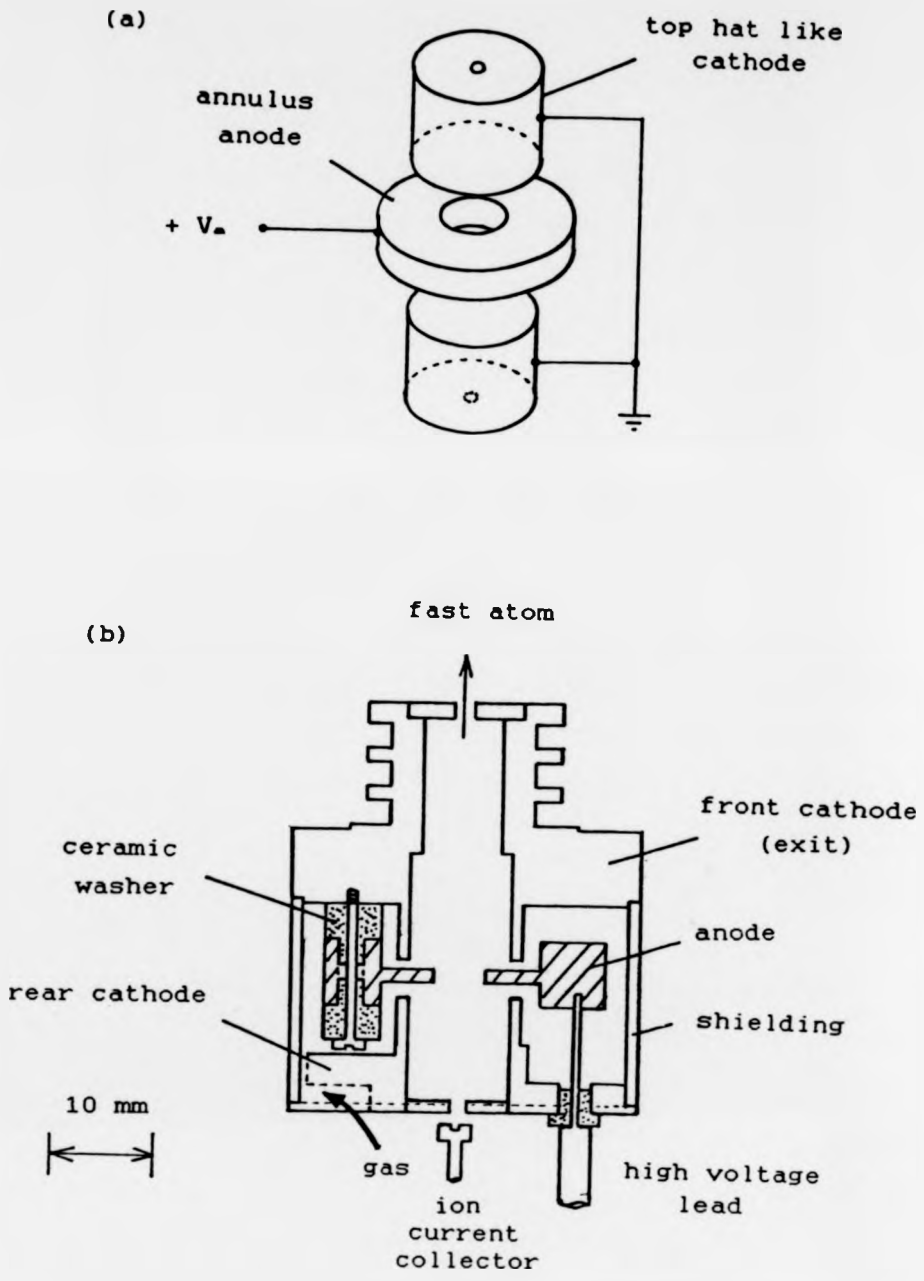

Fig. 4.13 : Saddle field fast atom gun

(a) Schematic construction

(b) cross-section of FAB11NF (saddle field cell only)

symmetry, in the sense that it induces a more intense and stable discharge at lower pressure and the beam is cylindrical in cross section. Due to its symmetrical construction, two beams of equal energy characteristics are self-extracted in opposite directions. Therefore, the study of the characteristics and working principle of a saddle-field atom gun, can in principle, be carried out by studying the ion beam produced by the field.

To date there is no entirely satisfactory explanation of how this source works. It is thought that ionisation of gas molecules by cosmic rays inside the cell provides the initial electrons, which in turn are accelerated into the saddle field region and subsequently oscillate stably to cause further ionisation. Each ionisation process produces an additional electron resulting in an electron avalanche; this multiplication effect, together with the generation of secondary electrons by the impact of the energetic ions on the cathodes, enables a steady discharge to be sustained inside the cell.

The positive ion beam formed in the discharge has energy and diameter depending only on the internal electrode structure. In a study using a thin annulus, with the saddle-field gun operating at 6 kV and argon pressure of 2×10^{-4} torr, Franks and Ghander [8] found that the ion beam was quite monoenergetic. The beam energy was 5.1 keV, i.e., 0.85 of the annulus potential, and its full width half maximum (FWHM) was 250 eV (i.e., 4.9%). However, the monoenergetic feature of the beam was shown to be less prominent by

Pomathiod et. al. [9] when a thicker annulus of 12 mm was used.

The monoenergetic nature of the beam implies that the ions are generated from a single point in the cell. In a recent study in the Physics Department, the discharge potential of a saddle field source was measured and compared with the potential obtained by solution of Laplace's equation. These two quantities were found to agree reasonably well and the ion energy, determined with a retarding field analyser, was found to be equal to the saddle point potential [10]. The FWHM of the atomic beam was consistently in the range of 110 - 150 eV depending on the anode voltage. Computer solution of the Laplace's equation shows that the saddle point potential is determined by the anode aperture aspect ratio. Thus, for a given diameter of anode aperture, increasing the anode thickness increases the saddle point potential. In the case of Source 2, according to the manufacturer's specifications, the beam energy is 0.85 of the potential applied to the annular anode.

The contents of the beam emerging from the saddle field are a mixture of positive ions, ground state neutral atoms and neutral atoms in their metastable states [11] and electrons [9]. After leaving the cathode opening for about 30 mm, the metastables are dissociated into positive ions and electrons [11]. The neutral atoms result when ions are neutralised inside the gun. As for the neutralisation process experimenters are divided in two lines of thought; it has been proposed that this occurs mainly through electron capture of the secondary electrons [12] or

resonance charge transfer [13,14]. The final central beam contains mainly ground state fast neutral atoms because its charged particle contents are deflected away due to their own mutual repulsion. Franks claims that the ion content of the final beam can be reduced to less than 1% by two modifications, namely, by careful shielding of the cathodes, and by decreasing the internal field at the cathode regions. These objectives are realised by making the exit side of the cathode longer.

Two series of preliminary experiments were carried out to study the characteristics of the gun's output, namely, the neutral content of the beam and its current-voltage relationships. The neutral content of the beams were measured by the following means. An electrostatic field deflector was inserted inside the UHV chamber, between the collimator and the gold target (this will be discussed further in Section 4.4.3). The gold target was connected to K602 and biased at -30 V with respect to ground; so that when the atomic beam strikes it, the total ejected electron current (I_e) can be measured and interpreted as proportional to the number of the incident atomic particles, neutrals or ions alike. When the deflector's DC voltage was increased slowly from zero, the ejected electron current decreased steadily until a point was reached where it stopped decreasing, which essentially means that the ejected electron current was due to the fast neutrals only. The deflection field for this to occur varied with the beam's energy; from about 200 Vcm^{-1} to 600 Vcm^{-1} for the beam's energy of about 2.5 keV to 8 keV. To speed up the

experiments, the ejected electron currents were measured at zero and at 1000 Vcm^{-1} deflection field strengths. The neutral beam content of the beam was taken as the ratio of the ejected electron currents, as follows:

$$\% \text{ of neutral} = \frac{I_e \text{ when electrostatic field } 1000\ Vcm^{-1}}{I_e \text{ without electrostatic field}} \times 100$$

The experiments were carried out at constant discharge current, i.e., at anode current of 1 mA, and the neutral contents were measured against the source pressure. Results from the experiments [Fig. 4.14] show that the neutral content of the beam varies proportionally with the source pressure, which suggests that the fast neutrals are produced through charge transfer mechanism.

Fig. 4.15 shows a typical current-voltage characteristics of the gun. It was found that the gun starts to operate above a threshold anode voltage of about 2.2 kV and up to 10 kV. However, it was found that the usable range of the anode voltage is between 3.0 to 7.0 kV; outside this range the beam current is practically too small. No attempt was made to measure the beam divergence; but the circular mark of diameter about 5 mm caused by the beam on the back of the collimator (about 20 cm away) suggests that the central beam divergence is about 1.5°.

The performance of a saddle field fast atom beam source of similar design (FAB11) was studied recently by Saied et. al. [14]. Their results show good agreement with ours in the area of general source current-voltage characteristics.

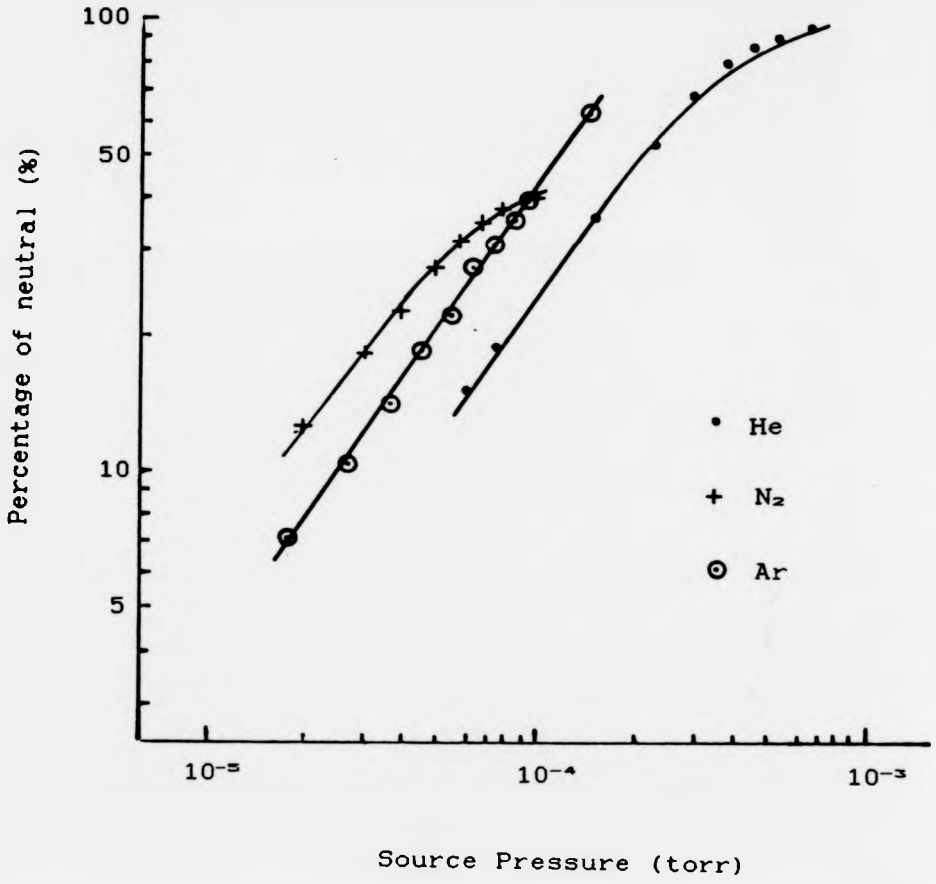

Fig. 4.14 : Logarithmic plot of percentage of neutral content of Source 2 against source pressure.

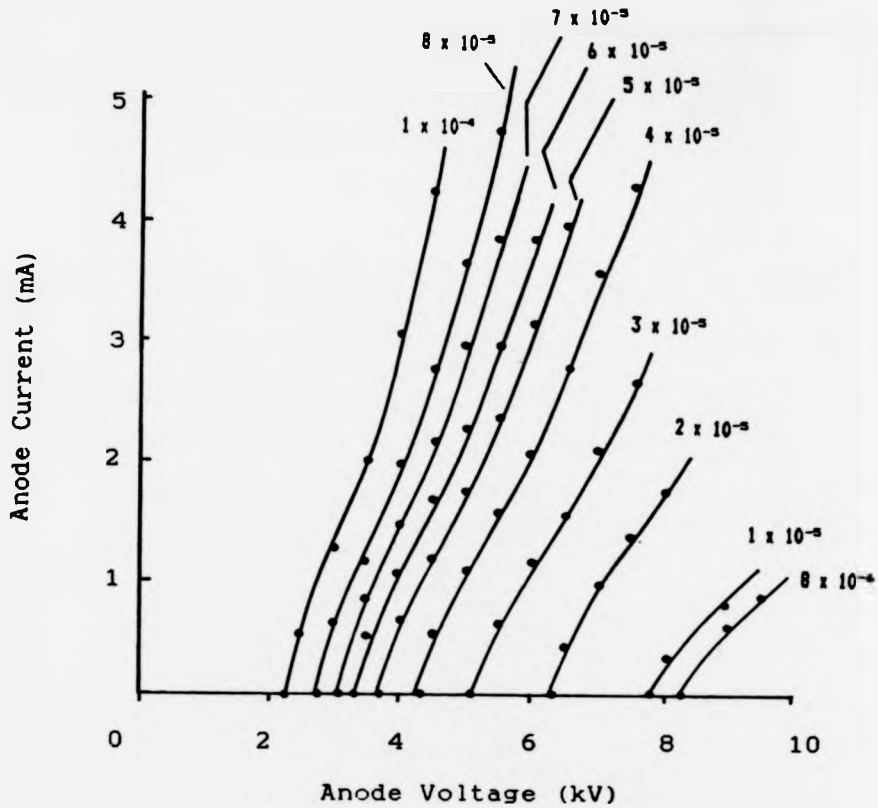

Fig. 4.15 : Graphs of anode current versus anode voltage of Source 2 at various source pressure (in torr). (Gas: N_2)

However marked differences can be seen in two aspects, namely, beam energy distribution and its neutral content.

By using time-of-flight technique, Saied et. al. found that the beam has a very broad energy distribution, typically producing 1100 eV FWHM at 4 keV, i.e., 27% resolution. This value is surprisingly high if compared with results obtained by other workers, such as that of Franks and Ghander (4.9%) [8], Pomathiod et. al. (3.6%) [9] and the ones obtained in the Physics Department (5%) [10].

The neutral content of the beam measured at this laboratory shows linear relationship between the percentage of the neutral with the source pressure, which concludes that the fast neutrals are formed through charge transfer. In the source pressure range of 1×10^{-5} torr to 1×10^{-4} torr, the neutral content of the beam increases from about 5% to 45% in the order of N_2>Ar>He; to be contrasted to 40% to 95% as obtained by Saied et. al. with Ar. The discrepancy may be due to the different condition applied in the two measurements; whilst Saied et. al. use a single deflection plate and apply no collimator, we collimate the beam before removing its ion content with a pair of parallel plate deflector.

4.4.3 Beam collimation

Beam collimation for both Source 1 and Source 2 was achieved by passing the beam through a bevelled metal aperture. The beam diameter at a point about 20 cm away from

the aperture, i.e., at the target, was found to be not more than 2.5 mm.

The introduction of the collimator can, in principle, add positive ions to the final beam by reionisation collisions even in the energy range of Source 1. This may well occur by the electron promotion mechanism proposed by Souda and Aono [15]. Therefore, an electrostatic field deflector, i.e., a pair of parallel conducting plates of 2 cm x 2 cm separated by 0.5 cm were placed about 2 cm away from the collimator but in the experimental chamber so that the positive ions resulting from the collision of the fast neutral atoms with the collimator edge, as well as the ion content of Source 2, could be deflected out of the central beam.

4.5 Sample preparation

Three surface samples were used in the experiments, they were gold and lithium surfaces. Since it was not intended to perform any scattering experiment on either samples, it was thought that polycrystalline samples would be adequate. All samples were bought from Goodfellow Metals and were delivered in the form of rolled films, as follows:

Sample	Purity (%)	Thickness (mm)
Gold I	99.99+	0.025
Gold II	99.99+	0.125
Lithium	99.9	0.25

4.5.1 Gold surface I

The gold foil I was cut into a circular shape of diameter 22 mm, and then clamped in between a pair of stainless steel circular frames of OD 22 mm and ID 16 mm. The frames were then spot welded to secure the gold foil. Two small holes of diameter 1 mm each were drilled in the stainless steel frame, at a distance of 10 mm apart, to provide connections to an aluminium sample holder and a sample heating filament. The heating filament was a single loop of diameter 10 mm, of rhenium-tungsten wire of diameter 0.20 mm, situated 3 mm behind the unpolished side of the gold foil. The filament was meant to provide the facility to study the effects of different surface temperatures and also to desorb weakly bound materials. A chromel-alumel thermocouple junction was set to have a good physical contact with the polished surface of the gold foil to provide for temperature readings. With 4 ampere current (r.m.s.) supplied to the filament, the surface temperature would reach 250°C after about 45 minutes.

A He-Ne laser gun was used to align the system and set a correct length for the sample holder by the following means. First, Source 1 was fitted into the Conflat flange at the end of the source chamber. Then, the laser beam was directed from behind the flat glass view port at the target chamber, to pass through the collimating aperture and impinge on the array of the hypodermic needles in Source 1. If the system was aligned, the laser beam could pass through the hypodermic needles and come out of the gun end through a

small flat glass window, and form a clear interference pattern on a white screen situated just behind it. The point where the laser beam fell on the view port was marked with a permanent ink for future reference. The perpendicular distance from the path of the laser beam to the end of the axial rod of the rotary manipulator was measured and the sample holder was cut accordingly. The holder was then connected to the axial rod of the rotary manipulator. Electrical connection to the sample was through a nichrome wire which was spot welded to the frame. The gold foil and the heating filament were isolated electrically from the axial rod by ceramic spacers [Fig. 4.16a].

It was found later that the sample could be used for experiments involving the measurement of secondary electrons energies and yields at normal incidence only owing to its slightly buckled surface. Attempts to perform experiments with other angles of incidence failed to show reproducibility because it was believed that the foil was too thin to form a reasonably flat surface. It was then decided that a thicker gold foil of the same purity was needed.

4.5.2 Gold surface II

This thicker gold foil was cut into a shape of a square of 10x10 (mm) with a tab of 5x5 (mm) on one of its sides. A hole of diameter 3 mm was punched through the tab to enable a 10 BA screw and a top hat ceramic washer pass through it. The gold foil was then clamped lightly in between two flat

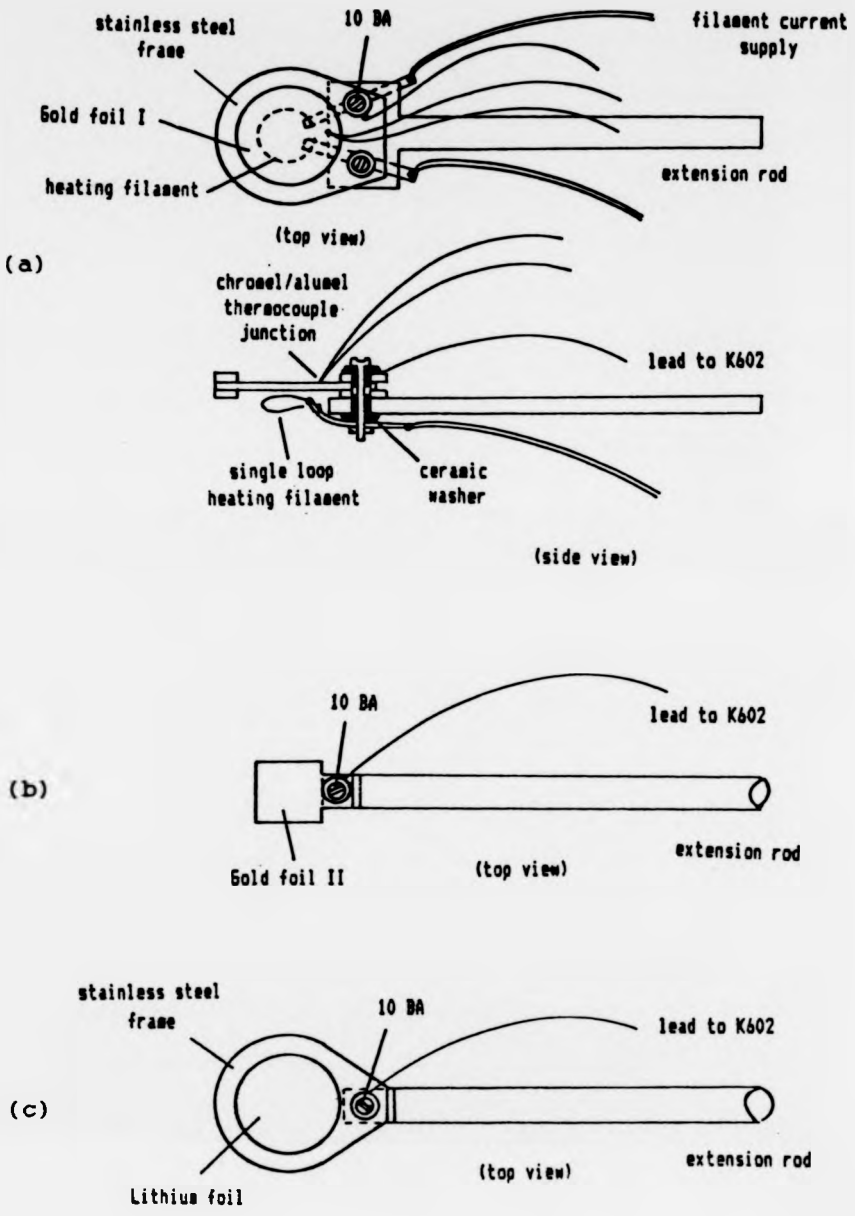

Fig. 4.16 : Sample holders

(a) Gold I (b) Gold II (c) Lithium

aluminium blocks so that it would have a reasonably flat surface. Electrical connection to the gold was via a nichrome wire which was spot welded to a 5 mm stainless steel washer, which in turn was sandwiched between the gold and the top hat washer. The gold foil was then fastened to one end of a stainless steel extension rod, with a flat ceramic washer between them providing the needed electrical insulation [Fig. 4.16b]. The other end of the extension rod was then connected to the axial rod of the rotary manipulator. With the aid of the He-Ne laser beam, the length of the extension rod was determined so that the fast atom beam would fall at the centre of the gold surface. In the described position, the gold surface could be rotated about an axis perpendicular to the path of the incoming fast atom beam.

Gold was chosen as a sample simply because it is inert chemically. This removed the necessity of a sample cleaning routine which is often very tedious and time consuming. Like other surfaces though, gold can become atomically dirty while being exposed to the atmosphere through physisorption. In the vacuum chamber, cracked vacuum oil products have been known to contaminate the chamber's inner wall as well as the sample, and gold is no exception. The sample heater provided a means of desorbing any adhering oil film. There was no special treatment undertaken to clean the sample, but its cleanness however was assumed based on two accounts:

(i) During bakeout loosely bound contaminants will certainly be desorbed off the surface, and

(ii) During the experiment the surface is constantly being bombarded with energetic atomic beams for a long duration; which can be expected to be equivalent to routine of bombardment by diffuse 500 eV argon ion beam usually performed in UHV condition for sample cleaning. This is not an over expectation case if we view the sputtering yields of gold for D^+ and He^+ measured by Bay et. al. [16], which show that in the energy range of Source 2, the sputtering yield is about 0.1 atoms ion^{-1}. Since H_2 is the lightest projectile and the sputtering yield increases with mass of projectile, we can expect that any of the atomic beams will sputter off the adsorbate from the area where exactly it falls on the surface, and eventually produce an essentially localised clean surface for the experiments. The UHV condition ensures that the rate at which the residual gas molecules stick to the clean spot will always much lower than the rate they are being removed, thus maintaining the localised cleanness throughout the experiments.

4.5.3 Lithium surface

Lithium is a very malleable metal; despite the fact that it is thicker than the gold foil, a support frame was needed for it. A pair of round stainless steel frames of ID 16 mm and OD 22 mm were cut, and the the lithium foil was clamped between them. The frames were spot welded so that the foil would sit firmly in them. Electrical connection was via a nichrome wire which was spot welded to the frame. The frame was then fastened to the extension of the rotary

manipulator's axial rod with a 10 BA screw which passed through a holed tab at the perimeter of the frame. A top hat and a flat ceramic washers were used to isolate electrically the sample from the rod [Fig. 4.16c].

The rolled lithium foil was delivered in a vacuum pack glass container because it is a very reactive element. Lithium reacts quite readily with moisture and oxygen, and is known to unite with nitrogen at 20°C. It was arranged so that the time taken from breaking the glass container to the point when the lithium target assembly being inserted into the vacuum chamber was less than 15 minutes, and this process was carried out in an inert gas (argon) atmosphere, so as to minimise surface deterioration. As a matter of note, at the time of insertion the lithium foil surfaces had already changed colour from silver metallic to dark grey despite the above precautions.

Lithium has a low melting point, that is 180.5°C; this means that the bakeout temperature had to be reduced. With the same arguments given for the gold surface, it was assumed that a localised clean surface would essentially be established on the lithium surface throughout the experiments.

4.6 Summary

A UHV environment was set-up to enable studies of the interactions of fast neutral atoms with clean metal surfaces be carried out in it. Two fast atom guns are used; the first was designed and built at the Physics Department and works

on the basis of charge-transfer, the second is the Ion Tech's FABNF11 which was found to be working on the basis of charge-transfer as well. The energy distribution of the secondary electrons formed in the interactions is analysed using a digital computer with the aid of a purpose-built computer-controlled ramp generator. A thermistor-based absolute bolometer of new design was built to be used in the measurement of the secondary electron yield coefficients. The targets are rolled gold and lithium foils of high purity (99.9%+); and without any provision of standard UHV in-situ sample cleaning device, a localised clean surface in the two targets is assumed.

4.7 References

[1] P. D. Johnson, Ph. D. Thesis (University of Warwick, 1978)

[2] P. L. F. Hemment, Vacuum 27 (1977) 611.

[3] C. A. van de Runstraat, R. Wijnaendts van Resandt and J. Los, J. Phys. E: Sci. Instrum. 3 (1970) 575.

[4] P. D. Johnson and T. A. Delchar, J. Phys. E: Sci. Instrum. 10 (1977) 428.

[5] H. B. Nielsen and T. A. Delchar, Surf. Sci. 141 (1984) 487.

[6] A. H. McIlraith, Nature 212 (1966) 1422.

[7] R. K. Fitch, T. Mulvey, W. J. Thatcher and A. H. McIlraith, J. Phys. D: Appl. Phys. 3 (1970) 1399.

[8] J. Franks and A. M. Ghander, Vacuum 24 (1974) 489.

[9] L. Pomathiod, D. Hendy, Y. Arnal and R Boswell, Inst. Phys. Conf. Ser. No. 54 (1980) 309.

[10] T. A. Delchar, private communication.

[11] J. Franks, Int. J. Mass Spectrom. Ion Phys., 46 (1983) 343.

[12] J. Franks, Vacuum 34 (1984) 259.

[13] R. K. Fitch, M. Khorassany and T. N. Mawlood, Proc 7th Int Vac Cong and 3rd Int Conf on Sol Surf, Vienna (1977) p. 285.

[14] S. O. Saied and J. L. Sullivan and R. K. Fitch, Vacuum 38 (1988) 111.

[15] R. Souda and M. Aono, Nucl. Instrum. Methods B15 (1986) 114.

[16] H. L. Bay, J. Roth and J. Bohdansky, J. Appl. Phys. 48 (1977) 4722.

CHAPTER FIVE

RESULTS AND DISCUSSION

5.1 Experiments on gold and lithium surfaces

Five gases were used in conjunction with Source 1 and Source 2; they were H_2, He, Ne, N_2 and Ar. Source 1 was used to provide fast neutral atom beam in the the energy range of 200-1000 eV while Source 2 was used for the energy range of 2.5-7 keV. All gases were of pure quality (99.998%) obtained from B.O.C. Ltd. The experiments were confined to three areas only, namely, the ejection of secondary electrons, reionisation of the fast atoms and the sputtering of surface atoms. In the area of electron ejection the following experiments were carried out:

(a) determination of the energy distribution of the ejected electrons, its dependence on the beam type and energy and on the surface temperature,

(b) determination of the electron emission yield coefficients (γ^*) and their dependence on the beam type and energy and on angle of incidence,

(c) determination of the angular distribution of the ejected electrons.

In the area of fast atom ionisation, the experiments were to determine ionisation efficiency and threshold energy (E_{th}) with respect to the beam type and energy; no attempt was made to measure the energy distribution of the resulting ions. The experiments to study the sputtered atoms were

arranged following the detection of "extra" positive ion current during the experiment to determine the energy distribution of the ejected electrons from a lithium surface. In the next sections, the procedure for each experiment will be described before reporting the experimental data.

5.2 The energy distribution of the ejected electrons

The experimental set-up for the determination of energy distribution of the ejected secondary electrons is as shown schematically in Fig. 4.3 (see Chapter Four ff. 59). Based on the results obtained with beams of electrons [1], ions [2] and metastables [3], it was anticipated that the secondary electrons would be of low energy, i.e., in the range of 0-25 eV ; therefore the ramp was programmed to sweep from about +6 V to about -25 V. The collector was floated at +27 V to suppress the emission of secondary electrons from its surface.

The retarding potential curve of the ejected electrons, i.e., the curve of the collector current versus the retarding potential, is displayed directly on the computer's screen and the data is simultaneously stored, in the form of 156 pairs of ADVAL number and the retarding voltage, in a destined file in the storage diskette. The computer program used to run the experiment is set out in Appendix 2. It must be noted here that the fast atom beam intensity had to be adjusted so that the collector current is greater than 10^{-11} A, if not it would be very susceptible to noise

interference. The measurement range of the K602 had to be selected accordingly, so that the collector current stays within a single range, or otherwise, the ADVAL number proportionality constant is not upheld.

The working principle of the energy analyser is simple. If the retarding voltage is - V, then only electrons with energy higher than eV will be able to overcome the potential barrier generated by the retarding grid and reach the collector. Thus, if N(E) is the energy distribution function of the electrons, the current at the collector (I_c) is a function of V as follows:

$$I_c(V) = \int_{eV}^{\infty} N(E)\, dE$$

Evidently, N(E) is obtainable by differentiating the collector current with respect to the retarding voltage.

Since the ADVAL number is directly proportional to the collector current, the energy distribution was actually obtained by differentiating the ADVAL number with respect to the retarding voltage. However, the energy distribution curve (EDC) obtained by direct differentiation on the raw retarding potential curve was of poor quality; therefore it was decided that the raw data should be fed into a smoothing routine prior to differentiation. In smoothing a retarding potential curve, the exactness of the smoothed curve is of prime importance; the final curve should look as close as possible to its original shape, or otherwise curvature which might carry vital information is lost in the process. Two types of smoothing methods were tried; the polynomial curve

fitting routine and the weighted averaging technique. The polynomial curve fitting works on the basis of least square principle, and with the BBC B (32K) microcomputer it works well up to order 10. The weighted averaging technique was due to R. E. Blake [4], modified to include correction for end point "lifting"; it works on the basis of averaging the value of a point with respect to its two nearest neighbours. A reasonably smooth retarding potential curve could be obtained after ten iterations of averaging cycle. It was found that for the retarding potential data, the weighted averaging technique performed better than the polynomial curve fitting routine in term of speed, exactness and ease of use. It then decided that only the weighted averaging technique would be used for the subsequent data analyses.

The details of the weighted averaging routine are now described:

Three consecutive points were averaged at a time using the following formula:

$$y_n = \frac{w_1 y_{n-1} + w_2 y_n + w_3 y_{n+1}}{w_1 + w_2 + w_3}$$

where $w_1, w_3 = 0$ for the end points or $= 1$ if otherwise, and $w_2 = 2$ for all points. The effect of end point "lifting" associated with this technique was avoided by incorporating two additional rules:

(i) the averaging starts from the second point and ends at the second last point, and

(ii) after each complete averaging cycle, the end points are re-evaluated such that each end point will lie in a straight line with its two nearest neighbours.
These two rules preserved the original feature of the raw retarding potential data. The computer program used for data processing is set out in Appendix 3.

Figs. 5.1-5.3 show examples of the retarding potential curve, its smooth averaged line and the ejected electron EDC. The use of arbitrary units for the electron intensity allows for the frequent change necessary for the fast atom beam intensity and the measurement range of the K602 electrometer, thus avoiding the need for recalculating the conversion constant following each change. Therefore the intensities of two EDCs obtained with this system can only be compared if the experiments were performed using the same fast atom beam intensity and the collector currents (I_c) were measured using the same measurement range on the K602 electrometer.

Experiments were carried out to study the effect of the beam type and energy on the ejected electron most probable energy (later called "peak energy"), and the results are shown graphically in Figs. 5.4-5.7. Not many ejected electron data in the energy range of Source 1 on the lithium surface were collected because the collector current was very small, generally $\approx 10^{-12}$ A , which might be due to the general deterioration of the target. This is possible because at the time Source 1 replaced Source 2, the lithium target had already been in the UHV chamber for about seven weeks. This view is supported by results from a recent AES

(a)

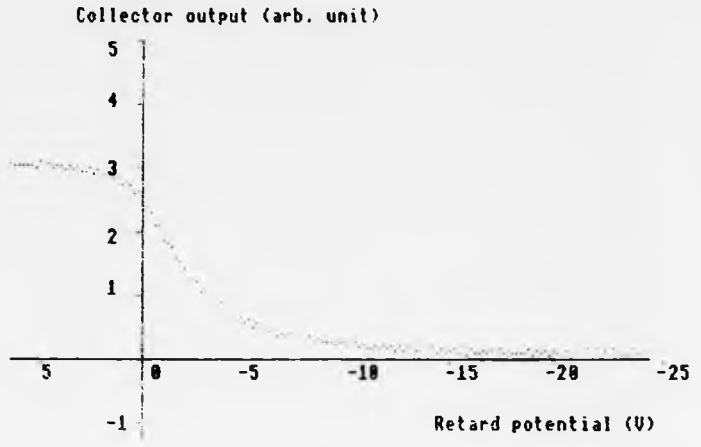

(b)

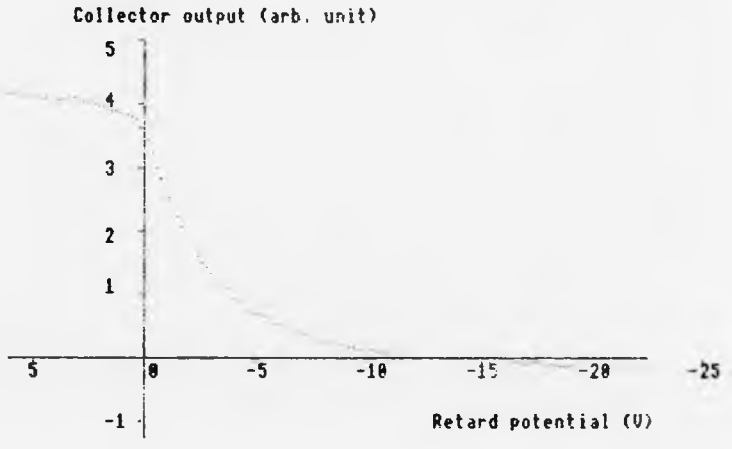

Fig. 5.1 : Samples of retard potential ADVAL number of the ejected electrons obtained with 4.25 keV He atom beam impinging on (a) Gold, and (b) Lithium.

(a)

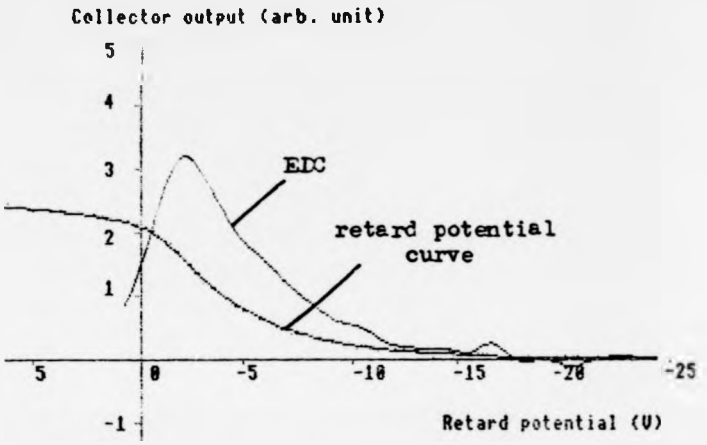

(b)

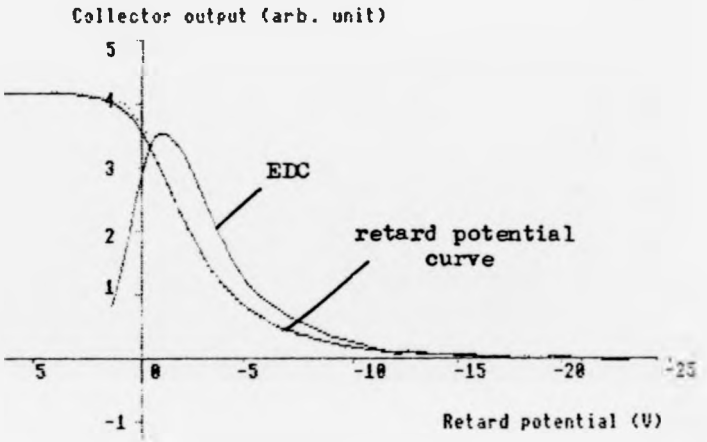

Fig. 5.2 :- Examples of smoothed retard potential curve of the ejected electrons and its derivative or EDC: a) 600 eV N_2 on Gold (b) 5.1 keV H_2 on Gold.

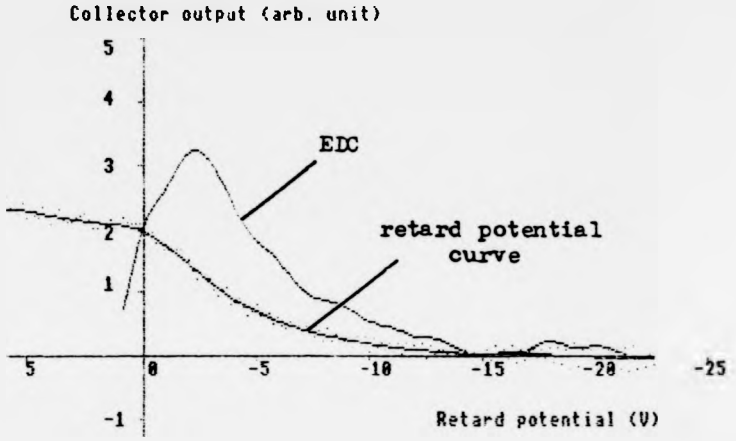

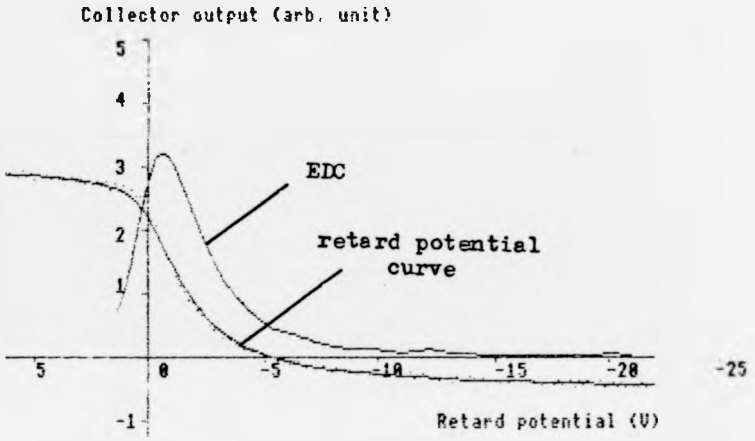

Fig. 5.3 : Examples of smoothed retard potential curve of the ejected electrons and its derivative or EDC: (a) 1 keV He on Li (b) 5.1 keV Ar on Li.

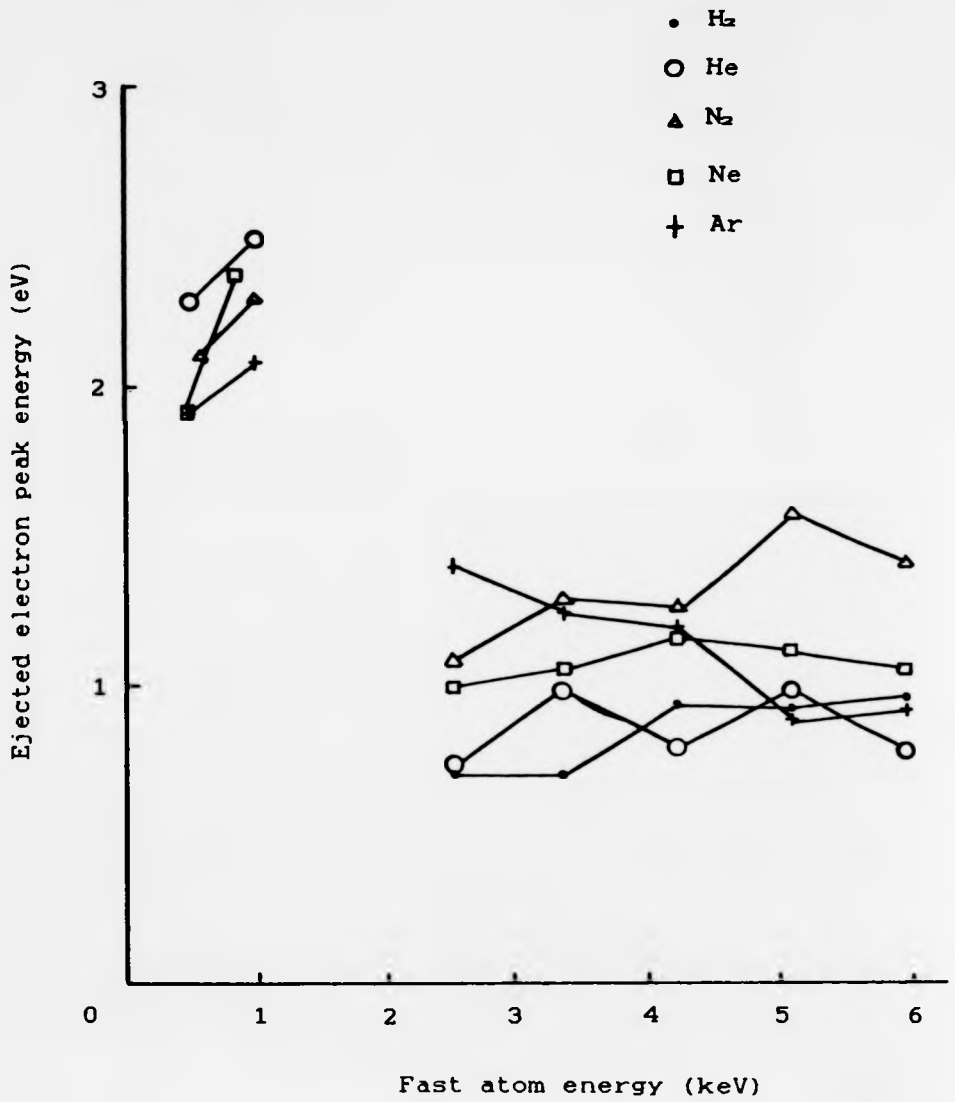

Fig. 5.4 : Variation of ejected electrons peak energy with fast atom beam energy and gas type (Gold surface).

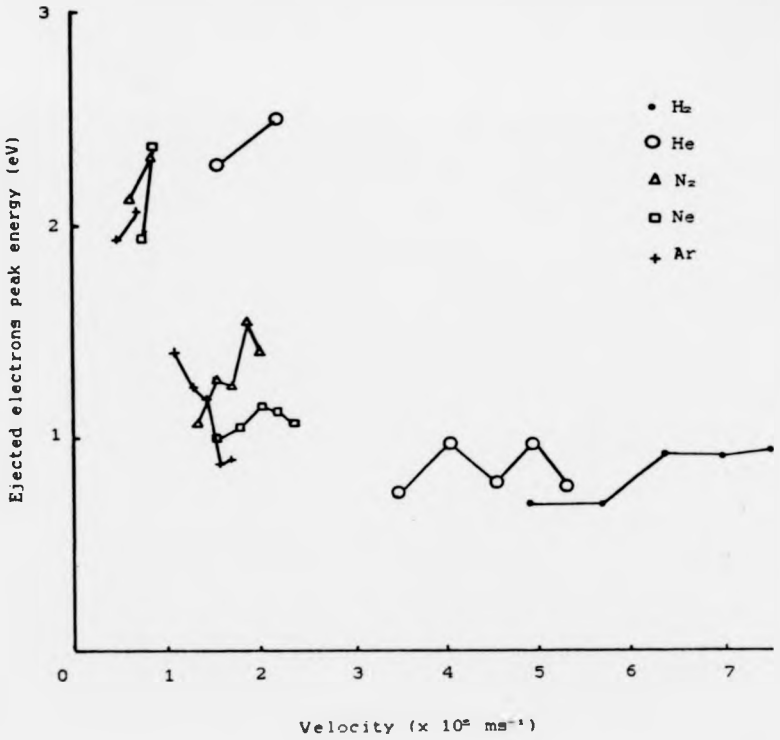

Fig 5.5 : Variation of ejected electrons peak energy with fast atom velocity and gas type (Gold surface).

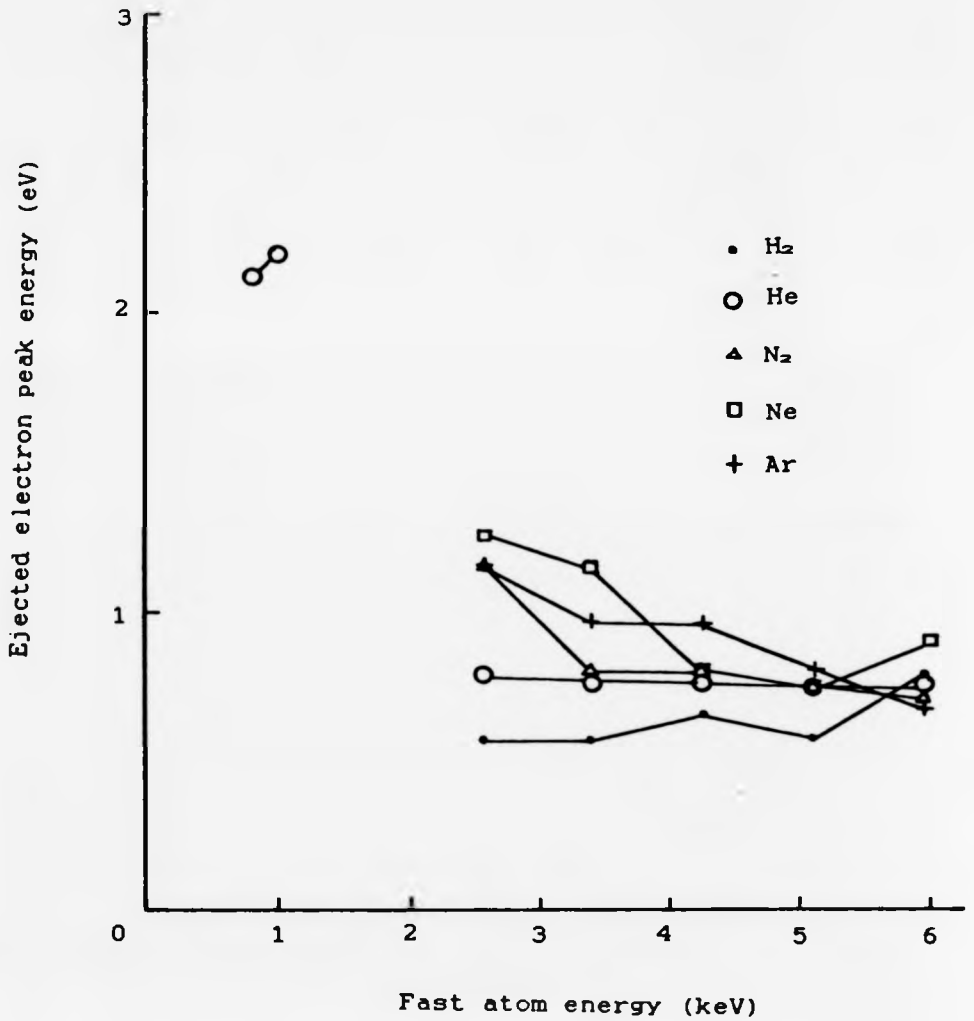

Fig. 5.6 : Variation of ejected electrons peak energy with fast atom beam energy and gas type (Lithium surface).

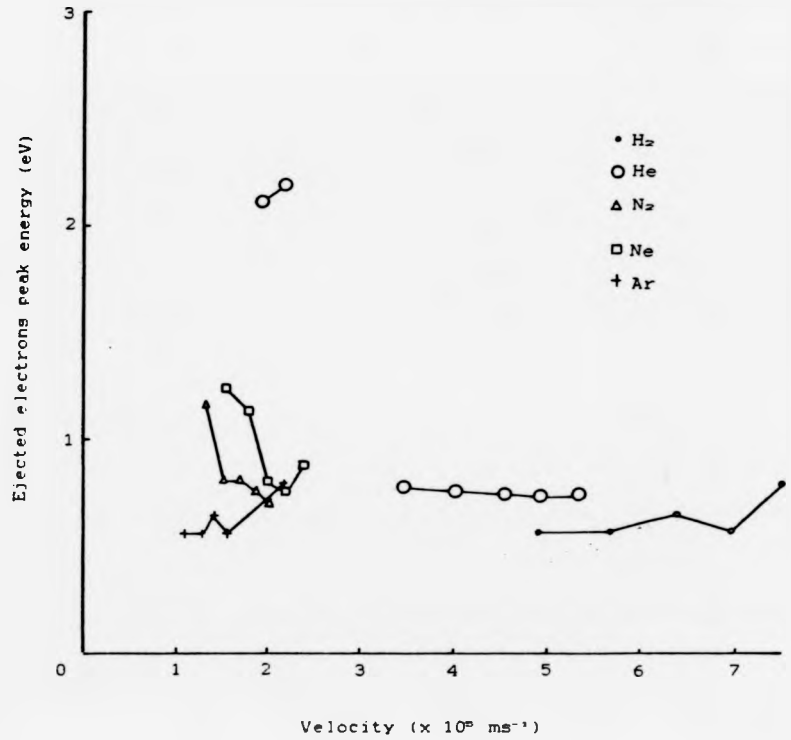

Fig. 5.7: Variation of ejected electrons peak energy with fast atom velocity and gas type (Lithium surface).

studies performed by Schowengerdt [5] on a polycrystalline Li surface, which was prepared by fracturing a research grade pure Li crystal inside a vacuum glove box prior to mounting in the UHV chamber. In the study, Schowengerdt identified oxygen contamination which only decreased, but not disappeared, when the surface was subjected to cleaning with Ar^+ ions (2.75 keV, 10 μA). Nevertheless, the EDCs obtained with He beams (800 and 1000 eV) show that, in the energy range of Source 1 the shape of the EDCs obtained from lithium surface are essentially identical to those obtained from the gold surface.

The EDCs show several interesting features:

(i) The ejected electrons are of low energy, i.e., the maximum energy is about 20 eV. The exact position of the cut-off point cannot be determined graphically because in the region higher than 10 eV the EDCs tend to be a very slow varying curve.

(ii) The EDCs peak at about 2 eV and shift to about 1 eV when the fast atom beam energy is increased from several hundreds eV to a few keV. In other words, the energy of the secondary electrons decreases as the energy of the fast neutral atom beam increases.

(iii) The full width half maximum (FWHM) of the EDCs decreases when the fast atom energy increases. In the examples from the lithium surface (Fig. 5.3), the FWHM decreases from 6 eV to 3.3 eV when the fast atom energy increases from 1 keV to 5.1 keV.

(iv) The ejected electron most probable energy, i.e., the peak energy, shows weak dependence on the mass of the

fast atom; in general, the lighter the atom the lower the peak energy.

These results must be contrasted with results from theoretical calculations of Kirson et. al. [6] who predicted higher electron energies (≈ 8 eV for Ar, H + Li (surface), and ≈ 25 eV for He + Li (surface)). While they predicted high energy tails that go beyond 100 eV, we observed cut-off energy a factor of five lower. This rather large discrepancy may be due to the assumption they made in the calculation, namely, the dominance of single electron-hole excitation. Furthermore, as they only dealt with the surface atoms, the attenuation factor was not included in their calculations. Further discussion on this subject will be given in Section 5.3.5 of this chapter.

In summary, given the same energy, the EDCs show nearly same structural feature irrespective of the beam type and the surface atom. A shift in the energy spectra along the energy axis due to work function difference as observed in INS, is not clearly evident here.

For the energy range up to 1 keV the peak energy was ≈ 2 eV but this peak shifted towards a lower value at higher fast atom beam energy (Figs. 5.4 and 5.6). Indeed a large portion of the ejected electrons appear to have energy close to zero or even negative. Negative energy electrons, or even zero energy electrons, are notions which are physically meaningless. To the best of the author's knowledge, there is no direct effect from the measuring system which may reduce the energy of the electrons before they can leave the surface. Therefore, reasons must be found to explain the

observed shift in the peak energy. This is not a new problem; it was observed before by experimenters working with electron beams [1], ion beams [7,8] and metastables [9]. There are several possibilities which may account for the problem:

(a) To address the same problem, Hagstrum [7] argued that the retarding grid works on the normal component of the electrons' momenta therefore electrons which are approaching the grid at grazing angle will be "seen" as having near zero energy. The use of hemi-spherical retarding grid must have minimised this effect tremendously and therefore it is probably not the responsible factor.

(b) In other INS experiments involving 40 eV singly charged inert gas ions on atomically clean Mo and W surfaces, Hagstrum [8] observed that the experimental values of the minimum secondary electron energy extended to negative values - the more so the heavier the incident ion. He related the phenomenon to the presence of an uncompensated magnetic fringing field in the neighbourhood of the target (about 45 gauss due to the magnetic mass analyser incorporated in the set-up). There was no intense magnetic field source being used in the author's experimental set-up; the only magnetic field presence was that of the earth, which was uncompensated. The earth magnetic induction near the experimental chamber was measured using Bell 3-axis Gaussmeter Model 640; and the magnitude of its components in three mutually perpendicular axes, with respect to the direction of the fast atom beam is shown in Fig. 5.19. As can be seen from the figure, the

horizontal component is about 0.18 gauss; a value which is too small to account for the energy shift.

(c) For this data to be physically meaningful requires an energy shift of ≈ 2 eV, i.e., an additional potential of ≈ 2 V between the target and the retarding grid with the target positive. The origin of this kind of potential might be from a space charge effect or from contact potential difference or both. Since the problem became observable only when Source 2 was in use, i.e., when the ejected electron current became relatively high (≈ 10^{-9} A to be contrasted with ≈ 10^{-11} A when Source 1 was in use), one is inclined to put the blame on the space charge effect. This is despite the fact that the measuring system was constructed from electrically good conducting materials which by itself will prohibit the building up of high concentration space charge. The space charge voltage can be estimated by considering the surface as a thermionic cathode and the grid system as anode of a parallel electrode diode. The presence of space charge will modify the velocity distribution of the emitted electrons which otherwise would be a Maxwellian. It can be shown that in an idealised case when the emitted electrons are of homogeneous velocity corresponding to the most frequent velocity of the Maxwellian distribution, a space current larger than that expected by Child's law will be injected into the space in front of the cathode [10], equivalent to a small potential V_m. The magnitude of V_m is given by

$$i = i_o \exp\left(-\frac{eV_m}{kT}\right)$$

where i is the current density which can overcome the space charge potential, while i_o is the current when the anode potential is high enough to collect all the emitted electrons. The quantity kT in this case is ≈ 0.025 eV. Inserting the experimental values for i and i_o into the equation, V_m was found to be in the order of 10^{-3} V. This value is far too small to account for the observed voltage shift.

(d) In the past, contact potential difference between the target and the grid was frequently quoted as the cause of the shift of the ejected electron energy peak. The contribution from contact potential was estimated by the following means. The retarding grid and the collector were connected electrically and then connected to two polystyrene capacitors (C_A = 100 pF, C_B = 1000 pF) as shown in Fig. 5.8. The capacitors were then connected to the target and to a Hameg Digital Storage Oscilloscope (HM208) which was floated. The technique works on the basis that if there is a contact potential difference between the grid and the target, then both capacitors will be charged up to that potential. When capacitor A is shorted out instantly, capacitor B will be discharged through the input impedance of the oscilloscope (1 MΩ); and a pulse will be registered on its screen which gives the value of the potential. With this technique, it was found that the contact potential difference was about 0.2 V with the target positive, a value which does not account to the ≈ 2 V shift observed in the EDCs.

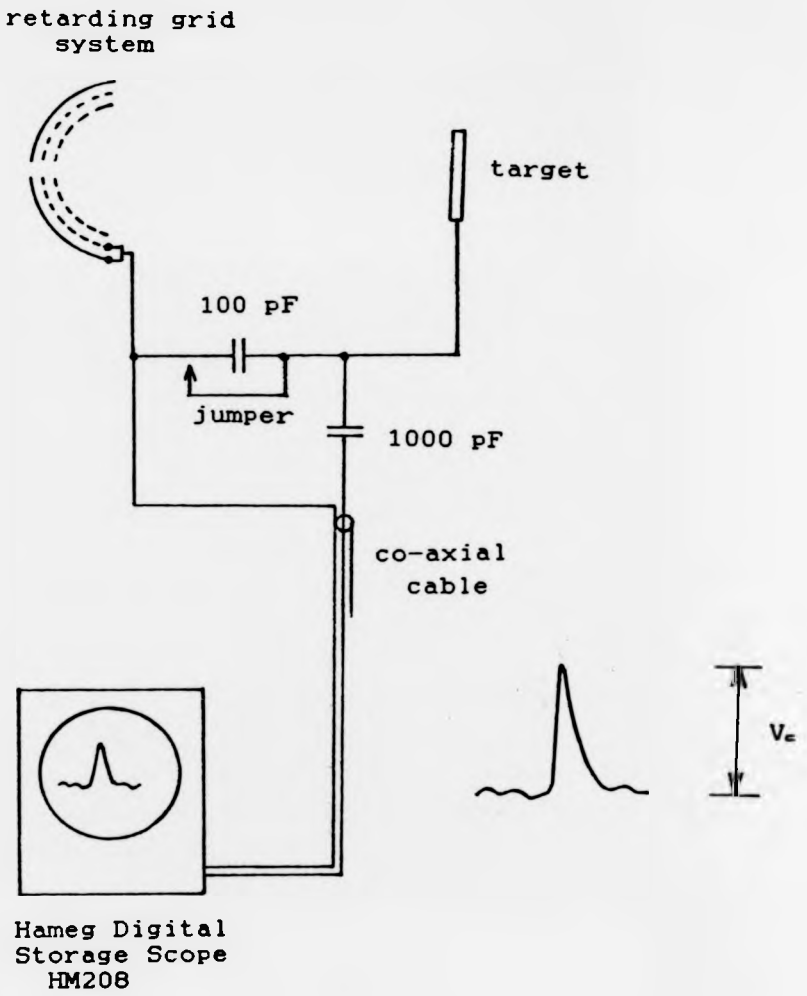

Fig. 5.8 : Experimental set-up to measure the contact potential difference between the target and the retarding grid.

It is a pity that the contact potential between the lithium target and the grid was not measured. The work function of the materials used in the experiments are: 2.38 eV for lithium, 4.3 eV for gold, and 4.5 eV for tungsten [11] (**NB**: the grids were made from gold plated tungsten mesh). Since contact potential is the difference in the metals' work function, then the Li - W/Au combination could show the energy shift the Au - W/Au combination could not, i.e., we may expect to see a difference of ≈ 2 eV in the energy shift between the two targets. As we may see from Figs. 5.1-5.3, the energy shifts shown by the two targets are almost equal, which suggests that contact potential difference is not the cause of the observed energy shift.

(e) The last and perhaps the most likely explanation is that the beam from Source 2 was itself directly or indirectly a source of "unwanted" electrons which were injected into the intergrid space. While an explanation as to how these electrons are related to the "negative energy electrons" has yet to be found; further experiments are necessary in order to confirm the existence of the "unwanted" electrons. One such experiment, for example, is to isolate the fast neutral beams from the grid system by incorporating a tube like passage for the beam from the collimator to the target. However, due to time constraint, no such experiment was tried. Furhter discussions on the purity of the fast neutral beams from Source 2 will be given in Section 5.6 of this thesis.

In summary, the puzzle of "negative energy electrons" as observed by the author has yet to be explained. Surely there is a logical expalanation for it, although nothing concrete the author can offer, at least for the time being.

The shifting of the ejected electron energy towards a lower value as the beam energy is increased can be explained if we subscribe to the idea that the electrons are generated deep under the surface. The mean depth of origin of the electrons should be comparable to the mean projectile range ($\langle R_p \rangle$) of the fast neutral atoms, i.e., the mean perpendicular distance measured from the target surface travelled by the fast neutral atoms before they lost their ability to transfer energy to the metal electrons. Lindhard and Scharff [12] calculated $\langle R_p \rangle$ for energetic ions in solid target, and found that for low energy range $\langle R_p \rangle \alpha E^{2/3}$.

where E is the ions' initial kinetic energy. The proportionality constant is a weak function of the atomic number and mass of the projectile and the target atom, which for a given target material has a value which is larger for a lighter projectile. This means that for a given projectile, the higher the energy the larger the mean depth of origin of the secondary electrons. Equally true, for a given projectile energy, the lighter the projectile the larger the mean depth of origin of the electrons. On their way to the surface the electrons lose their energy through interaction with lattice electrons and lattice vibrations (phonons), a process which is essentially governed by the exponential law [13]. Therefore, secondary electrons which have to travel a longer distance towards the surface will lose more energy in the process, and on exit the surface, are left with less kinetic energy.

The effect of surface temperature on the process of electron ejection was investigated by determining the EDCs of the electrons at three different target temperatures, i.e., 310 K, 380 K and 510 K. The experiments were carried out with 5 keV Ar beam and the gold surface. In this temperature range, the electrons were essentially the secondary electrons; the chance of having contribution from thermoelectrons is negligible. The EDCs obtained from the experiments are shown in Fig. 5.9. The results show that in the temperature range the electron ejection process is unaffected by the target temperature. This observation suggests that during escape the secondary electron's interaction with the lattice vibrations is marginal. In

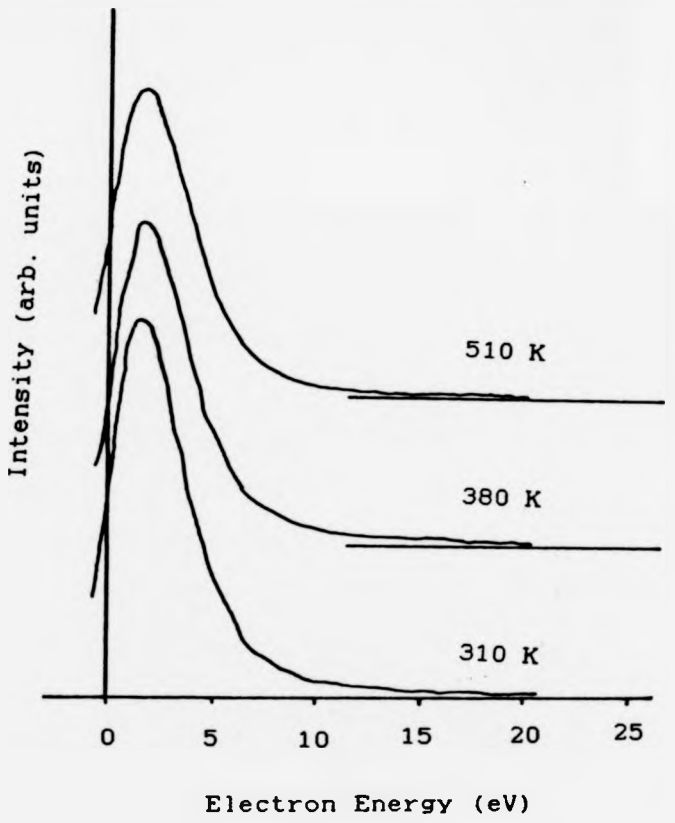

Fig. 5.9 : The EDCs of the ejected electrons from gold surface under the bombardment of 5.1 keV Ar beam: Target temperature as a parameter.

theory, we may expect a small target temperature effect on the ejected electrons in terms of their intensity and energy. This is so because as the target temperature increases the Debye-Waller factor of the target increases as well, which means that the electrons mean free path will decrease and hence their energy and chance to escape from the surface. To observe this effect, the target temperature must be raised to a value close to its melting point. However, this idea was not tested.

To conclude this section, the discussions are summarised as follows:

(i) The energy spectra of the ejected secondary electrons show a common structural feature irrespective of the beam type and the surface atom. The majority of the electrons have energy below 5 eV, and a significant portion of them have zero energy, which remains unexplained.

(ii) The electrons are produced in the bulk of the surface, and on escape their interaction with phonons is negligible.

5.3 The measurement of the secondary electron emission yield coefficients (γ^*)

5.3.1 The measurement technique

The secondary electron emission yield coefficient was determined by measuring the average number of secondary electrons ejected from the surface per incoming fast neutral atom. The measurements were for normal incidence and the

experimental set-up is shown schematically in Fig. 5.10. The target was floated at -27 V to ensure that all the secondary electrons would leave the surface, and the ejected electron current read by K602 would give their number. Assuming we know the beam energy, the number of the incoming fast neutral atoms can be measured using the thermistor-based absolute bolometer which was described earlier. In order to avoid a collision between the bolometer and the target, the former was positioned 2 cm in front of the latter and when the fast atom beam was required to hit the target it was retracted from the path of the beam by a distance of 2 cm. The reading of the position dial on the manipulator on which the bolometer was mounted was taken so that the collector could be positioned back in the path of the fast atom beam when necessary. If I_e is the ejected electron current in ampere (A), E is the energy of the fast atom beam in electron-volt (eV) and P is the beam power in Watt (W), then by assuming a total energy accommodation, the secondary electron yield coefficient (γ^*) is given by

$$\gamma^* = \frac{I_e E}{P}$$

5.3.2 The dependence of yield coefficients on energy and type of the fast atom

Measurement of the yield coefficients was carried out with all the five gases (H_2, He, Ne, N_2 and Ar) on lithium and gold surfaces. The experiments started with the heavier gas so that at the target localised cleanliness could be

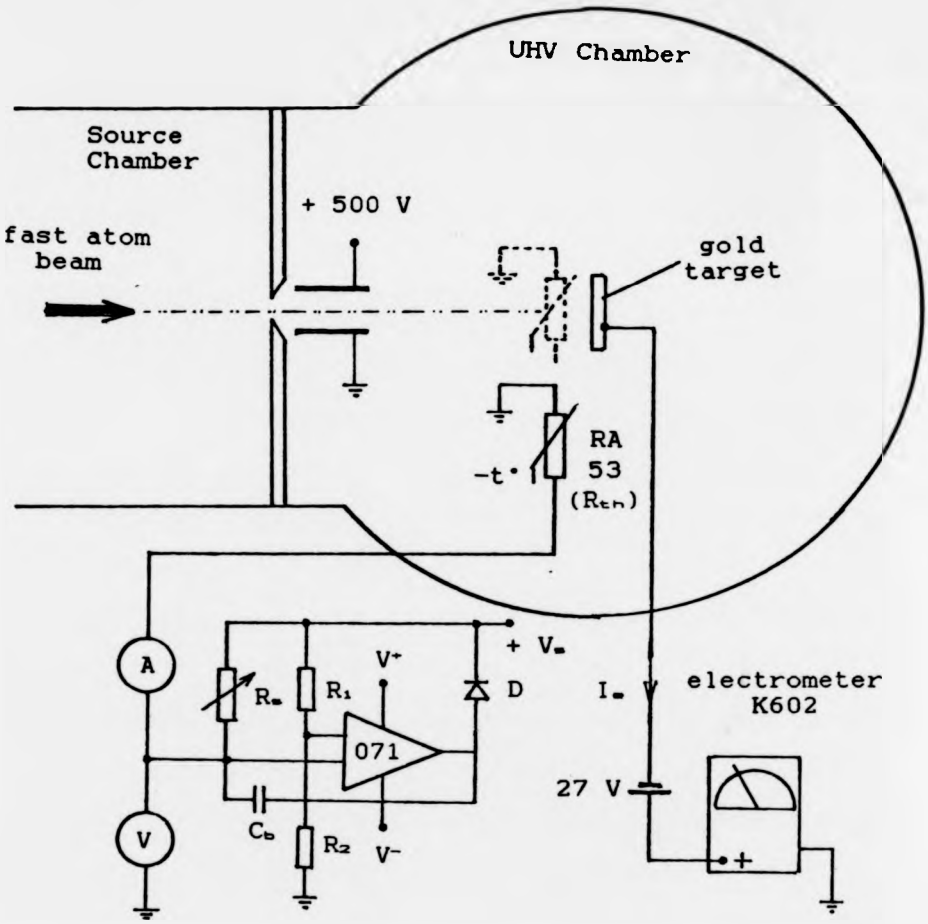

Bolometer

Fig. 5.10 : Schematic diagram showing the experimental arrangement for the measurement of secondary electron yield coefficient (γ^{o}).

achieved and maintained. Unfortunately only data in the energy range of Source 2 could be obtained; attempts to measure the yield coefficient with Source 1 were not fruitful because the beam power produced by the source was comparable to or less than the sensitivity of the bolometer. Results obtained from the gold surface are shown graphically in Figs. 5.11-5.12 and those from the lithium surface are in Figs. 5.13-5.14.

In the beam energy range of 2.5-7 keV, results from the gold surface show two distinct features:

(i) γ^* increases linearly with the beam energy

(ii) the yield coefficient shows strong dependence on the type of the collider; γ^* decreases with increasing atomic number of the fast atom.

Secondary electron yield coefficient data between fast neutral atoms with metal surfaces are very scarce - the list for such experiments is quickly exhausted (See Chapter One). Except the degassed Mo surfaces used by Arifov et. al. [14] and Medved et. al. [15], the other surfaces were not treated beyond rinsing with detergent. All the experiments were performed before 1970 and were in poor vacuum conditions, i.e., not better than 10^{-7} torr, therefore it is not surprising then that the yield coefficients obtained in some of the experiments are nearly independent of the type of gases and targets used [16].

In the era of UHV, there is again an unfortunate general lack of experiments involving fast neutrals with surfaces. In the case of this experiment, comparison with data from other laboratories cannot be made simply because

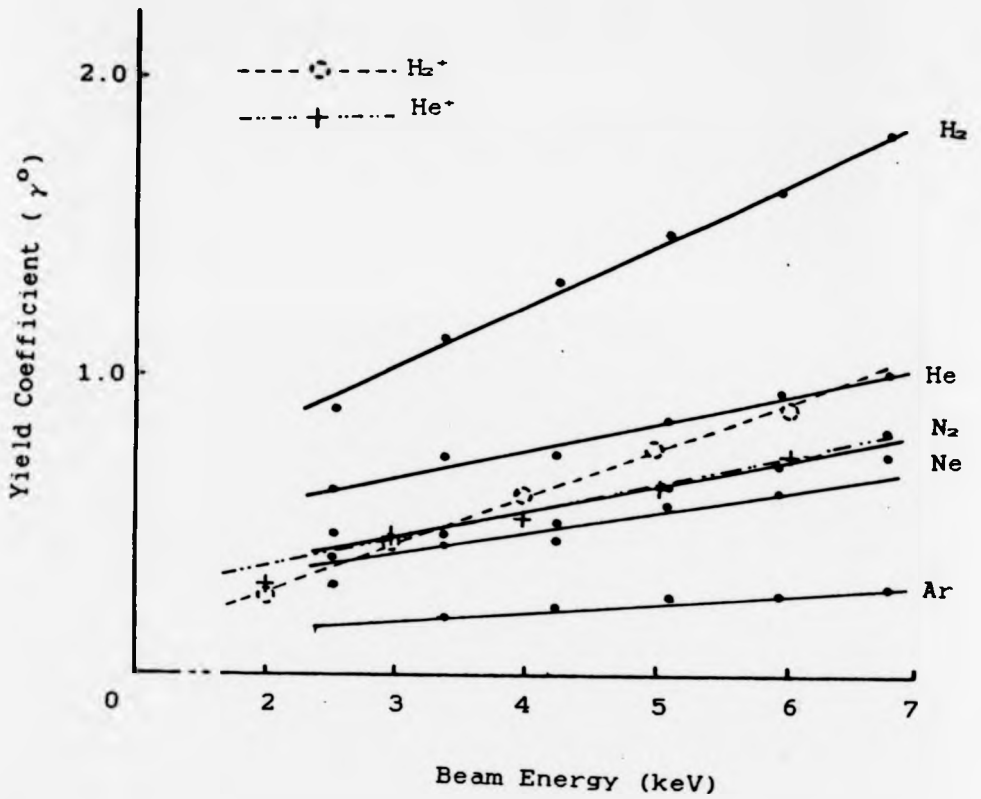

Fig. 5.11 : Graphs showing variation of ejected electron yield coefficient with fast atom energy (Gold surface). Dashed lines are results interpolated from graphs of ion-induced kinetic electron emission yield coefficient measured by Baragiola et. al. [18].

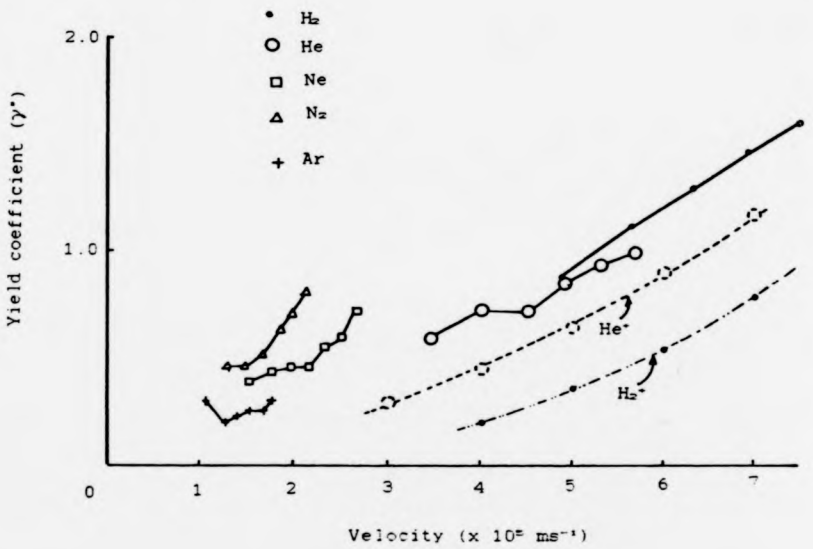

Fig.5.12: Graphs showing variation of ejected electron yield coefficient with fast atom velocity (Gold surface). Dashed lines are results interpolated from graphs of ion-induced kinetic electron emission yield coefficient measured by Baragiola et. al. [18].

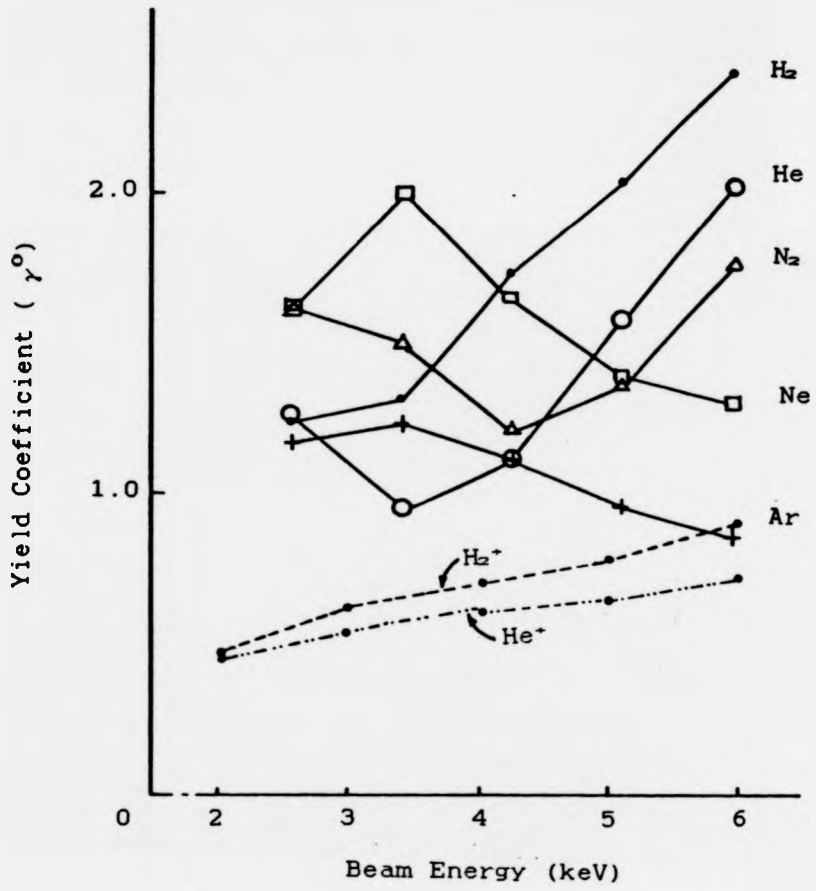

Fig. 5.13 : Graphs showing variation of ejected electron yield coefficient with fast atom energy (Lithium surface). Dashed lines are results interpolated from graphs of ion-induced kinetic electron emission yield coefficient measured by Baragiola et. al. [18].

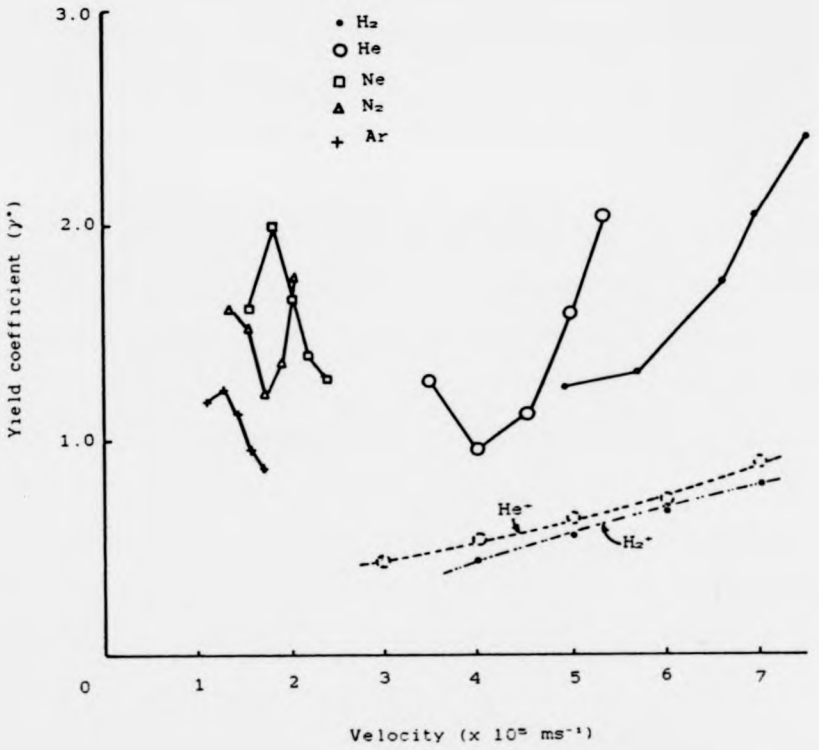

Fig. 5.14 Graphs showing variation of ejected electron yield coefficient with fast atom velocity (Lithium surface). Dashed lines are results interpolated from graphs of ion-induced kinetic electron emission yield coefficient measured by Baragiola et. al. [18].

such data is not available. But however, since the interaction between the fast atoms and the target is purely kinetic in nature, given the same target and projectile species, the secondary electron data could be expected to be the same as those obtained from "kinetic emission" using ion beams. This idea has been considered by Medved et. al. [15] who pointed out that in the energy range smaller than 1.5 keV, neutral inert gas atoms are more readily reflected from metal surfaces than their ionic species. They went on to suggest that in the energy range below 1.5 keV, the yield coefficient obtained with fast neutrals is less than yield coefficient obtained with ion kinetic emission. However, the idea was not well received on the ground that there were several uncertainties in the methods and conditions of their experiments on the particle reflection behaviour. Quite recently, Dixit and Ghosh [17] claim to have verified experimentally that "kinetic ejection of secondary electrons for a given target bombarded by projectiles having identical electronic shell structure and similar masses is the same". The statement certainly means that for a given target and projectile energy, the secondary electron yield coefficient obtained with fast neutrals is the same as those obtained from kinetic emission from positive or negative ions of the same species as the neutrals. On this footing, coefficients of ion-induced kinetic electron emission from clean lithium and gold surfaces (prepared by in-situ evaporation in UHV 99.9% of the target metals followed by sputtering with Ar^+ ions), measured by Baragiola et. al. [18], are interpolated from their yield graphs and inserted in Figs. 5.11 and 5.13.

It must be pointed out that comparing yields of secondary electrons obtained from different laboratories cannot be done without reservation. That is because of the following reasons: (i) in the case of secondary electrons from ion beams, the yields are sensitive to the surface cleanliness and therefore results obtained from different laboratories are bound to differ, sometimes, widely [19], and (ii) as pointed out by Magnuson and Carlston [20], results obtained with polycrystalline targets pose another problem, i.e., possibility of differences in the grain structure which may lead to differences in transmissivity (a quantity which is inversely proportional to the density of lattice points projected on a plane normal to the beam), and hence the secondary electron yield. They measured secondary electron yield using Ar^+ ions (0-10 keV) on three different clean copper single crystal planes ({111}, {100} and {110}) and found that, on all the targets the yield increases with projectile energy, with magnitude for a given projectile energy in the order $\gamma^+_{\{111\}} > \gamma^+_{\{100\}} > \gamma^+_{\{110\}}$. The transmissivity of the three planes is in the order {110} > {100} > {111}.

The lithium surface generally shows higher yield coefficients than those from the gold surface. The lithium's lattice constant of 3.49 Å must be contrasted with gold's 4.08 Å [11], which means that the former is more closely packed than the latter and hence has lower transmissivity. Apart from that, lithium's work function is lower than gold's; since the electrons have had to surmount the surface

barrier prior to their ejection, this quantity must have some bearing on the yield.

The yield coefficients obtained from the lithium target show a mixed dependence on the fast atom energy and its type, as follows:

(i) in the high end of the energy range, the yields show strong dependence on the atomic number of the fast atom; the lower the atomic number the higher the yield,

(ii) with the exception of He, the yield due to the inert gas beams (Ne and Ar) decreases with beam energy, and

(iii) again, with the exception of He, the yield due to the reactive gas beams (H_2 and N_2) increases with beam energy.

The complicated nature of the dependence of the yield coefficients on the beam type and energy is thought to be due to the reactive property of the surface. A layer of a complex mixture of chemical products between Li and H_2, O_2, N_2 and halogen gases might have been formed on the surface and prevented the latter from interacting directly with the fast neutral atoms. The presence of Li_2O has been reported from AES studies on carefully prepared Li surfaces. In one of the reports, the surface was prepared from molten lithium poured into a pre-heated Mo cast (800 °C) and then filed to expose fresh Li surface in UHV chamber (4×10^{-9} torr) which had background gas of mainly H_2 and Ar [21]. In the other, the surface was prepared by fracturing a research grade Li crystal in a strictly argon atmosphere followed by Ar^+ ions bombardment in UHV chamber. In short, the lithium surface used in the experiments was not atomically clean due to

chemisorption, a view which to some extent is supported by the experimental data.

The steady increase shown by the yield curves of H_2 and N_2 with beam energy, may suggest that the two gases see the target as a solid surface made of lithium compounds in their stable chemical phases. The same is also true for the He atoms, which although inert are too light to destabilise the surface. The decrease with beam energy of the yield curves of Ne and Ar may lead one to conclude that as they hit the surface the chemisorption layer is being etched through sputtering, resulting in a cleaner surface, a process which manifests itself in lower yield of secondary electrons. Li_2O, as observed by Schowengerdt [5], stubbornly sticks to the lithium surface even after the surface was bombarded with Ar^+ ions (2.75 keV, 10μA) for 30 minutes. If the theory about the overlayer is true, further increasing the beam energy should cause the yield to pass through a minimum, which coincides with an atomically clean lithium surface, followed by an energy dependent yield increase. However, due to limitation on Source 2, the idea was not tested.

In summary, the efficiency of ejection of secondary electrons depends on the mass of the fast atom and its energy, and also on the type of the surface. There is further evidence that the secondary electrons are generated deep under the surface. The complicated nature of the dependence of the lithium surface's yield coefficient on the fast atom type and energy, is thought to be due to the surface reactive property.

5.3.3 Variation of yield coefficient with angle of incidence ($\gamma^*(\theta)$)

Experiments to determine the variation of the yield coefficient with angle of incidence was carried out with the thicker gold surface only; the other two surfaces were not flat enough for the purpose. Three gases were used with Source 2, i.e., H_2, Ne and Ar. The experimental procedure was very similar to the one used for obtaining normal incident yield coefficients except with one addition, i.e., to provide for the different angle of incidence the gold surface was rotated about an axis perpendicular to the path of the fast atom beam. The yield coefficients were measured in 5° intervals of incident angle, in range 60° either sides of the surface normal.

Qualitatively the results show similar dependence of yield coefficient (γ^*) on angle of incidence (θ) as those obtained by Morita et. al. [22] and Ohya and Mori [23]. The angular dependence also qualitatively similar to those obtained using primary electron beams [1] and ion beams [19]. The yield increases with angle of incidence, and does not depend on the direction of rotation of the target, i.e., $\gamma^*(\theta) = \gamma^*(-\theta)$. A typical plot of $\gamma^*(\theta)$ versus θ is shown in Fig. 5.15; and the rest of the results are presented in Fig. 5.16, in the form normalised to the yield coefficient at normal incidence (θ=0), i.e., as $\gamma_N^*(\theta)$ versus θ, where $\gamma_N^*(\theta) \equiv \gamma^*(\theta)/\gamma^*(0)$.

The dependence of the yield with angle of incidence can be predicted by using the semi-empirical model of kinetic

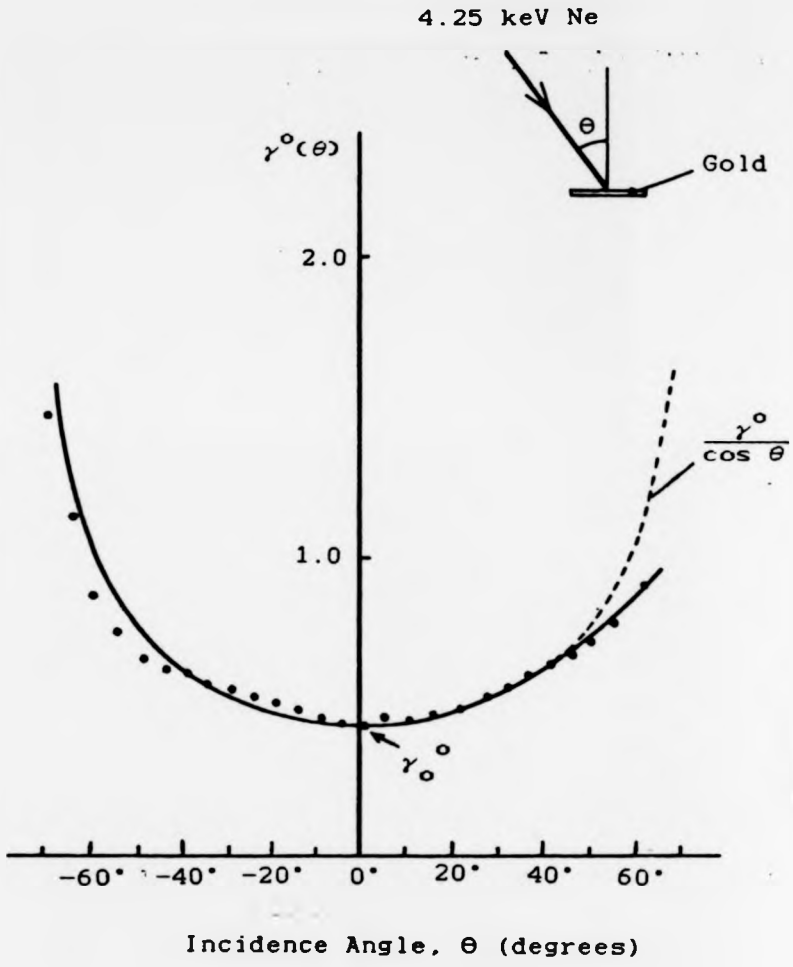

Fig. 5.15 : Graph showing the variation of yield coefficient with angle of incidence (4.25 keV Ne on Gold surface).

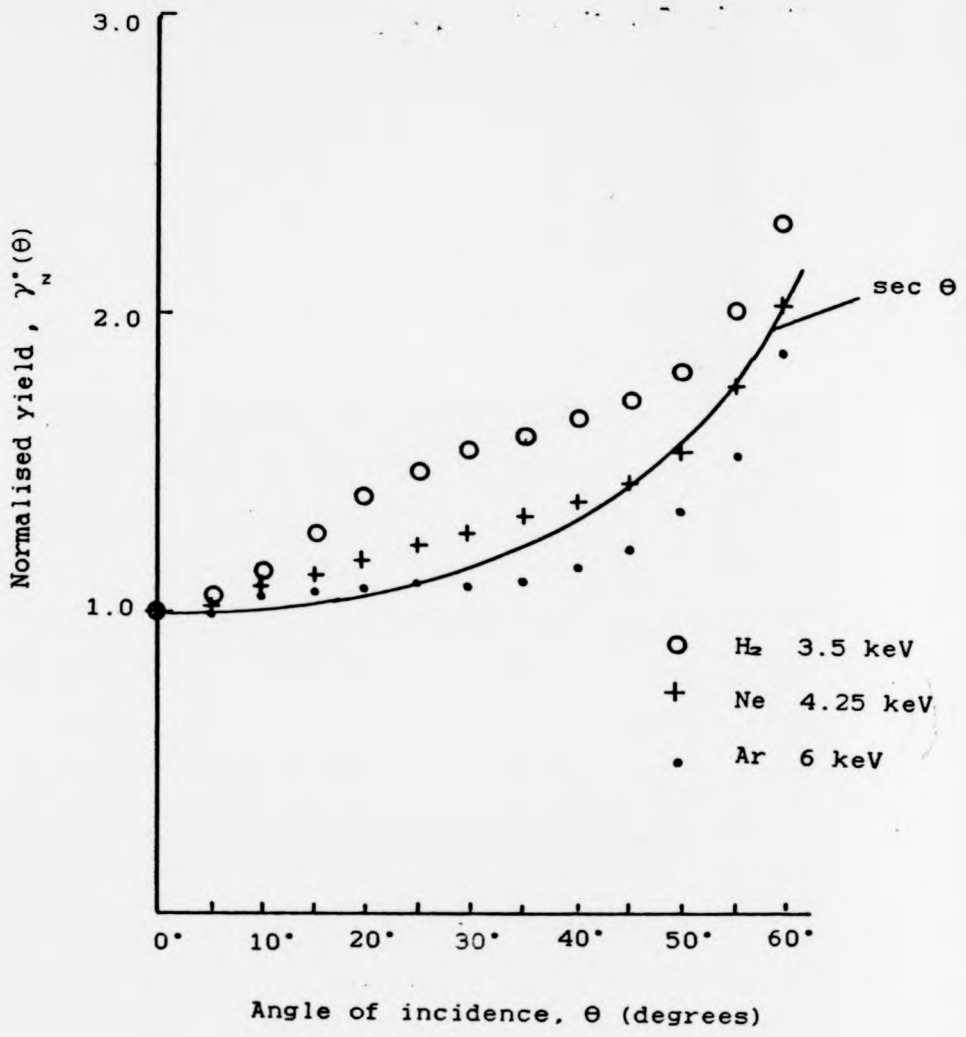

Fig. 5.16 : The variation of normalised yield coefficient with angle of incidence (Gold surface). Solid line is sec θ curve.

electron emission of Baragiola and co-workers [18,24]. Without paying attention to the details of the electron ejection process, the ion-induced yield of secondary electrons can be calculated as follows:

$$\gamma^{\circ} = C \int_{0}^{x_n} N(R)\ e^{-x/L}\ dR$$

where R is the path traversed by the projectile, x the perpendicular distance of the projectile from the surface, N(R) the number of excited electrons produced in dR at R, L the mean electron attenuation length, C is a target-dependent constant, and x_n the distance at which the projectile loses it capability to eject secondary electrons from the lattice atoms. Assuming the projectile takes a rectilinear path, i.e., R = x sec θ, and its electron excitation efficiency is constant over a distance much larger than L, i.e., N(R) = N, the yield equation can be approximated to give $\gamma^{\circ}(\theta) = CLN \sec \theta$.

Results from the experiments show that the normalised yields deviate from the predicted sec θ (solid line in Fig. 5.16). On the one extreme, the normalised yields of H_2 grow faster than sec θ, the higher the energy. On the other hand, the normalised yields of Ar, fall below the sec θ line between θ = 25° to 60°. Following Ferrón et. al. [25], within the range of the experimental incident angles, the normalised yields can be adjusted to the expression $\gamma^{\circ}(\theta) = \sec^{f}\theta$. The exponent f depends on energy and mass of the projectiles - increasing with increasing energy and

decreasing with increasing mass of projectiles. By introducing a correction factor in N(R), i.e.,

$$N(R) = N(0) + R \left(\frac{dN}{dR} \right)_{R=0}$$

the authors obtained

$$f = 1 + \frac{AL}{1 + AL} \qquad \text{where} \qquad A = \frac{1}{N(0)} \left(\frac{dN}{dR} \right)_{R=0} .$$

where A is the normalised gradient of the density of excited electrons at the surface (i.e., $|AL| < 1$). The equation is valid only for $\Theta < 60^{\circ}$ and small A. Evidently, the exponent f will be greater than 1 if A positive, and otherwise when A negative.

Physically, f<1 means fewer electrons per unit path length are being ejected as the projectiles traversed into the near surface region. Evdokimov et. al. [26] pointed out that the near surface region, especially the second layer atoms, are shadowed by the surface atoms, and creates what they called a "transparency effect". The larger the incidence angle the more opaque the region; hence, less collisions take place which result in lower yield of ejected electrons. The significance of the near surface region in this context is that it is the region of larger escape probability. If the model is true, the larger the incidence angle the further down the normalised yields fall below the sec Θ line, which is generally the trend of the results. Morita et. al. [22] attributed the lower yields to the reflectance of fast neutral atoms, which presumably increases with angle of incidence.

On the contrary to the situation discussed above, f>1 means more electrons per unit length produced as the

projectiles traverse their way into the solid. According to Ferón et. al., this may be brought about by three processes:

(a) generation of excited electrons by recoiling atoms,

(b) non rectilinear trajectory of the projectiles, and

(c) anisotropy in the source of the excited electrons.

By means of Monte Carlo simulations, the authors followed the trajectories of the projectiles and the recoiling atoms and found that the effect of (a) and (b), if they are acting alone, will cause $f>1$. The recoiling of the target atoms becomes important only if $(M_{target}/M_{projectile}) > 1$. However, the collective contribution from both effects is small and practically negligible.

Knowledge of angular dependence of secondary electron yield has two applications:

(1) Following Bruining [1], it is possible to estimate the mean depth of origin of the secondary electrons from the yield coefficients. Let 0 and Θ denote the angle of incidence, then

$$\gamma^*(0) = C\, e^{-x_m/L} \quad \text{and} \quad \gamma^*(\Theta) = C\, e^{-(x_m/L)\cos\Theta}$$

where C is a target characteristic constant, x_m the mean depth of origin and L the mean attenuation length of the secondary electrons. Cancelling C from the equations, we obtain

$$x_m = L\,\frac{\ln(\gamma^*(\Theta)/\gamma^*(0))}{1-\cos\Theta}$$

Note that, this equation is only valid in the range of incidence angle for which the sec Θ law is obeyed.

(2) According to Ohya and Mori [23], at incidence angle greater than 60°, the normalised yield is a linear function of fast atom energy, i.e.,

$$\gamma^*(\theta,E) = k(\theta,E) = a\,E + b$$

where a, b are constants which are characteristics of the target material and E is the beam's mean energy. They showed that the equation can be utilised in designing a secondary electron detector (SED), which can be used for measurement of absolute flux density of fast neutrals of unknown energy distribution, and determination of ion temperature of a Maxwellian plasma.

In summary, the angular variation of the secondary electron yield shows little variation with the sec θ law, which provides another evidence that the electrons are generated in the bulk of the surface.

5.3.4 The angular distribution of the secondary electrons

The geometrical arrangement of the fast atom beam, gold target and rotating probe for the determination of the angular distribution of the secondary electrons is shown in Fig. 5.17. The probe for the electrons was a tungsten strip 1.5 mm wide and 30 mm long, mounted on a simple rotary manipulator so that it could be rotated around the surface plane in a 40 mm radius. With that arrangement, the probe subtended 2° at the target surface and 40° at right angle to the plane of rotation. The target was at earth potential and the probe was connected to K602 with its output connected to the ADVAL Port of the BBC microcomputer. The experiments

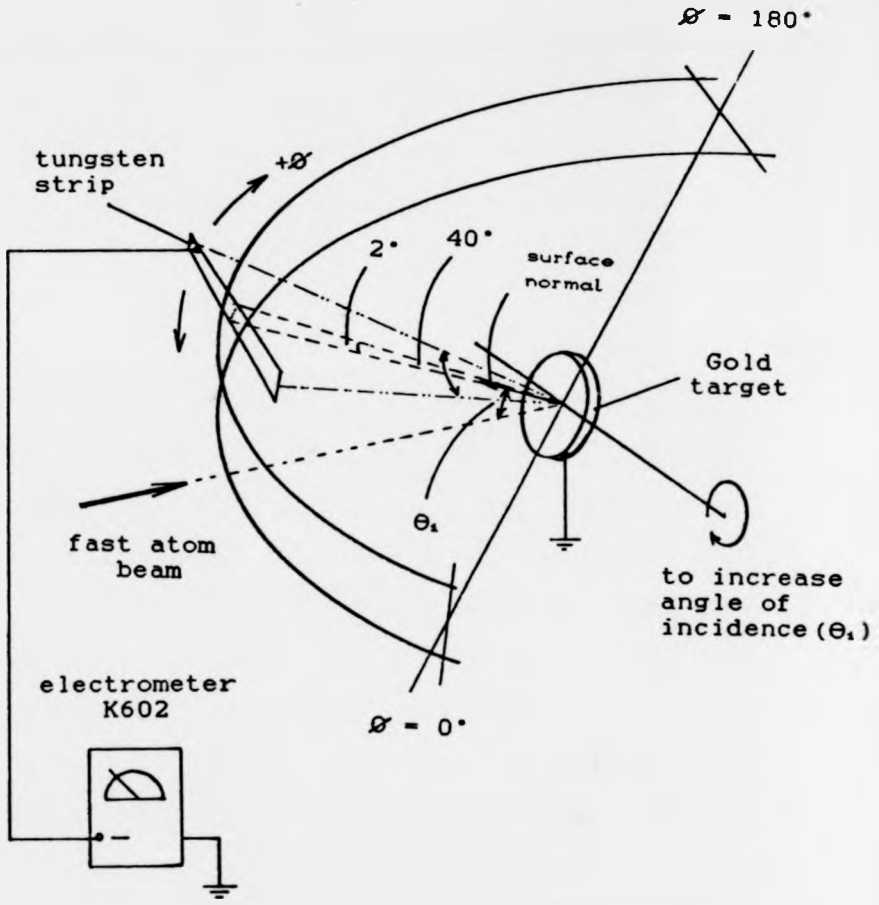

Fig. 5.17 : Schematic diagram showing the geometrical arrangement of fast atom beam, gold target and a rotating tungsten strip for the determination of angular distribution of the ejected electron.

were run by rotating the probe at 5° intervals around the surface plane, through a full 180°. Fig. 5.18 shows the angular distribution of the secondary electrons (polar plot) for various fast atom beam angles of incidence.

In general, the polar plots show that most of the secondary electrons are ejected in direction around the normal of the target surface. The increase in area bounded by the curve with the increasing angle of incidence is just another indication that the electron yield is increasing with angle of incidence. The lobes which appear in the lower half of the graph are due to the secondary electrons leaving the probe as the latter is hit by the backscattered fast neutral atoms. These lower lobes show that the number of the backscattered fast atoms peaks at angles around 65°-70° irrespective of the angle of incidence, and it increases sharply with angle of incidence. This suggest that the backscattered fast atoms are not due to specular reflection, but to the so-called rainbow scattering as observed by Nielsen and Delchar from a single crystal tungsten surface [27]. This is possible since a rolled foil of gold may have patches of ordered facets on its surface, which collectively contribute to the observed rainbow scattering effect, and anyway fast atom scattering does not require long range surface order. However work in this area with the gold surface was not pursued due to the fact that fast atom scattering data will only be useful if it is associated with a surface of known geometry, or at least of known structure.

Qualitatively, the angular distribution of the ejected electrons is similar to those obtained with electron and ion

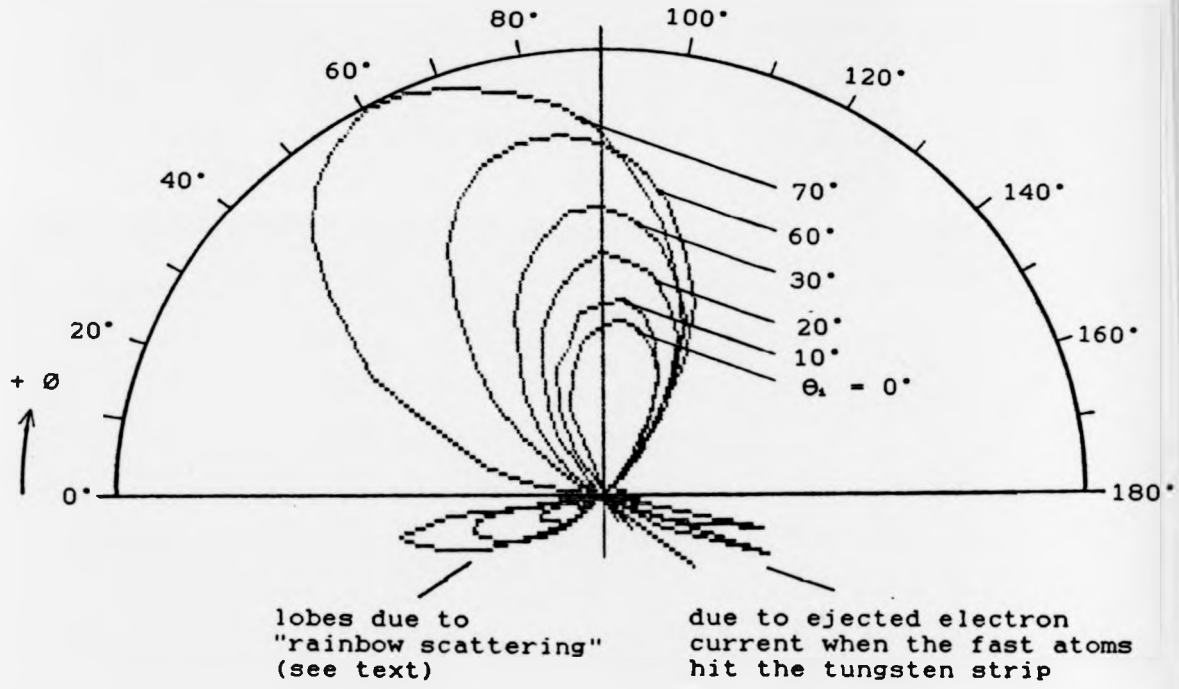

Fig. 5.18 : Angular distribution of the ejected electrons: angle of incidence (θ_1) is a parameter.

beams, although the polar plots do not exhibit a perfect cosine distribution as shown by electron [1] and ion beam [28]. A cosine distribution associated with backward ejected secondary electrons has been taken in the past as a proof of isotropy in the ejection process.

Closer examination of Fig. 5.18 shows that at large incidence angles, the ejected electrons leave the surface in a preferential direction, i.e., at angles slightly tilted towards the fast atom direction. It is a pity that the experiments were only carried out on a single quadrant of the surface (see Fig. 5.17), therefore the behaviour cannot be concluded without doubt. If the behaviour is real, there are two possibilities which may explain it: the effect of the earth magnetic field, and or, the existence of an anisotropic element in the ejection process.

To evaluate the effect of the earth magnetic field, the latter was measured using a three axis Bell 640 Gaussmeter with respect to the direction of the fast atom beam, and the measured components are shown in Fig. 5.19. By taking the electron initial energy as 1 eV, and its initial direction as normal to the surface plane, the trajectory of the electron in the three dimensional space defined by unit vectors $\hat{x}$, $\hat{y}$, $\hat{z}$, under the influence of the Lorentz force $\vec{F} = -e\,\vec{v} \times \vec{B}$, is calculated by solving the equation of motion point-by-point in time intervals of 5×10^{-10} s. The point where the electron reaches the strip detector is determined by imposing the condition that $\sqrt{(x^2+z^2)} = 40$ mm, i.e., the sweep radius of the strip detector. Results from the calculations with three electron initial velocities,

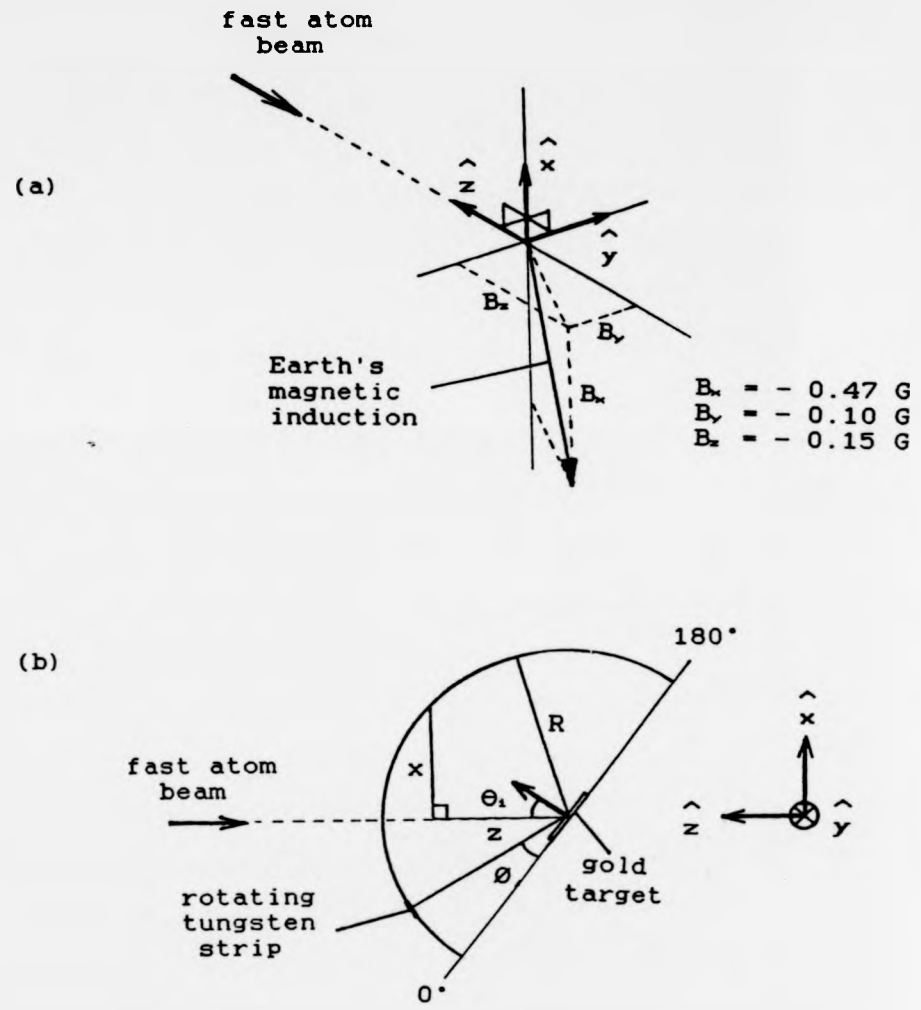

Fig. 5.19 : (a) The components of earth's magnetic induction (B) with respect to the direction of the fast atom beam.

(b) Side view showing the ejected electron initial velocity with respect to the fast atom beam direction and the earth's magnetic induction.

i.e., 1 eV, 2 eV and 25 eV, are given in Table 5.1. It was found from the calculation that for the incidence angle between 0° to 70°, the electron reaches the strip detector within 0.2°-3.4° from the surface normal, towards the fast atom beam. In other words, the earth's magnetic field is not the cause of the observed direction preferring behaviour shown by the ejected electrons at large incidence angle.

In a similar study using 40 keV Ar^+ ions on a clean Al polycrystalline target, Mischler et. al. [29] found that the angular spectra of the ejected electrons follow cosine distribution but have additional structure which is persistently linked to the Ar^+ ion beam angle of incidence. They tentatively proposed that the ejected electrons are a mixture of true secondaries and Auger electrons $L_{23}M_1M_{23}$; whilst the true secondaries are produced isotropically and formed the cosine background of the spectra, the direction preferring structure is thought to be due to the Auger electrons which are produced anisotropically. There are two competing reasons with which the direction preferring behaviour of Auger electrons may be explained, namely, the inherent anisotropy of the three electron state from which they originated, and the "easy" channeling formed by the lattice ion and adatom cores in the exit vicinity. With the polycrystalline target used in this experiment, the second reason seems to be unfounded. More experiments with a perfectly flat and well defined surface are needed before the idea can be fairly judged.

Table 5.1 : The calculated position of the ejected electron (in mm) in the direction of the unit vectors **x**, **y** and **z** (see Fig. 5.19), in the presence of earth magnetic field, for three different electron initial energies (E_i) and various fast atom beam angle of incidence (θ_i).

Angle of Incidence (θ_i)	E_i = 1 eV			E_i = 2 eV			E_i = 25 eV		
	x	y	z	x	y	z	x	y	z .
0°	−2	12	40	−2	8	40	−1	2	42
10°	5	11	40	5	7	40	6	2	42
20°	12	10	38	12	7	38	14	2	40
30°	19	8	35	19	5	35	21	1	37
40°	24	6	31	25	4	31	27	1	33
50°	29	4	27	30	3	26	32	1	27
60°	34	2	21	34	2	21	36	0	21
70°	37	0	16	37	0	15	40	0	15
80°	39	−2	9	39	−1	8	42	−1	8

In summary, the ejected electrons leave the surface in a solid angle about the surface normal, and the polar plot does not follow exactly the perfect cosine distribution.

5.3.5 Model for fast atom interaction with a metal surface

In principle, we may draw a parallel between the ejection of secondary electron from metal surface caused by bombardment with fast neutrals and that of ion-induced kinetic electron emission. Results from the experiments have shown very good agreement, at least qualitatively, between the two processes in the following aspects: very low secondary electron energy (< 5 eV), emission yield coefficient which varies linearly with projectile energy and follows sec Θ law with angle of incidence, and cosine angular distribution.

There are several theories proposed for ion-induced kinetic electron emission [19]; we shall examine each of them to see if it fits with the results obtained with fast neutral atoms:

(i) It was proposed that the ejected electrons are thermal electrons emitted from a microscopic hot zone as a result of the surface been heated by the impact of the energetic incident projectile. By assuming a statistical thermodynamic equilibrium for the very rapid energy exchange between the projectile and the surface atom, the theory predicts that the ejected electrons would have a Maxwellian energy distribution with mean energy equivalent to tens of thousands of Kelvin, a figure which is smaller than the experimental value, obtained with fast neutrals and ions alike, by three orders of magnitude. This "thermal" theory was severely criticised by many authors [19,39] for its

improper use of Richardson's thermionic emission formula, and also to the fact of very poor energy exchange between the lattice of the target and its conduction electrons.

(ii) It was also proposed that the secondary electron emission is due to an interaction between the free metal electrons and the electromagnetic field generated by the rapidly retarded charged projectile. Clearly it is hard to see how this could be applied to fast neutrals which carry no nett charge to generate the electromagnetic field.

(iii) One may be tempted to think that the secondary electrons result from a direct "knock out" of the metal free electrons by the incoming projectile. In this case, the transferred energy, $T \alpha Eo$; but however, experimental results obtained with fast neutrals and ions alike show that the EDC of the ejected electrons remains virtually unchanged with the projectile's energy. It was also pointed out that, due to the large size and mass difference between the projectile and the free electron, the probability for a direct collision between the two is very small.

(iv) Perhaps the most successful theory for low energy ion-induced kinetic electron emission is the so-called "standard theory" of Parilis and Kishinevskii (PK) [30]. PK proposed that like the potential ion-induced electron emission (i.e., INS), the kinetic electron emission is formed mainly by Auger electrons, although the mechanisms of excitation in the two processes are different. During the violent collision energy is transmitted from the ion to the lattice atoms due to deformation and overlap of the electron shells, analogous to the Firsov's friction model. In the

process, the lattice atom is ionised, in which a hole is created in the filled band. Thus PK assumed that the inner shell ionisation cross-section is essentially the cross-section for the formation of an electron-hole pair. Then with relatively large probability, "there occurs a recombination of a conduction electron with the hole, accompanied by the transfer of energy to another conduction electron (the so-called Auger recombination)". The ejection of electron into the vacuum is energetically possible if the inequality $\delta > 2\emptyset$ is fulfilled, where δ the depth of the filled band where the hole is created and $\emptyset$ the work function. PK proposed that analogous to the Auger transition in potential extraction of metal electron under the action of inert gas ions, Hagstrum's empirical formula for the electron ejection $w(\delta)$ is equally applicable in kinetic ejection, that is,

$$w(\delta) = 0.016\ (\delta - 2\emptyset)$$

which already includes the probability of surmounting the surface potential barrier.

PK's theory can explain the form of the ejected electrons' EDC, which has a maximum in the low energy region (1-3 eV). It also predicts that the electron maximum energy equals $(\delta - 2\emptyset)$. Up to this stage, the theory shows good qualitative agreement with the EDCs obtained from experiments with fast neutral atoms, although due to the shape of the high energy tail of the EDCs it is not clearly evident if the maximum energy $(\delta - 2\emptyset)$ is strictly obeyed. In the case of a gold target, $\delta = 20.5$ eV and $\emptyset = 4.3$ eV, applying the theory we may expect maximum electron energy at

11.9 eV. However, it is inappropriate to dismiss PK's theory simply on this basis because the high energy tail may well contain the energy loss electrons originated during the creation of holes in the filled bands. Nevertheless, to some extent the theory can explain the seemingly equal maximum energy of ejected electrons obtained with different fast atom gases on the gold surface.

In the case of lithium target, δ = 76 eV and $\emptyset$ = 2.4 eV; following PK we may expect maximum electron energy at 71 eV, whereas the observed value is a factor of five lower. Since results obtained with the lithium target have indicated that the surface is not atomically clean, therefore it is inappropriate to speculate on the applicability of PK's theory in this respect.

By assuming an exponential decay law PK calculated the coefficient of electron emission using

$$\gamma^{+}(u) = \int_{0}^{x_n} \sigma(u)\ w(\delta)\ N\ e^{-(x/L)}\ dx$$

where N is the density of the metallic atoms, $\sigma(u)$ the ionisation cross-section, u the projectile velocity, x_n the depth at which the projectile loss ability to ionise the lattice atom and L the characteristic attenuation length. PK's theory predicts that in the energy range immediately after the threshold energy, $\gamma^{+}(E) \propto E$, where E is the ion energy, and in the higher energy range the energy dependence gradually changes to $\gamma^{+}(E) \propto E^{\frac{1}{2}}$. The energy dependence of the fast neutral induced KEE yield coefficients obtained

from the gold surface show a very good agreement with the PK's prediction.

(v) Quite recently, Baragiola et. al. [18,24] dismissed the importance of inner-shell excitation and subsequent Auger decay, which the central idea of PK's theory, as the main mechanism for ion-induced electron kinetic emission. Their argument was based on the experimental data of ion-induced L-shell ionisation cross-section of aluminium which are very low (σ_i = 8 x 10^{-23} m^2 at 15 keV and = 7 x 10^{-22} m^2 at 50 keV). They also pointed out that the energy dependence of the yield coefficient in the energy range does not contain the increase in σ_i which is about 10 whereas the former is only about 1.6. Since data of fast atom-induced inner-shell ionisation cross-section for gold is not available, we cannot evaluate PK's theory on the same footing.

As an alternative Baragiola et. al. proposed that the kinetic emission results mainly from the escape of excited valence electrons. This is equivalent to the theory put forward by Kirson et. al. [6] who assume a dominant single electron-hole excitation for the ejection process. Although Baragiola et. al. did not discuss the form of the ejected electrons' EDC, following results from calculations of Kirson et. al. on a lithium surface, single electron-hole excitation will yield electrons with most probable energy of 10 eV and higher, and maximum energy which goes beyond 100 eV. Again, due to the poorly defined lithium surface, we are not in a position to dismiss Kirson's results based on our experimental observation with the lithium surface.

To explain the energy dependence of the yield coefficient, Baragiola et. al. proposed a semi-empirical model for the ejection process, as follows:

The number of electrons excited by the projectile above the vacuum level in the depth interval x and x + dx is

$$n(x)\ dx = \frac{S_e(E)}{J}\ dx$$

where $S_e(E) \equiv -(dE/dx)$ is the electronic stopping power and J the average energy spent by the projectile to excite an electron into the vacuum. On escape, the electron cascade and attenuation follow the exponential decay law, that is, P exp(−x/L) where P is the average escape probability and L the attenuation characteristic length. Thus, in the path-length approximation:

$$\gamma^+ = \frac{P}{2J} \int_0^\infty S_e(E)\ e^{-(x/L)}\ dx$$

Since L is in the order of nm, they expect the energy of the projectile and therefore S_e, not to vary very much over the escape distances. When the term $S_e(E)$ is taken outside the integral, they obtain:

$$\gamma^+(E_o) = \frac{PL}{2J}\ S_e(E_o)$$

where E_o is the projectile initial energy. Results from calculation of atomic projectile range in solid by Lindhard and Scharff [12] show that $S_e(E_o) \propto E_o^{2/3}$. Substitute this into Baragiola's yield equation, we may expect that $\gamma^+(E_o) \propto E_o^{2/3}$, which clearly does not agree with the observed experimental results obtained with fast neutrals on

the gold surface which show $\gamma^{*}(E_o) \propto E_o$. The discrepancy of this theory with the experimental results may be due to the omission of the effect of nuclear stopping in Baragiola's model. Calculations of total stopping power which are based on Lindhard, Scharff and Schiott (LSS) theory, show that the individual contribution of nuclear and electronic stopping power varies over the projectile energy range [31], with the nuclear stopping dominates at low energies. The inclusion of nuclear stopping power into Baragiola's model is necessary in order to evaluate it fairly, especially in the low energy region. At higher energies electronic stopping dominates, and following the LSS theory in the energy region, $S_e(Eo) \propto E_o^{\frac{1}{2}}$; which means that both PK and Baragiola KEE models predict the same energy dependence for the yield coefficients.

So far the experimental results agree quite well with the PK's KEE model. However, PK's theory does not free from shortcomings. It is impossible to use the model to explain the observed high secondary electron yields from insulator surfaces, which are known to have no conduction electrons. The concept of direct excitation of valence electrons, which is the central idea of Baragiola's KEE model, when applied together with the concept of dominance electron-electron interactions during escape process, can be used to explain the high KEE yields of insulators [37]. The same arguments also explain the comparable KEE yields of metals and semiconductors. Judging the PK and Baragiola models together, the eminent question is the relative importance between the two mechanisms used. Using the Al L-shell

excitation cross-sections which were measured by Benazeth et. al. [38], Baragiola et. al. show that the KEE mechanism as proposed by PK is not significant especially at low energies and with light ions. However, more reliable data of valence electron ionisation cross-section are needed before PK's KEE model be dismissed confidently. This is true because, with the aid of sensitive electron spectrometer of high resolution, Auger electrons resulting from ion bombardments have been observed by Benazeth et. al. [35]. It was found that the Auger spectra not only originating from the target but from the collider as well. This certainly subjects the modelling of the KEE mechanism to an even wider possibilities.

In summary, there is no conclusive model to account for the kinetically emitted secondary electrons, and thus the same is true for fast neutral-induced KEE. Kirson et. al. have shown that fast neutral-induced electron-hole excitation in metals is a process of observable probability; therefore Baragiola's empirical model for KEE is a thing to be seriously considered. More data on fast neutral induced secondary electron in general, and on valence electron ionisation in particular, is needed in order to develop a working model of neutral induced KEE.

5.4 Ionisation of fast atoms by metal surfaces

According to Souda and Aono [32], during the ionisation of fast neutral atoms by metal surfaces, the former suffer inelastic energy loss which in general is slightly less than

their first ionisation potential. Therefore, it was anticipated that any positive ions produced in the process would have energy comparable to the energy of the fast neutrals.

A series of experiments was carried out to study the the efficiency of the ionisation process with respect to the fast atom energy and its mass. In the experiments, the ionisation efficiency was taken as the average number of fast atoms being ionised per incoming atom. The number of the incoming fast neutrals was determined by measuring the current of the ejected secondary electrons, with the surface held at -27 V with respect to earth potential [Fig. 5.20a]. In that arrangement, the current read by the electrometer was essentially due to the secondary electrons which were leaving the target, and therefore, the number of fast atoms can be determined by consulting the yield coefficient-energy curves measured before (Figs. 5.11, 5.13). The positive ions were produced at the time the fast neutrals were about to leave the surface, and being of high energy they were not affected by the relatively small potential of the target, and hence did not contribute to the reading. The number of positive ions produced in the ionisation were determined by measuring the electron current produced by the process: it was achieved by biasing the target at +27 V with respect to the earth potential, which had the effect of suppressing both the secondary and the ionisation electrons from leaving the target [Fig. 5.20b]. In that arrangement, the current read by the electrometer was essentially due to the ionisation electrons; although it must be noted here that a small error will be introduced because the target will also collect stray secondary electrons which are emitted from surrounding surfaces upon their interactions with the scattered fast neutrals and ions. The fast neutral-induced secondary electrons which are supposedly emitted from the target will not have enough energy to overcome the -27 V bias potential, and hence they will not contribute to the

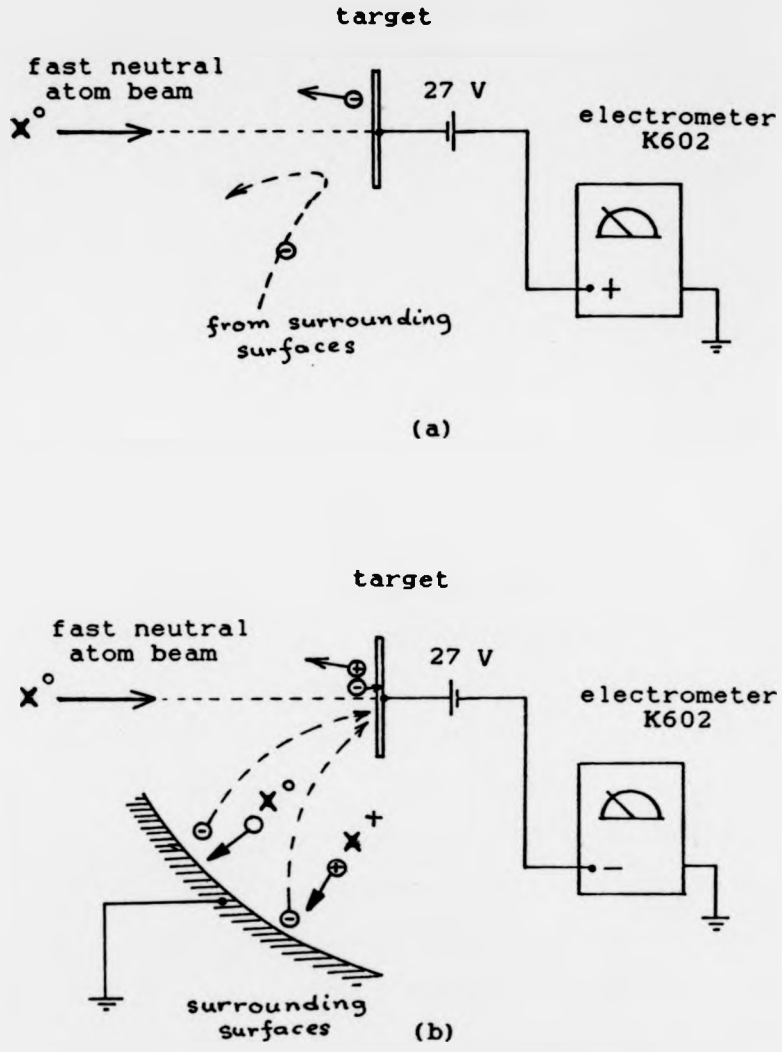

Fig. 5.20 : Schematic diagram showing the methods used to measure:

(a) total ejected electron current,

(b) positive ion current due to ionisation of fast neutrals by the surface.

reading because they never leave the target. Results from the experiments are shown in Figs. 5.21-5.22.

Attempts to determine the ionisation efficiency in the energy range of Source 1 with the lithium surface was not fruitful because both the secondary and ionisation currents were too small to be measured accurately, i.e., in the order of 10^{-11} and 10^{-12} A respectively. These values were in the same order with the leakage current of the measuring system ($\approx 10^{-12}$ A) which render the results erroneous and irreproducible.

With the gold surface, in the energy range of 500 to 1000 eV, the ionisation efficiency increases with the fast atom energy. In that energy range, H_2 is the most efficiently ionised (up to about 17%), followed by the other four gases, with N_2 being the least ionised (as low as 5%). In the energy range of 2.5-6 keV, with the exception of Ar, the ionisation efficiency decreases with the fast atom energy. For the energy range where no experiment was carried out, i.e., 1-2.5 keV, it may not be far too wrong to expect a maximum in the ionisation efficiency. By interpolating a maximum in the energy range mentioned, the threshold energy (E_{th}) for the ionisation process can be extrapolated, and found to be about 350 eV for all the five gases. This is different from results obtained by Souda et. al. [33] which generally showed that E_{th} increases with the atomic number of the fast atom. The E_{th} for the ionisation process via electron promotion mechanism, depends on the ability of the target atom unfilled valence states to receive electron from the fast neutral atom. Souda's values for E_{th} of helium on

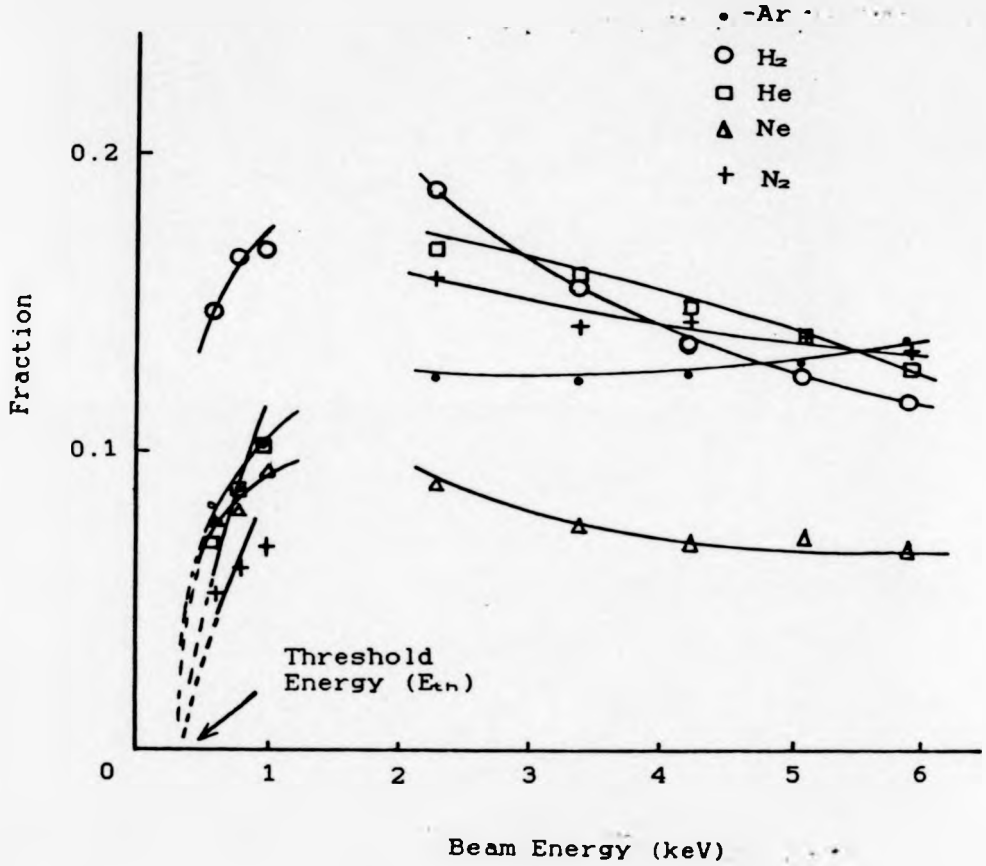

Fig. 5.21 : Curves showing variation of fraction of fast neutral atoms ionised during collision with the Gold surface, with the beam energy.

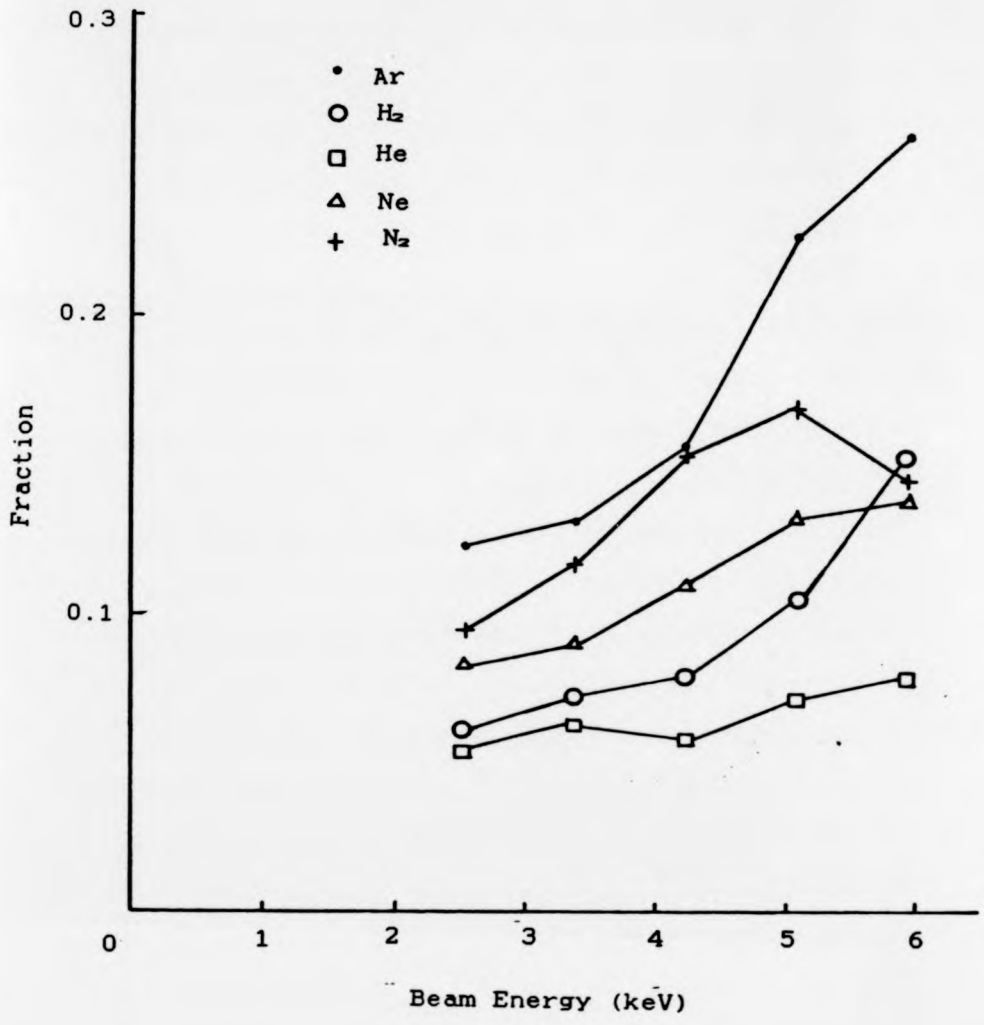

Fig. 5.22 : Curves showing variation of fraction of fast neutral atoms ionised during collision with the Lithium surface, with the beam energy.

copper (electronic configuration: Cu = [Ar]$3d^{10}4s^1$) and silver (Ag = [Kr] $4d^{10}5s^1$) are larger than 2000 eV. Being in the same column in the Periodic Table with Cu and Ag, gold (Au = [Xe]$4f^{14}5d^{10}6s^1$) might well have been expected to have E_{th} in the same energy range, but in fact the value measured is a factor of six lower.

In the energy range of 2.5-6 keV, with the exception of Ar, results obtained with the lithium surface show comparable ionisation efficiency with those obtained with the gold surface, i.e., from about 5 to 17%. The efficiency, however, increases with the fast atom energy; with Ar being the most efficiently ionised while He being the least. The rather large ionisation electron current observed with lithium target was not solely due to the ionisation electrons but also to the positively charged sputtered fragments, which were indistinguishable from the former. In this energy range, established data of the sputtering ratio (S) of noble gas ions, i.e., average number of sputtered surface atom per incident ion, shows that at any ion energy, the sputtering ratio increases with the atomic number of the ion [19,34]. Since sputtering is a kinetic process, the sputtering data obtained with ions, in principle, should also be applicable to the fast neutrals. This is indeed shown by the results; the contribution from the positively charged sputtered fragments to the measured "ionisation electron current" increases with the mass of the fast atom. Accordingly, results obtained with H_2 should lie below those of He, but as the former reacts chemically with lithium there might well be some elements of chemical sputtering

taking part in the process. The same might as well be true with the interaction involving N_2.

In summary, upon impact with a surface a portion of the fast neutral atoms are ionised. The threshold energy of ionisation at gold surface is about 350 eV and independent of the beam type. The curve of ionisation efficiency versus fast atom energy has similar form with those of electron impact ionisation cross-section of molecular gas. It is believed that the lithium target is covered with a layer of its chemical compounds, which cast doubt over the results obtained in the measurement of fast atom ionisation efficiency on its surface.

5.5 Measurement on the slow sputtered positive ions

The presence of a significant number of slow positive ions was consistently found throughout the experiments with lithium target. During the experiments to determine the energy distribution of the secondary electrons (see Fig. 5.3), their presence caused the collector current (I_c) to change sign from +ve (which means the positively biased collector receiving electrons) to -ve (which means the collector receiving positively charged particles). Again, in the ionisation experiments discussed earlier, the notion of the production of slow positively charged particles seems to fit well into the results.

Experiments were carried out to determine the species of the positively charged particles and their energy distribution. To determine the type of the charged species,

mass spectrographs of the UHV were recorded at two target biasings; at +60 V above earth potential to ensure that all positively charged particles were ejected , and -60 V to suppress them from leaving the target. In both conditions, sputtering of neutral particles were not affected. A typical mass spectrograph obtained from the experiments is shown in Fig. 5.23. The peaks due to lithium were very small because the spectrometer's detector subtended a solid angle of only 0.02 steradians to the centre of the target surface, at 45° in front of the surface. With the angular distribution of the sputtered material obeys a "below cosine" distribution [19], the arrangement was not expected to produce better results. No improvement was made to to the arrangement of the spectrometer due to the physical constraint imposed by the UHV chamber and the spectrometer. However, the quality of the mass spectrum produced was adequate to convince us that Li^+ ions and neutral Li atoms were sputtered from the target surface during bombardment with fast neutral atom beam.

The energy distribution of the Li^+ ions was determined in the same way as the secondary electrons, except with two changes, i.e., the ramp was programmed to sweep from -6 V to +30 V, and the collector was biased at -27 V with respect to the earth potential. The secondary electrons ejected from the target's surface were repelled by the collector's potential and hence did not pollute the data. Fig. 5.24 shows an example of the energy distributions of the sputtered Li^+ ions. The curves show two interesting features:

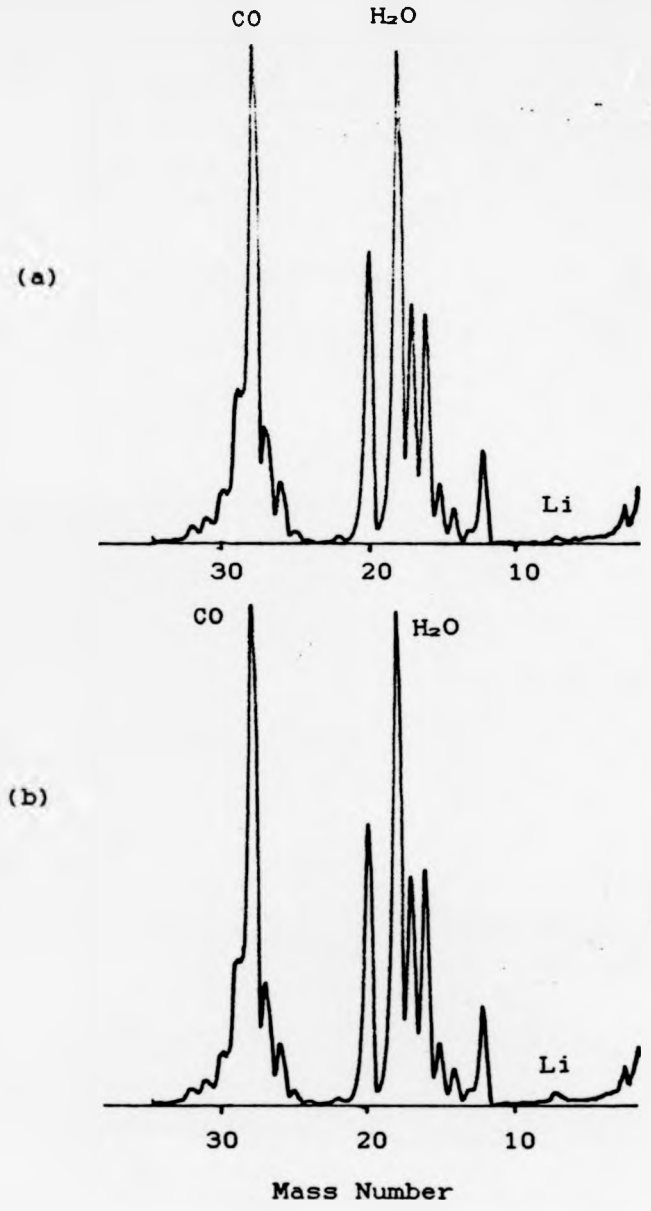

Fig. 5.23 : Mass spectra of the UHV condition when 4.25 keV Ar beam impinging on the Lithium target, which is biased at: (a) - 60 V , and (b) + 60 V with respect to the earth potential. Chamber pressure 1 x 10^{-8} torr.

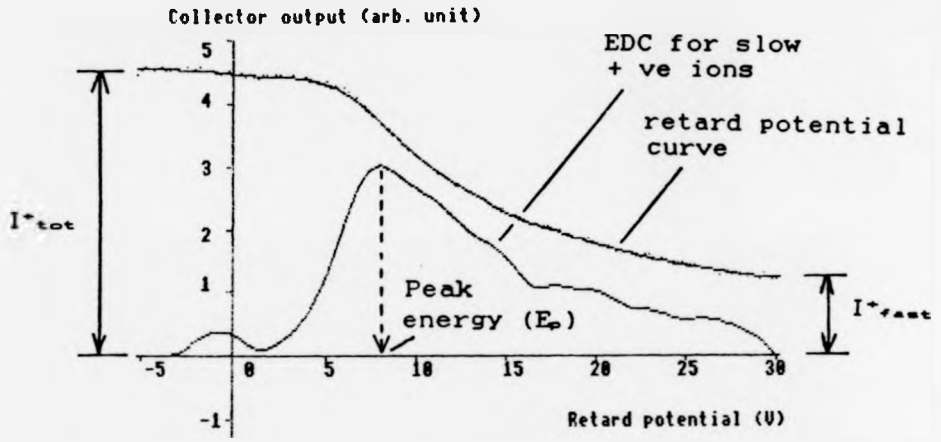

Fig. 5.24 : An example of a retard potential ADVAL number of the slow positive ion current ejected from Lithium surface. The data was obtained with 3.4 keV Ne atoms.
The percentage of the slow ions is estimated using

$$\% \text{ neutral} = \left(\frac{I^+_{tot} - I^+_{fast}}{I^+_{tot}} \right) \times 100$$

(i) the EDCs peak at about 10 eV with the peak energy depends on the type and energy of the fast atoms,

(ii) from the retarding potential curves, the positive ion current consisted of two components, i.e., the slow positive ions and the high energy positive ions.

From the same pool of data, the variation of the Li^+ ion peak energy and its ratio to the total number of the positive ions are plotted against the fast atom energy for all the five gases, and the graphs are depicted in Figs. 5.25-5.26.

Fig. 5.26 shows that the energy of the Li^+ ions increases with the fast atoms' energy and it also depends on the mass of the latter, i.e., the lighter the fast atom the higher the peak energy. The absence of data for H_2 deserves an explanation. During bombardment with H_2, the ratio of slow Li^+ ions to the total number of positive ions was decreasing with time until it reached a point where the ratio was less than 5%. With that small amount of slow Li^+ ions, the EDC would not be determined accurately, and it was then decided not to continue the experiments. However, experiment to determine the slow Li^+ ions were not affected.

Fig. 5.26 shows a general decrease in the content ratio of the slow Li^+ ions with the fast atoms' energy. For a given fast atom energy, the content ratio depends on the mass of the fast atom; the heavier the atoms the higher the content ratio. This seems to agree with the general feature of sputtering process which dictates higher sputtering yield (S) from heavier projectiles [34].

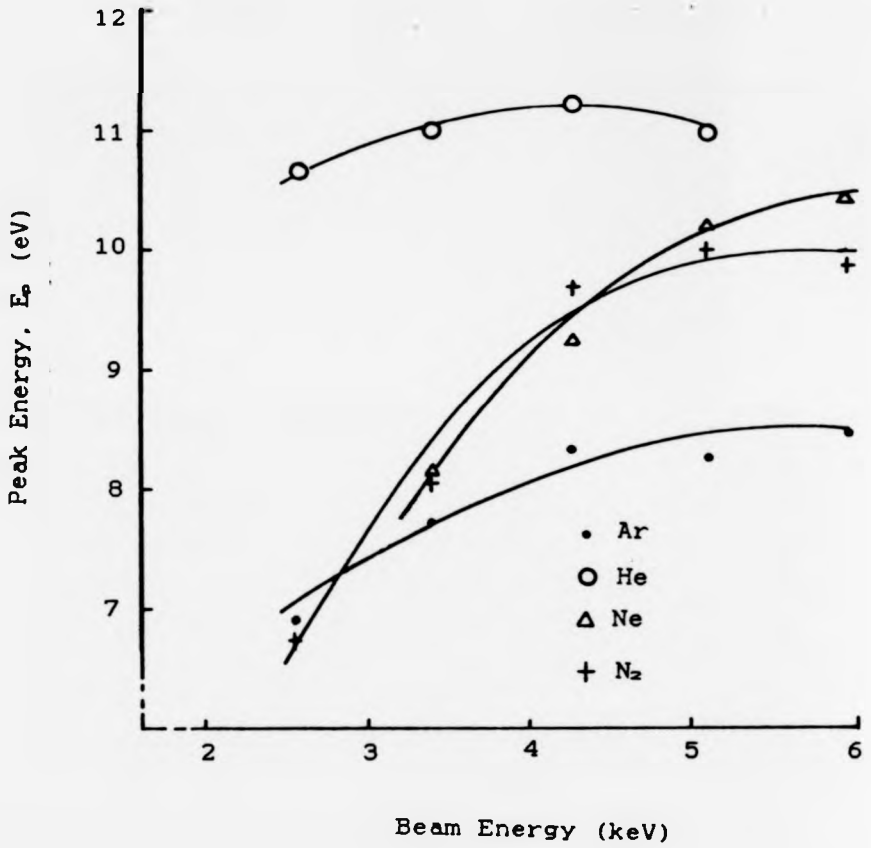

Fig. 5.25 : Variation of slow positive ions peak energy (E_p) with fast atom energy and gas type, incident on a lithium surface.

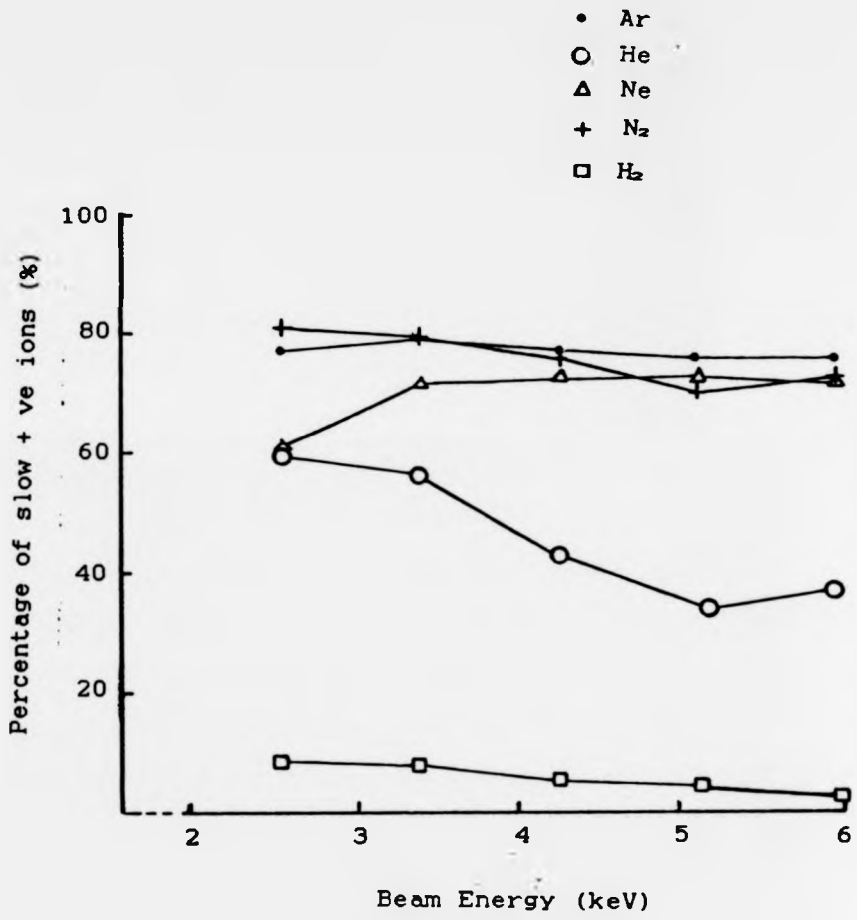

Fig. 5.26 : Variation of percentage of slow positive ions with fast atom energy and gas type, incident on a lithium surface.

In summary, with a lithium surface, the fast neutrals are not only undergoing neutralisation but also causing the ejection of neutral lithium atoms and slow Li^+ ions from the surface.

5.6 General critique on the experimental technique and results

As a whole, the results obtained from the experiments are generally illuminating, but they are not up to the author's fullest satisfaction. The reasons for this, range from the choice of fast atom guns, sample preparation techniques and generally to the experimental arrangement itself. Unfortunately, due to the lack of time and financial constraints, during the course of this work no major improvement to the experimental system was undertaken. Nevertheless, working with fast atom beams to study their interactions with metal surfaces in UHV condition is a new experience to the author, which he enjoys most and takes it as part of his learning process. In the following paragraphs, the weak points of the experimental system from the author's point of view is discussed, and where appropriate suggestion for improvement is given.

From the previous discussions on the ejected secondary electrons, at times the surface cleanliness was mentioned. For that matter, in any surface study, the sample's cleanliness is of prime importance. It is now clear that, the surface's "localised cleanliness" which was assumed throughout this work is not satisfactory, nor it is

adequate; the data obtained just shows otherwise. Even if we were permitted to assume that "localised cleanliness" is an achievable reality, certainly the perimeter of the area on which the beam falls will not be etched away, and thus not atomically clean. Depending on the size of the beam cross-section, the area of the dirty perimeter may account up to 50% of the total area of interactions. In summary, in the context of surface study the concept of a "localised cleanliness" is not appropriate and must be avoided.

Evidently, the reason for the dirty surface is the absence of any in-situ cleaning facility in the system. The provision of a single loop tungsten heating filament behind the sample is not adequate. The incorporation into the system a standard surface cleaning routine, that is, repeated flashings of the target to a temperature of several tens of hundreds degrees below its melting point followed by bombardments with diffuse Ar ion beam, is indeed necessary. The inclusion into the system, of a surface cleanliness monitoring device, namely, Auger Electron Spectrometer, used in conjunction with the cleaning routine is the perfect way of establishing an atomically clean surface.

Meanwhile, in the context of the surface cleanliness, the fast atom guns used in the experiments need to be commented. Source 1 has no apparent contribution to the surface contamination; its rather wide aperture ($\approx$ 1 cm in diameter) ensures that the central beam is free from any interaction with the electrostatic lens wall. However, the problem with the source is with its rather low output. When used with He gas, the ejected secondary electron current at

800 eV was 2×10^{-9} A. If we extrapolate the KEE yield coefficient versus ion energy curve for He^+ on gold reported by Baragiola et. al. [18], the yield coefficient at 800 eV is about 0.1. This means that the number of fast He atoms which reach the gold surface is 1.25×10^{11} atoms/s. Taking the beam diameter at the target as 2.5 mm, the beam flux is 2.55×10^{12} atoms/cm^2/s. Now, the rate of arrival of molecules of a residual gas of molecular weight M at a surface in a vacuum of P (torr) at T (K) is given by [35]

$$r = 3.51 \times 10^{22} \, P/(TM)^{\frac{1}{2}} \text{ molecules/cm}^2\text{/s} .$$

With the gun is in operation, the typical pressure reading for the target chamber is 2×10^{-9} torr. By taking nitrogen as the main constituent of the residual gas, and the room temperature as 20°C, the rate of nitrogen molecules arriving at the target surface is 7.8×10^{11} molecules/cm^2/s. This value is at par with the number of the probing atoms itself. Certainly the ejected electron data obtained with this gun is bound to be erroneous and indeed was found to be hardly reproducible.

The saddle field atom gun, despite its manufacturer's claim that it produces 99.99% fast neutrals, is actually an active source of the surface contamination itself. The intense and energetic flux of atomic particles it produces, sputters the small perimeter of the aluminium aperture on exit. Thus the beam not only contains the fast neutral atoms but the sputtered aluminium fragments as well - a serious problem of beam contamination indeed ! This problem manifests itself in the form of shining concentric ring-like patterns of fringes deposited on the wall about the

collimating aperture. It is rather an unfortunate experience for the author, for although he has observed the ring-like patterns during changing the source flange, his lacking of experience in the field made him continues his work with the gun without any suspicion of beam contamination at all. The author was made aware of this problem rather unexpectedly by Dr. M. G. Dowsett ** in one private occasion.

Compared to Baragiola's results, the yield coefficients obtained from these experiments are systematically larger, although the slopes of the yield coefficient versus energy curves for both sets of results are the same (See Fig. 5.11). Baragiola's results are highly reproducible and agree very well with results of other experimenters [18]; therefore his results are not far too wrong and may be taken as a reference. According to his results, the KEE yield coefficients of Al for He+ and H_2^+ ions in the energy range of 2 - 50 keV are lower than the yields from gold. Therefore, the presence of aluminium fragments on the gold surface is not the reason for the systematically larger yield coefficients obtained by the author, although it must be emphasised here that it is an unwanted effect. There are two possible explanations which the author can provide to account for the larger yield coefficients:

** Dr. M. G. Dowsett has worked with saddle field atom guns of the same type for SIMS experiments; the mass spectrometer helped him to notice the beam contamination. He also studied the gun's beam profile which he found to be most intense at its centre and loses it intensity almost gradually towards its perimeter. Although this important piece of information was conveyed to the author when he has completed the writing of the thesis, never the least, he greatly appreciated Dr. Dowsett's kindness.

(i) After some time, the area on which the beam hit the surface will be etched away according to the beam's intensity profile. Following Dr. Dowsett's finding on the beam's profile, the contour of the surface area where the beam falls during a normal incidence, will make the angle of incidence (θ_i) effectively larger than 0°. Following the sec θ_i law (Sec. 5.3.3), we can rightly expect for a larger value of yield coefficient.

(ii) In calculating the yield coefficients, the author assumed that the fast atoms dissipate their energy totally on the thermistor's collector plate. Evidently, if that is not the case, then the calculations will carry systematic error which pushed the results larger than their true values. A precise information on energy transfer for such collisions is necessary for a correct yield calculation. Another alternative is to attach a cage like collector at the thermistor's bead [36] to ensure for a total energy dissipation by the fast atoms.

The "negative energy electrons" problem discussed in Sec. 5.2, as have been pointed out before, only observed when Source 2 was in use. The beam contamination associated with the source may have some bearings on the problem, although it is not easy to relate them. One may think of the effect of the sputtered aluminium fragments, which may carry charges of both signs; but it is not understood why they are being bothered by only a small voltage of about 2 V and do not disappear even when the collector plate is biased at + 60 V ? The same question will arise when one thinks of the possibility of contributions from the ionised residual gas

molecules. Certainly the problem will become clearer if we perform a series of controlled experiments, such as by using a tube from the collimator to the sample, to avoid any interaction of the fast atoms with the residual gas. This will help us to eliminate the possible causes of the problem, one at a time, and so on.

Finally, but not the least, the technique of sample preparation requires some comments. Since gold is a very inert element, direct use of its rolled foil as a target is indeed an acceptable practice. However, it is better if the gold foil is put through an electropolishing process prior to its insertion into the target chamber. The preparation of a lithium surface needs a very careful planning and must not be compromised. The metal's reactive properties demands for an in-situ preparation. The easiest way of doing this is by evaporating the metal onto an unreactive substrate in a high vacuum inside the target chamber. Even by preparing the samples as discussed, we still need to subject them through the sample cleaning routine.

In summary, the author realises some of the weak points found in his experimental system. As to that effects, the need for a source of high intensity and clean atomic beam is strongly recommended. The better method of preparing the gold and lithium surfaces is outlined, and the need for incorporating the standard surface cleaning and monitoring devices into the experimental system is emphasised. In the next section some suggestions for future experiments are given.

5.7 Suggestions for future experiments

As a rule, any undertaking for a surface study in future, which involves the use of a fast atom gun needs to begin with a series of thorough investigations on the gun's performances and output characteristics. Particular attention should be given on the beam's purity, intensity profile and energy range (NB: the missing energy range encountered in the author's work is a very unpleasant disadvantage and needs not be repeated!). As for the gun's performances, taking the manufacturer's claim blindly may lead to serious experimental errors. Inclusion of a magnetic mass analyser into the system will help establish the beams contents. Equal emphasis should also be given to the surface cleanliness.

As for the ion induced KEE yield coefficients, any experiments on fast atom induced KEE should be welcome. This is equally true for both the energy distribution of the secondary electrons as well as the yield coefficients, an area where reliable experimental data is very scarce. As for the fast atom induced valence electron ionisation cross-sections, experimental method employed by Benazeth et. al. [38] may be followed.

In the context of this work, interesting experiments may be carried out on the atomic beam bolometer, particularly in the design of an efficient beam collector and on the gross behaviour of the energy transfer between the fast atoms and the metal collector. The use of

controlled ion beams of the same species as the fast neutrals will be very helpful here.

5.8 References

[1] H. Bruining, **Physics and Applications of Secondary Electron Emission** (Pergamon, London, 1954).
H. A. Ghalib, **Ph. D. Thesis** (University of Cincinnatti, 1964).

[2] H. S. Masey and E. H. S. Burhop, **Electronic and Ionic Impact Phenomena** (Clarendon Press, Oxford, 1952).

[3] W. Allison, F. B. Dunning and A. C. Smith, J. Phys. B: Atom Molec. Phys. 5 (1972) 1175.

[4] R. E. Blake, in **Design Techniques for Electronics Engineers** (McGraw Hill, 1977) p. 350.

[5] F. D. Schowengerdt, in **Lithium** (ed. R. O. Bach) (John Wiley, New York, 1985) p. 217.

[6] Z. Kirson, R. B. Gerber and A. Nitzan, Surf. Sci. **124** (1983) 279.

[7] H. D. Hagstrum, Phys. Rev. **89** (1953) 244.

[8] H. D. Hagstrum, Phys. Rev. **104** (1956) 317, 672.

[9] P. D. Johnson, **Ph. D. Thesis** (University of Warwick, 1978).

[10] See for example, O. Klemperer, **Electron Physics** (Butterworth, London, 1961).

[11] N. W. Ashcroft and N. D. Mermin, **Solid State Physics** (Holt Saunders Int., 1976).

[12] J. Lindhard and M. Scharff, Phys. Rev. **124** (1961) 128.

[13] E. J. Sternglass, Phys. Rev. **108** (1957) 1.

[14] U. A. Arifov, R. R. Rakhimov and Kh. Dzhurakulov, Soviet Phys.-Doklady **7** (1962) 716.

[15] D. B. Medved, P. Mahadevan and J. K. Layton, Phys. Rev. **129** (1963) 2086.

[16] R. C. Amme, J. Chem. Phys. **50** (1969) 1891.

[17] S. D. Dixit and S. N. Ghosh, Indian J. Phys. **B55** (1981) 87.

[18] R. A. Baragiola, E. V. Alonso and A. Oliva-Florio, Phys. Rev. **B19** (1979) 121.

[19] M. Kaminsky, **Atomic and Ionic Impact Phenomena on Metal Surfaces** (Springer-Verlag, Berlin, 1965).

[20] G. D. Magnuson and C. E. Carlston, Phys. Rev. **129** (1963) 2409.

[21] R. E. Clausing and D. S. Easton, Surf. Sci. **36** (1977) 377.

[22] K. Morita, H. Akimune and T. Suita, Jpn. J. Appl. Phys. **5** (1966) 511.

[23] K. Ohya and I. Mori, Jpn. J. Appl. Phys. **19** (1980) 2027, L281.

[24] E. V. Alonso, R. A. Baragiola, J. Ferrón, M. M. Jakas and A. Oliva-Florio, Phys. Rev. **B22** (1980) 80.

[25] J. Ferrón, E. V. Alonso, R. A. Baragiola and A. Oliva-Florio, Phys. Rev. **B24** (1981) 4412.

[26] I. N. Evdokimov et al, Phys. Status Solidi **19** (1967) 407.

[27] H. B. Nielsen and T. A. Delchar, Surf. Sci. **141** (1984) 487.

[28] R. C. Abbott and H. W. Berry, J. Appl. Phys. **30** (1959) 871.

[29] J. Mischler, N. Benazeth, M. Nègre and C. Benazeth, Surf. Sci. 136 (1984) 532.

[30] E. S. Parilis and L. M. Kishinevskii, Soviet Phys.-Solid State 3 (1960) 885.

[31] See for example, S. M. Sze (ed.), VLSI Technology (McGraw- Hill, International edition, 1983) Ch. 6.

[32] R. Souda and M. Aono, Nucl. Instr. Methods B15 (1986) 138.

[33] R. Souda, M. Aono, C. Oshima, S. Otani and Y. Ishizawa, Surf. Sci. 179 (1987) 199.

[34] H. H. Andersen, Appl. Phys. 18 (1979) 131.

[35] D. P. Woodruff and T. A. Delchar, Modern Techniques of Surface Science (Cambridge Univ. Press, 1986).

[36] C. A. van de Runstraat, R. Wijnaendts van Resandt and J. Los, J. Phys. E: Sci. Instrum. 3 (1970) 575.

[37] K. H. Krebs, Vacuum 33 (1983) 555.

[38] C. Benazeth, N. Benazeth and L. Viel, Surf. Sci. 78 (1978) 625.

[39] U. A. Arifov, Interaction of Atomic Particles with a Solid Surface (Consultants Bureau N.Y., 1969) Ch. 11.

CHAPTER SIX

COMPUTATION OF THE SCATTERING POTENTIAL FOR HELIUM ON COPPER (ENERGY RANGE 150 - 1000 eV)

6.1 The interatomic potential

The scattering of a fast neutral atom by a surface is a phenomenon governed by the force that exists between the fast atom and the target atom in the surface. The final scattering trajectory will be determined not only by the fast atom initial energy and angle of incidence, but also by the nature of the colliding atoms and spatial arrangement of the surface atoms.

The force F between two atoms, distance r apart, is expressible in terms of their potential energy of interaction, better known as interatomic potential, V. To a first approximation on r, the potential is an r-dependent quantity, that is, a central force field. The force is related to the interatomic potential as follows:

$$F(r) = - \frac{dV(r)}{dr}$$

The interatomic potential, in vacuum, between two ground state atoms of atomic numbers Z_1 and Z_2 with their nuclei already fully constituted is as follows:

$$V(r_{12}) = \frac{1}{4\pi\varepsilon_o}\left(\frac{1}{2} \sum_{i=j}^{n} \frac{e^2}{r_{ij}} - \sum_{i=1}^{n} \left(\frac{Z_i e^2}{r_{i1}} + \frac{Z_1 e^2}{r_{i2}} \right) + \frac{Z_1 Z_2 e^2}{r_{12}} \right)$$

where r_{12} the distance of inter nuclear separation, r_{ij} the distance between the i-th and j-th electron, r_{i1} and r_{i2} the distance of the i-th electron to the nucleus of the 1st and 2nd atom respectively, and ε_o the permittivity of free space.

The equation shows that even for a relatively simple interaction system such as that between He and Li atoms, the calculation for the interatomic potential is too complicated to handle. Luckily, as we can choose to work in the energy range in which only the repulsive part of the potential is dominant, there exist several empirical approximations for the interatomic potential which are simpler and easier to use. Two popular examples are the Thomas-Fermi-Molière and Born-Mayer approximations.

The Thomas-Fermi-Molière equation takes the following form:

$$V(r) = \frac{1}{4\pi\varepsilon_o} Z_1 Z_2 \frac{e^2}{r} \phi(x)$$

where $\phi(x)$ is the Molière electronic screening function:

$$\phi(x) = 0.35\, e^{-0.3x} + 5.5\, e^{-1.2x} + 0.1\, e^{-6x}$$

$x = r/a$

a = Firsov's characteristic screening length

$= 0.88534\, a_B\, (Z_1^{\frac{1}{2}} + Z_2^{\frac{1}{2}})^{-2/3}$

a_B = Bohr radius $= 0.529 \times 10^{-10}$ m

The Born-Mayer repulsive potential offers a simpler form:

$$V(r) = A \exp(-br)$$

For two unlike atoms, the empirical combining rule is

$$V_{12} = \sqrt{(V_{11}V_{22})} = A_{12} \exp(-b_{12} r)$$

where $A_{12} = \sqrt{(A_{11}A_{22})}$ and $b_{12} = \frac{(b_1+b_2)}{2}$

Values for coefficients A and b for atoms of Z=2 to 102 were calculated by Abrahamson [1]. The Molière screening function is more accurate for interaction systems with atoms of high atomic numbers because of the high electronic densities and well defined electron average positions. On the other hand the Born-Mayer approximation is good only for interactions with energy up to about half the value of the pre-exponential coefficient [2]. It has been used extensively for interaction distances within 0.5 to 2.0 A.

6.2 The calculation of fast atom scattering trajectories

At this stage it is best to look back at some terms usually used in describing scattering process. In Fig. 5.1, A and B are two atoms which are set to have a collision; A is the projectile and B is the target. At the initial instance of $t=t_o$, A is at P, a point far away from B, approaching the latter at a velocity v_i. The interacting force which acts between A and B is attractive in nature and of negligible magnitude. As A comes closer towards B, such as at point Q, the interacting force becomes repulsive in nature and its magnitude becomes increasingly significant. The action of this force makes A changes its velocity and hence its course. The process goes on until A is far from B such that the interaction force between them is no longer

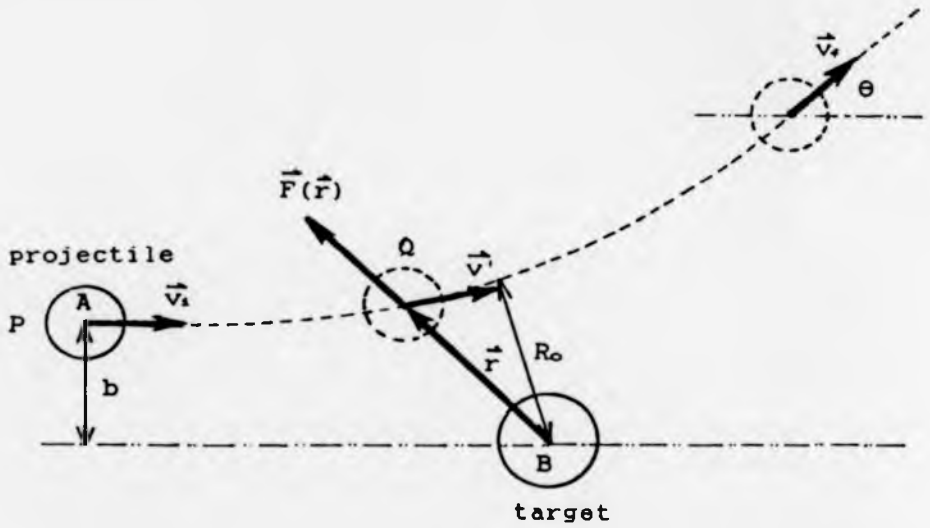

b : impact parameter
θ : scattering angle
R_o : distance of closest approach

Fig. 6.1 : The scattering trajectory

able to alter A's velocity. Atom A then proceeds in flight with its final velocity, v_f. In the diagram, b is called the impact parameter, R_o is the distance of closest approach. The angle between v_i and v_f, i.e., θ, is called the scattering angle.

The scattering process described above is a simplified scattering model in which it was assumed that the target atom remains stationary. However, in the case of fast atom scattering by surfaces, it is not a bad assumption because the surface atoms are strongly held in place by their neighbouring atoms and in some cases the scattering experiments are between light fast atoms and a heavy atom surface.

The calculation for a scattering process is really a matter of solving the equation of motion, as follows:

$$m \frac{d^2 r(t)}{dt^2} = F(r(t),t)$$

where m is the mass of the fast atom, r(t) is the position vector of the fast atom with respect to the target surface atom at time t and F(r(t),t) is the interactive force at time t. The complexity of the calculation depends very much on the nature of the interactive force. Strictly speaking, to have a mathematically rigorous solution for the equation the scattering process has to be treated quantum mechanically as a many-body problem.

Luckily, it had been pointed out by Bohr in 1948 [2], that for a two-body collision there exists a critical scattering angle, θ_c, above which a classical treatment is

adequate. The critical scattering angle is related to the other scattering parameters as follows:

$$\Theta c = \frac{\lambda}{2R_o} = \frac{\pi\hbar}{\mu v R_o}$$

where λ is de Broglie's wavelength of the collider, R_o is distance of closest approach, v is relative velocity and $\mu \equiv (M_A M_B)/(M_A+M_B)$ is the reduced mass of the colliding atoms.

The equation shows that Θ_c is smaller for a system of heavier atoms in inverse proportion to their reduced mass. It also becomes smaller as the collision energy is increased. Since most experimental scattering events are both of large reduced mass and high collision energy, therefore it is adequate to treat their theoretical calculations on the basis of classical mechanics.

The calculation for a fast neutral atom/surface scattering can benefit from the experiences gain from LEIS. The LEIS spectra for the back-scattered ions have most of their energy peaks located near the energies the ions would retain after a single binary elastic collision (SBEC) with one of the surface atoms. This means that despite an array of close neighbours, surface atoms can be assumed to be acting as individual targets, i.e., the impinging atom interacts with only one surface atom at a time. This is indeed a legitimate assumption because in the regime of the fast atom energy, the atom/surface collision time is very

brief, i.e., $\approx 10^{-15}$ s (*), and the mutual interaction potential between the surface atoms is negligible compared to that of the incoming fast neutral atom. A series of computer simulations for LEIS performed by Chang et. al. [3] showed that identical results can be obtained by neglecting the interactions among the surface atoms.

6.3 Routine for computer simulation

By assuming a stationary target, a scattering process between two atoms can easily be simulated on a computer. It is carried out through a series of time intervals, δt, and employs the following routine:

(i) Select the position and velocity for the collider

(*)

In the context of fast atom scattering, collision time is actually the interaction time, i.e., the time taken by the fast atom to be within the vicinity of the surface. Its magnitude depends on the following set of factors: fast atom energy (E), angle of incidence, interatomic spacing (d) and the distance above the surface (y) for which the surface vicinity is defined. For a given set of factors, the interaction time varies according to the impact parameter the fast atom make with the first surface atom. This idea is best illustrated by the following table showing the interaction time calculated from the scattering of He on Cu(111) at 50° incidence:

	E = 250 eV		E = 750 eV	
y	d=2.56 Å	d=4.43Å	d=2.56 Å	d=4.43Å
≤ 1 Å	1.6 – 3.5	1.7 – 4.7	1.3 – 2.3	1.4 – 3.4
≤ 2 Å	4.1 – 8.4	2.9 – 7.2	2.6 – 4.2	2.9 – 7.2
≤ 3 Å	6.4 – 9.6	6.4 – 11.9	4.0 – 6.2	4.4 – 9.5

NB: All times are in 10^{-15} s.

(ii) Calculate the interactive force between the collider and the target atom(s) using the relation:

$$F(r) = -\frac{dV(r)}{dr}$$

(iii) Calculate the new velocity and position of the collider after an interval δt

(iv) Move the collider to its new position and test for conservation of momentum and energy

(v) Repeat through (ii), (iii), and (iv) until there is no change in the collider's velocity.

The choice of the magnitude of the time interval δt affects the exactness of the simulations; in general, the smaller the magnitude δt takes the better the results will be. However, there exists a critical value for δt below which no further dramatic improvement will be achieved in the exactness of the simulation. In practice, the overall computing time will be the major consideration in choosing an optimum magnitude for δt.

6.4 The relation between impact parameter and scattering angle

A simulation to study the relation between impact parameter and scattering angle in He-Cu and Ar-Cu scattering systems was carried out on a BBC B microcomputer using the routine described above . The time interval used, δt, was 5.7×10^{-17} s and the Born-Mayer interatomic potential for

the interacting systems was calculated using Abrahamson's potentials:

He-Cu: $V(r) = 1805 \exp(-3.867\, r)$ eV, r in Å

Ar-Cu: $V(r) = 9843 \exp(-3.594\, r)$ eV, r in Å

The results of the computations are depicted in Fig. 6.2. From the figure it is easily seen that there is a well defined boundary behind each Cu atom in which the He or Ar atom has no trajectory. In other words, atoms which lie inside the cone-like boundary will not be "seen" by the collider; this space is called the shadow cone. Atoms inside the shadow cone do not contribute to the overall scattering result. Close examination of Fig. 6.2 shows that for a given scattering system, increasing the collision energy will slightly reduce the size of the shadow cone. A Change in the nature of the colliding atoms has a significant effect on the shape of the cone. Fig. 6.3a shows that at incident angle of 50° the shadow cones of an array of surface atoms effectively prevent the second layer atoms from being "seen" by the fast atoms; hence they do not have to be included in the calculation. This adds support to the validity of a two-atom surface model which is applied in all simulations reported in this chapter. However, it must be made clear here that at small incident angle and particularly at normal incidence, the shadow cone of the first layer atoms may no longer effectively conceal all the second layer atoms. In this situation, the second layer atoms will contribute to the overall scattering yield.

There are four types of trajectories possible for a fast atom when it is being scattered by a surface. They are

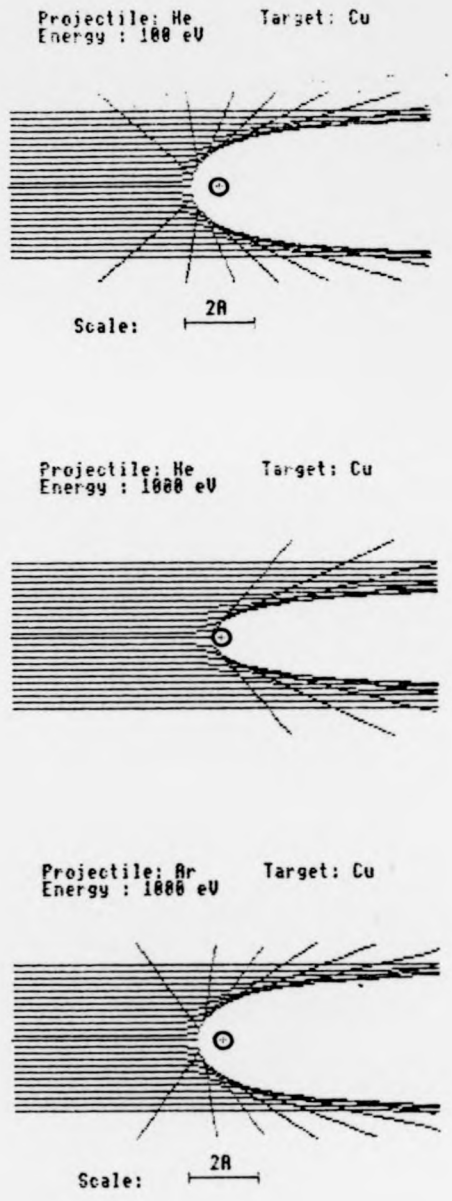

Fig. 6.2 : Variation of scattering angle with impact parameter and energy - shadow cone.

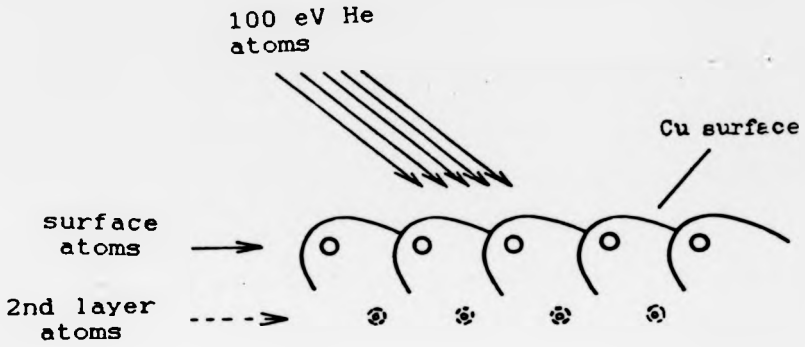

(a) Figure showing shadow cones of surface atoms effectively conceal the 2nd layer atoms.

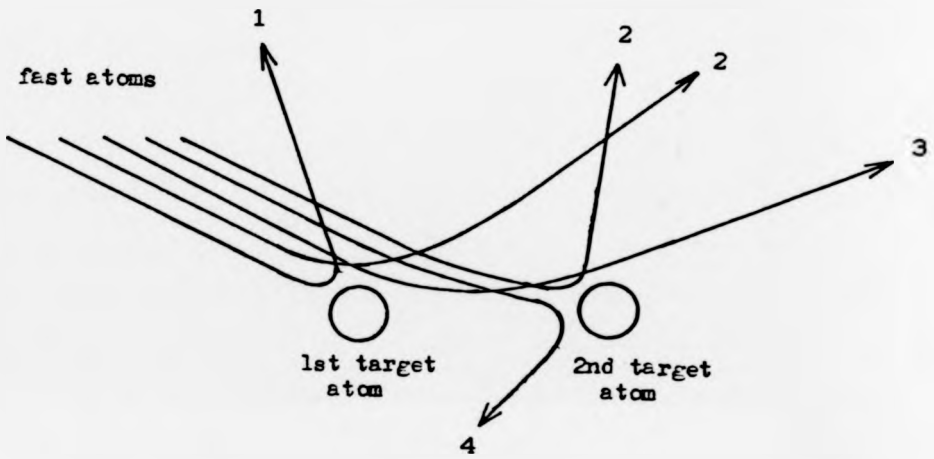

(b) Figure showing four types of trajectories of fast atoms scattered by a two atom surface.

Fig. 6.3

the results of either a single or double scattering or a near double scattering. Fig. 6.3b shows all the four types of trajectories from an in-plane scattering of fast atoms impinging on a two atom surface. Of all the four, the third trajectory is the most interesting; it is the result of a near double scattering by two adjacent surface atoms. It sets the minimum forward scattering angle, and therefore by a weak optical analogy it is called rainbow scattering. The angle obtained from rainbow scattering is called the rainbow angle. From now on, angle of incidence and rainbow angle are measured with respect to the surface normal.

The occurrence of rainbow scattering is best explained in terms of shadow cone and impact parameter. For rainbow scattering to occur, the fast atom must start with a certain impact parameter to encounter the first atom, such that it will leaves the latter at an angle that gives it an impact parameter for the second atom tangential to the latter's shadow cone at a far distance behind it. It is the impact parameter that plays the important role, and hence the rainbow angle is strongly dependent on the spacing between the two surface atoms concerned; larger spacing will result in a smaller rainbow angle. As for the shape of the shadow cone, the rainbow angle will be weakly dependent on the collision energy and angle of incidence.

6.5 The variation of rainbow angle with interatomic spacing

A series of scattering simulations were designed to study the effect of varying the interatomic spacing and

angle of incidence on the rainbow angle. In the simulations a beam of 250 eV He atoms was scattered by a pair of Cu atoms whose separation was varied from 2.0 Å to 5.0 Å. It must be emphasised here that in a real Cu surface the interatomic spacing between the atoms is fixed and there is no way of varying it over a large range. However it is still possible to have two different interatomic spacings on a surface, for example, on the Cu{111} surface [Fig. 6.4] the interatomic spacing along azimuths $\langle 1\bar{1}0\rangle$ and $\langle 1\bar{2}1\rangle$,$\langle 2\bar{1}\bar{1}\rangle$ are 2.56 Å and 4.43 Å respectively.

Results from the simulations are shown graphically in Fig. 6.5. Two conclusions can be drawn from them:

(i) For each angle of incidence, as expected, the rainbow angle increases with the interatomic spacing though they are not linearly dependent. To illustrate the relation between the two quantities we define a quantity which we may call spatial sensitivity, S_r, as follows: For any interatomic spacing, S_r is the increment in rainbow angle per unit spacing. The graphs show that the spatial sensitivity decreases as the spacing increases. For example, for normal incidence scattering, S_r decreases from $13.6^{\circ}\text{Å}^{-1}$ to 6.5°Å^{-1} to 3.2°Å^{-1} as the interatomic spacing increases from 2.0 Å to 3.5 Å to 5.0 Å respectively.

(ii) For any interatomic spacing, rainbow angle increases with angle of incidence. However, there must be an upper limit for the angle of incidence above which the shadow cone from the first atom will effectively screen the second atom and rainbow scattering ceases to occur. We may define angular sensitivity, S_θ, as increment in rainbow angle per

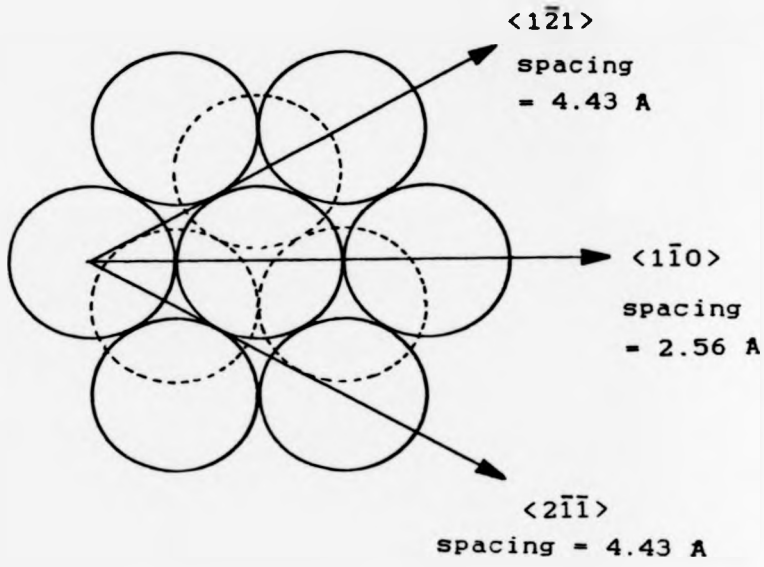

Fig. 6.4 : An unreconstructed Cu(111) surface. Solid line represents surface atoms, dashed line is for the 2nd layer atoms.

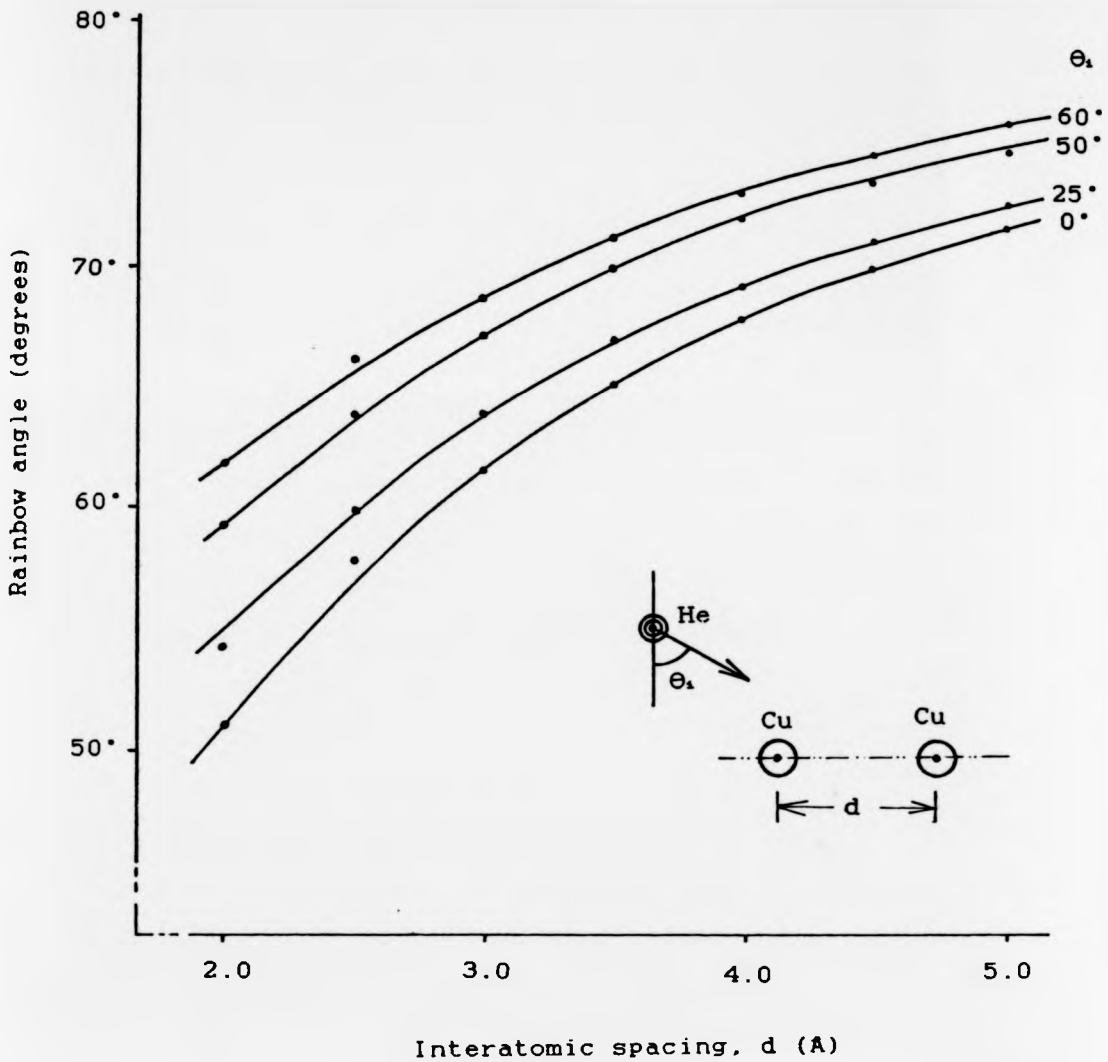

Fig. 6.5 : Graphs showing variation of calculated rainbow angle with interatomic spacing (d) and angle of incidence (θ_i). The scattering is between 250 eV He atoms with a two atom copper surface; and the interatomic potential used is

$V(r) = 1805 \exp(-3.867\ r)$ eV, r in Å.

unit increment in angle of incidence. Like the spatial sensitivity, S_θ decreases as the spacing increases.

From the experimental point of view large spatial sensitivity means better accuracy in determining the rainbow angle.

6.6 Experiments for fast atom scattering

Basic requirements for angle-resolved fast atom scattering from surfaces do not differ very much from other surface sensitive experiments. Since the angular distribution of the scattering yield is sensitive to the orientation of the surface atoms, it is therefore necessary for the surface sample to be a single crystal type which is cut to expose a particular surface orientation. Apart from that, the surface under study must be atomically clean and this means that it must be mounted in its own ultra-high vacuum chamber equipped with in situ cleaning facilities and surface cleanness monitoring devices.

There are two immediate possibilities for the type of experiments involving fast neutral atom scattering, namely:

(i) performing the procedures of Low Energy Ion Scattering (LEIS) with the fast neutral beam taking the place of the ion beam. Selective energy measurements can be done by mean of the time-of-flight technique. This approach seems a natural extension of LEIS with the added bonus of not having neutralisation at the surface.

(ii) performing ARFAS, i.e., measuring the in-plane

scattered beam intensities with respect to the polar angle measured from the surface normal.

6.7 The scattering of fast He atom by Cu{111} surface

Rainbow scattering arises from a near double collision involving only two surface atoms, therefore rainbow angles can be used to gain a better knowledge of the interatomic potential. In order to do just that we need ARFAS data from a surface of known geometry. A practical example of such a surface is the Cu{111} surface which is known not to reconstruct. ARFAS data for a fast He atom beam impinging on an atomically clean Cu{111} surface was supplied to the author by Dr. T. A. Delchar [4]. The complete data and experimental technique are described elsewhere [5]. However, the spectra from the scattering experiments are reproduced in Fig. 6.6 and data for the rainbow angles are given in Table 6.1.

A series of computer simulations were carried out to search for a "good" interatomic potential between He and Cu atoms. The model used employed the SBEC approximation and applied to a two-atom surface. In the computations, the Born-Mayer interatomic potential was used, and it was chosen because of two reasons:

(i) It has only two coefficients, hence simpler and easier to use

(ii) A trial preliminary simulations for the scattering of fast He atoms on an assumed unreconstructed W{100} surface was carried out by the author using the Born-Mayer

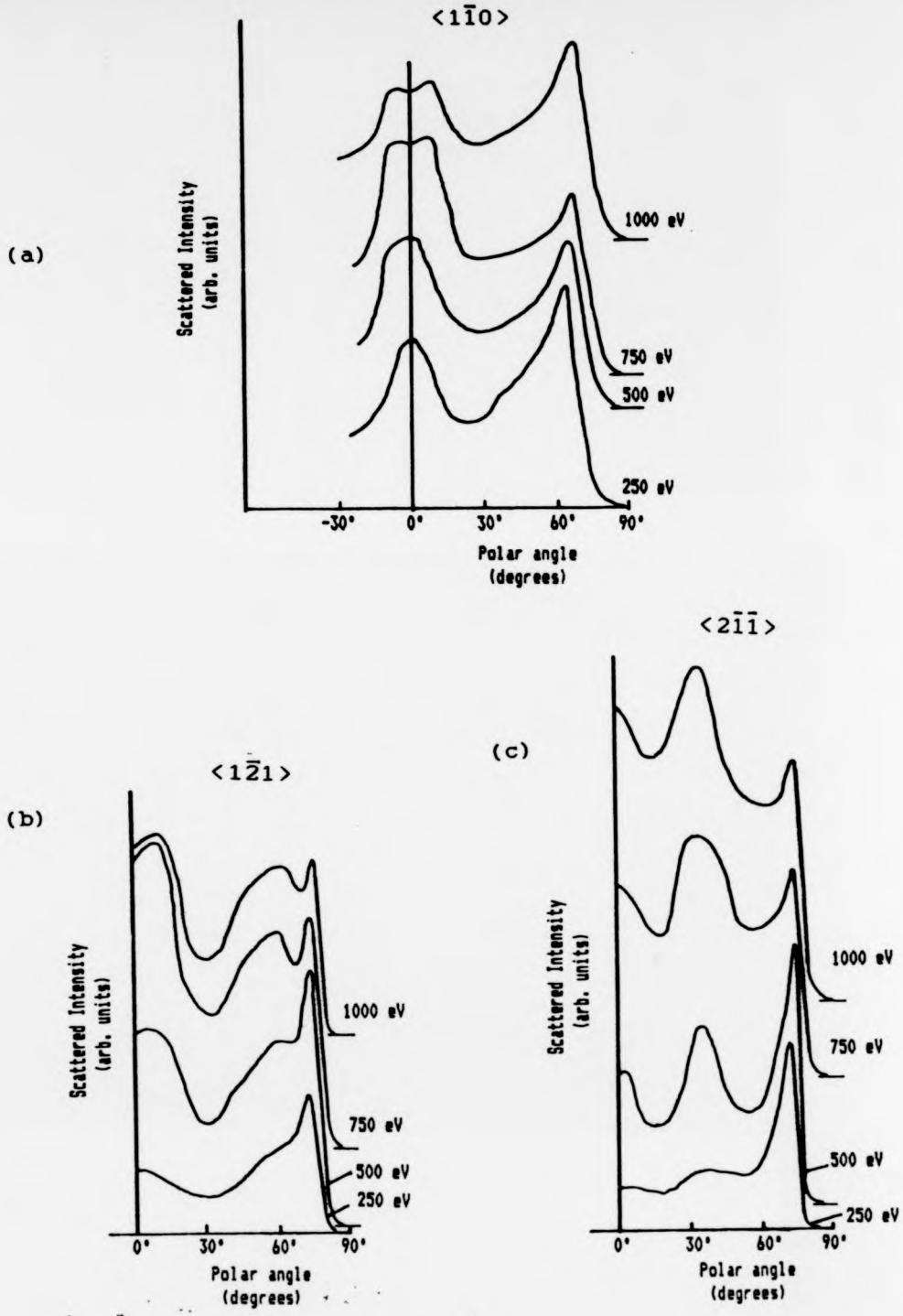

Fig. 6.6 : Scattered intensity versus polar angle for fast He atoms incident at 50° to the surface normal along azimuth (a) <1$\bar{1}$0>, (b) <1$\bar{2}$1>, and (c) <2$\bar{1}\bar{1}$> of a Cu{111} surface: beam energy as a parameter [4].

Table 6.1 : Values of rainbow angles (in degrees) from ARFAS experiments : He on clean Cu(111) [4].

Energy (eV)	azimuth $\langle 1\bar{1}0 \rangle$	azimuth $\langle 1\bar{2}1 \rangle$,$\langle 2\bar{1}\bar{1} \rangle$
250	63.8 ± 0.3	73.5 ± 0.2
500	66.0 ± 0.4	74.4 ± 0.2
750	66.0 ± 0.0	75.7 ± 0.3
1000	68.5 ± 0.1	76.3 ± 0.3

Table 6.2 : Average gradient of decrement of the calculated rainbow angle with respect to the value of A. for various fast atom energy in two different azimuth of incidence.
(Values are in 10^{-4} degrees per eV).

Energy (eV)	azimuth $\langle 1\bar{1}0 \rangle$	azimuth $\langle 1\bar{2}1 \rangle$,$\langle 2\bar{1}\bar{1} \rangle$
250	8.45	7.76
500	9.42	7.10
750	10.53	6.51
1000	10.94	6.23

potential with the coefficients calculated using Abrahamson's values, that is, A = 3562 eV and b = 3.837 A^{-1}. The rainbow angles obtained were 72° at 250 eV and 73° at 1000 eV, to be contrasted with the experimental value of 72° ± 1° [6]. The Thomas-Fermi-Molière potential was used by Chang et. al. [7] in their simulations for the same scattering system; the rainbow angles they obtained were generally lower than the experimental value by ≈ 2° at 1000 eV to ≈ 8° at 150 eV. The rather large discrepancies obtained with the Thomas-Fermi-Molière potential might be due to its unsuitability with scattering system containing He atoms because of the latter's less dense electronic distribution, a regime in which the Molière screening function is known to be less accurate.

Fig. 6.7 shows a computer generated scattering profile superimposed on the experimental result. Clearly, while the curves agree very well over the position of the so-called rainbow peak, the real result has two additional peaks, situated at ≈ 0° and 36°. Besides, the real rainbow peak is broader (FWHM ≈ 11°) than the computed one (FWHM ≈ 4°). The two additional peaks observed in the real results are due to the scattering of the fast atoms from the inner layer surface atoms, which was purposely disregarded in the computation. The chance of fast atom penetration into the subsurface region increases with its energy and the transmissivity of the surface with respect to the azimuth of incidence. Therefore one can expect that the relative intensities of the additional peaks increase with fast atom energy and those obtained in azimuth <121>,<211> should be

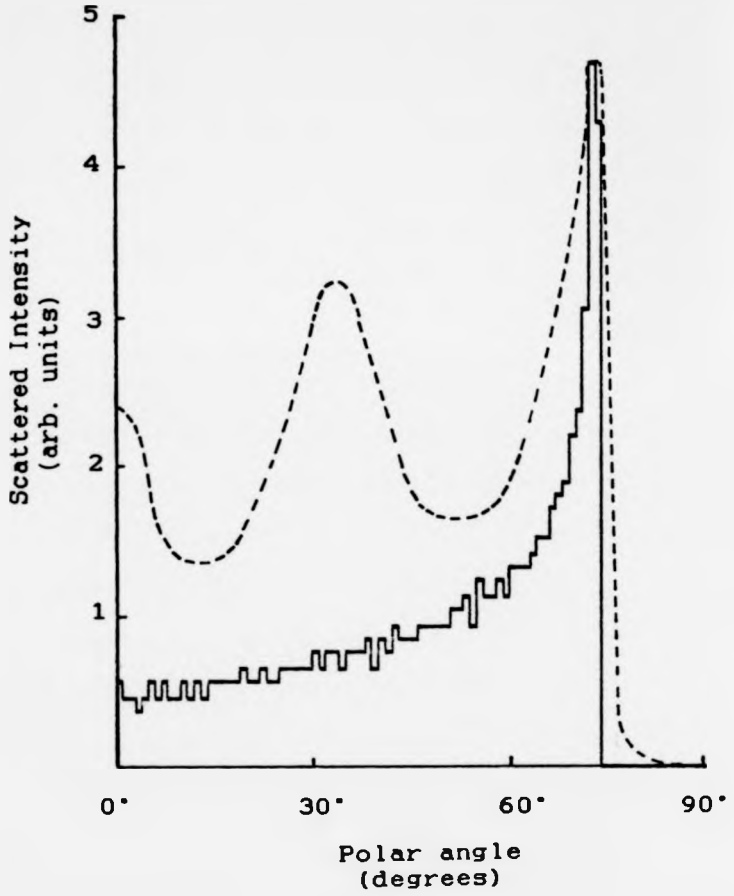

Fig. 6.7 : Polar angle distribution of scattered 500 eV He atoms incident at 50° to the surface normal along azimuth <2$\bar{1}$1> of a Cu{111} surface. The solid line is the calculated result, the dashed line is from the experiment [4].

higher than the one obtained in azimuth <1$\bar{1}$0>; features which the experimental results show. The broader rainbow peak showed by the experimental result is thought to be due to the Debye-Waller factor which was excluded in the computation. Nevertheless, the interaction potential must still be chosen to give a correct prediction of rainbow peak position as the beam energy, angle of incidence and surface atom spacing are varied. Fig. 6.8 shows the variation of the rainbow angle with exponential parameter b while the pre-exponential parameter A was kept constant at 1805 eV.

For each experimental rainbow angle a value of b was found graphically from Fig. 6.8, for which the calculated rainbow angle equals the experimental data. It was found that the average value for a "good" b is 4.136 Å^{-1} with standard deviation of 0.314 Å^{-1}. This value of b is higher than that of Abrahamson's potential by ≈ 7 %. Gaydaenko and Nikulin (GN) [8] have pointed out some mistakes in Abrahamson's calculation; and by using quantum mechanical electron distribution instead of the Thomas-Fermi-Dirac like Abrahamson, GN proposed their own calculation for A and b for atoms up to krypton. By using the same empirical combining rule, GN's Born-Mayer parameters for He-Cu are A = 1313 eV and b = 4.23 Å^{-1}. GN's value for b is only ≈ 2 % higher than the average value for "good" b. It must be emphasised here that the value of "good" b applies only in the energy range of the experiments and its accuracy obviously only as good as that of the experiments.

By letting b = 4.136 Å^{-1}, another series of scattering simulations was carried out to study the effect of varying

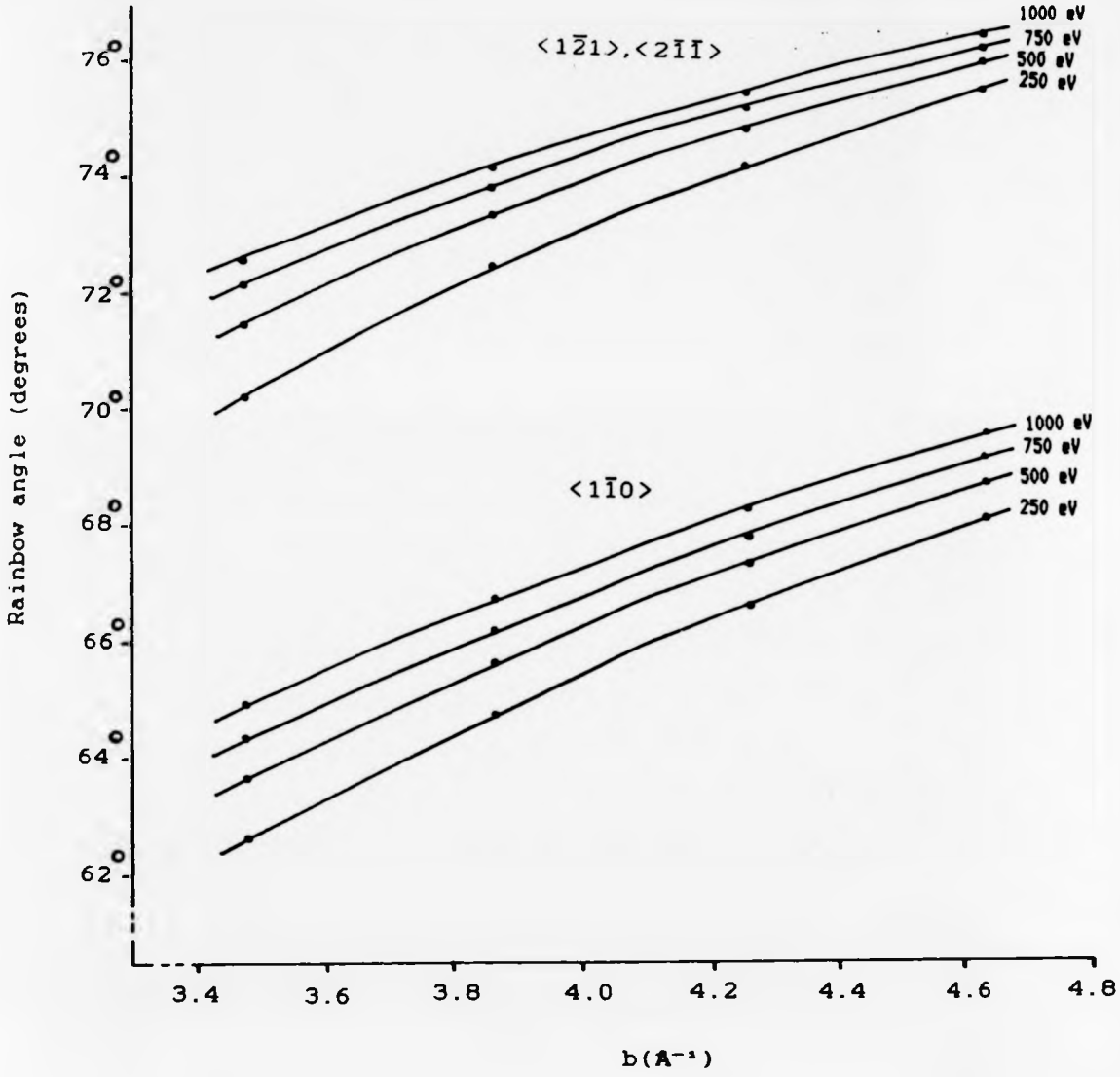

Fig. 6.8 : Graphs showing variation of calculated rainbow angle with exponential parameter, b, of the Born-Mayer's potential V(r) = A exp(-br). Incidence angle = 50°, A = 1805 eV.

the value of the pre-exponential parameter, A, on the rainbow angle. Results of the computations showed that the rainbow angle decreases slowly as A increases [Fig. 6.9], and the average gradient of decrement depends on the beam energy and interatomic spacing [Table 6.2]. It was found that there is no single value of A which provides a "good" fit between the calculated rainbow angles and those from the experiment.

The choice of the value of parameter A is likely to affect the shape of the calculated rainbow peak [Fig. 6.10]; small values of A tend to yield broad rainbow peaks. Since the half-height width of the calculated rainbow peaks are about 4° to be contrasted with 11° from the experimental data, it was decided that good value for A could not be found on this basis. It was therefore felt appropriate to use A as calculated using Abrahamson's data, that is, A = 1805 eV.

As mentioned before, the surface Debye-Waller factor is thought to have contributed to the broadening of the rainbow peaks observed in the experiments. This view is in line with the fact that the typical value for frequency of vibration of surface atoms is $\approx 10^{13}$ Hz; which means with the collision time in the order $\approx 10^{-15}$ s the surface atoms will appear to be relative stationary to the incoming fast neutral atom, at any phase of their vibration. Theory dictates that surface atoms should have larger mean square displacements than the corresponding bulk atoms, and as a consequence the surface Debye-Waller factor becomes important here. The same effect was known to reduce

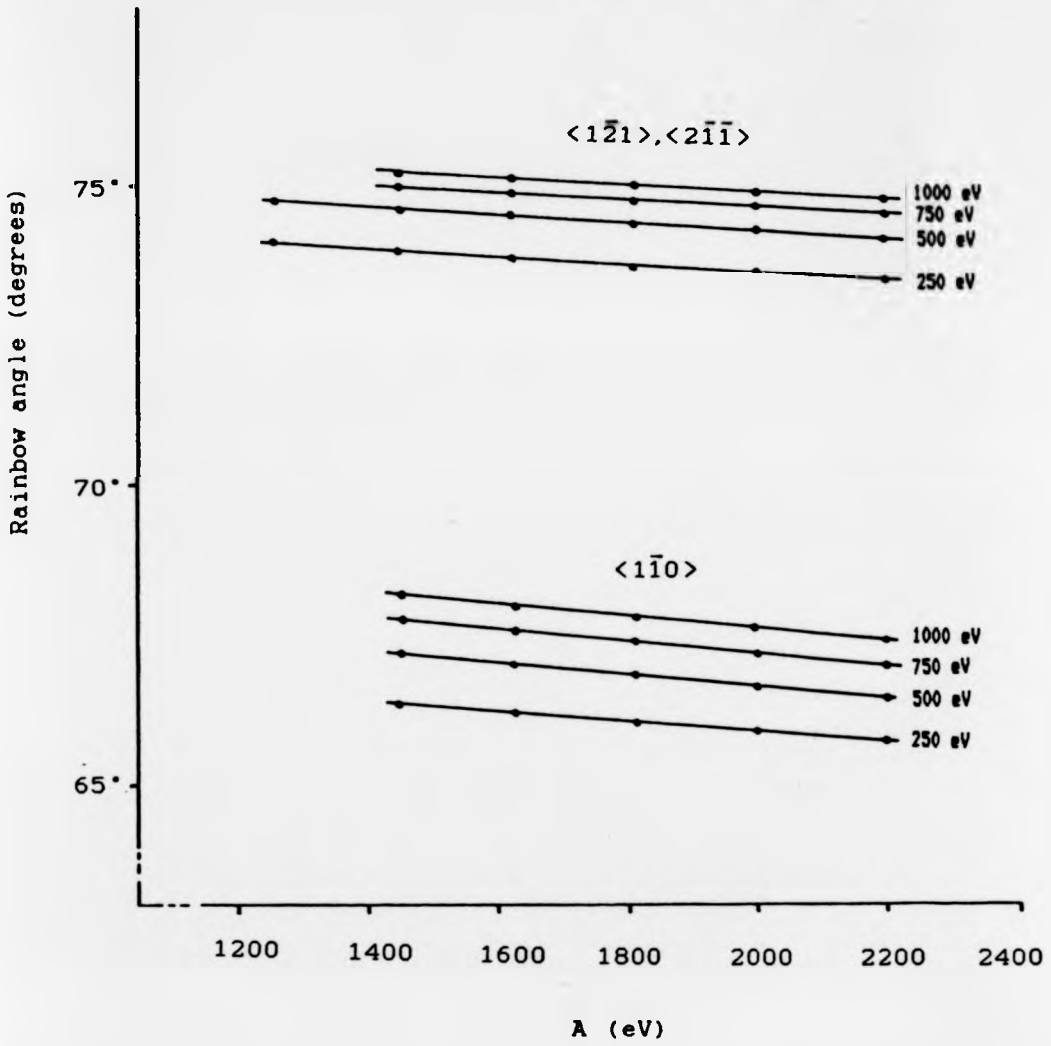

Fig. 6.9 : Graphs showing variation of calculated rainbow angle with pre-exponential parameter, A, of the Born-Mayer's potential $V(r) = A \exp(-br)$. Incidence angle = 50°, $b = 4.136$ Å^{-1}.

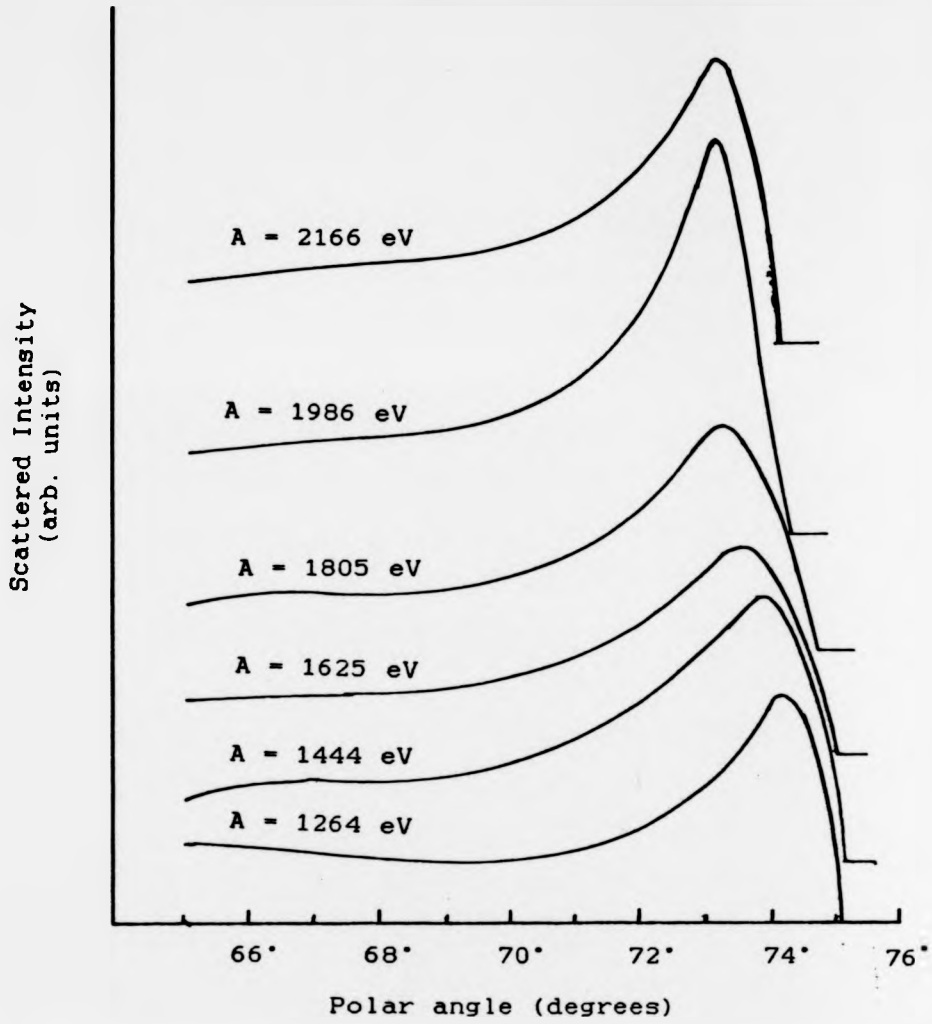

Fig. 6.10 : Graphs showing variation in the shape of the calculated rainbow peak with the pre-exponential parameter, A.
The scattering is of 500 eV He atoms from a Cu{111} surface, incident at 50° to the surface normal along azimuth <1$\bar{2}$1>.

scattering coherence of the electron beam, which in turn reduces the diffracted beam intensities in LEED experiments. The mean square vibrational amplitude of surface atom is given by [9]

$$\langle u^2 \rangle = \frac{3\hbar^2 T}{m k_B \Theta_D}$$

where m being mass of the atom, T surface temperature, Θ_D surface Debye temperature and k_B Boltzmann's constant. For Cu, Θ_D = 315 K and m = 1.055 x 10^{-25} kg. Taking T = 300 K, we get u_{rms} = 0.083 Å. It is usual to assume that $\langle u^2 \rangle$ is isotropic; therefore, at 300 K the interatomic spacing of Cu(111) in azimuth $\langle 1\bar{1}0 \rangle$ varies in the range 2.39–2.73 Å and in azimuth $\langle 1\bar{2}1 \rangle$,$\langle 2\bar{1}\bar{1} \rangle$ it varies within 4.26–4.60 Å. By consulting Fig. 6.5, the broadening of the rainbow peaks due to the thermal effect is found to be by ≈ 2.5° in azimuth $\langle 1\bar{1}0 \rangle$ and ≈ 1.5° in azimuth $\langle 1\bar{2}1 \rangle$,$\langle 2\bar{1}\bar{1} \rangle$. These values are in good qualitative agreement with the experimental results [Fig. 6.6] which show larger broadening effect in azimuth of smaller interatomic spacing, thus confirms the assumption of isotropic Debye-Waller effect made earlier. Adding the value for azimuth $\langle 1\bar{2}1 \rangle$,$\langle 2\bar{1}\bar{1} \rangle$ to its initial FWHM will give 5.5°. This value still far smaller than the experimental FWHM, but it does prove the contribution of Debye-Waller factor in the broadening the rainbow peak.

6.8 Summary

In the collision energy range of 150–1000 eV, classical treatment is adequate for calculating the scattering

trajectory of a fast neutral atom by a two atom surface. Scattering simulations based on that simple model, show the existence of the so-called "rainbow peaks" which were observed experimentally. By suitable choice of the interatomic potential used in the calculations, it was possible to achieve a good fit between the calculated "rainbow angles" and the experimental results.

6.9 References

[1] A. A. Abrahamson, Phys. Rev. 178 (1969) 76.

[2] I. M. Torrens, Interatomic Potentials (Academic Press, New York, 1972).

[3] C. C. Chang, L. A. DeLouise, N. Winograd and B. J. Garrison, Surf. Sci. 154 (1985) 22.

[4] T. A. Delchar and H. B. Nielsen , private communication.

[5] M. N. Yusuf and T. A. Delchar, Surf. Sci. 182 (1987) 231.

[6] H. B. Nielsen and T. A. Delchar, Surf. Sci. 141 (1985) 487.

[7] C. C. Chang, B. J. Garrison, H. B. Nielsen and T. A. Delchar, Surf. Sci. 155 (1985) 327.

[8] V. I. Gaydaenko and V. K. Nikulin, Chem. Phys. Letters. 7 (1970) 360.

[9] See for example, D. P. Woodruff and T. A. Delchar, Modern techniques of surface science (Cambridge, 1986) Ch. 2.

CONCLUSIONS

The secondary electrons ejected from gold surface when the latter interacts with fast neutral atoms, have many properties similar to those shown by ion-induced kinetically emitted secondary electrons from metal surfaces. The energy spectra of the ejected electrons have a maximum in the low energy region, i.e., 1-3 eV, and the effect of different types of projectile and the target's temperature on the structure is not clearly evident. The electrons are ejected into a solid angle around the surface normal, and follow a "near cosine" angular distribution. With the fast atoms in the energy range of 2-7 keV, the ejected electron yield coefficient (γ^*) increases linearly with the fast atom energy, i.e., $\gamma^*(E) \alpha E$, and for any given energy in the range, the magnitude of γ^* for the five gases is in the order $\gamma^*_{H_2} > \gamma^*_{He} > \gamma^*_{N_2} > \gamma^*_{Ne} > \gamma^*_{Ar}$ .The variation of γ with angle of incidence (θ_i) slightly deviates from the sec θ_i law. Based on these observations, it is believed that the majority of the secondary electrons are formed deep under the surface.

As to the general state of the kinetic electron emission theory, no model of electron emission could be offered. At present there are two competing models, namely, the Parilis-Kishinevskii inner shell ionisation model and the Baragiola's empirical model of direct valence electron ionisation. Following any of these models, data obtained from the interaction is bound to be self-convoluted. Hence, within the energy range, a fast neutral atom beam will not be a useful probe for surface electron spectroscopy.

In the step of collision with a metal surface, a small fraction of the fast atoms are ionised. The threshold energy for the ionisation on gold surface is ≈ 350 eV for all the five gases used. This value is a factor of six lower than values measured by Souda and co-workers for elements in the same group with gold, i.e., copper and silver. The result is also in apparent conflict with those obtained by Souda and co-workers, which shows that for a given metal target the threshold energy for ionisation increases with the atomic number of the projectile. Further experiments with atomically clean surfaces are needed in order to understand the phenomenon.

Computer simulations of the scattering of He atoms (150-1000 eV) from an unreconstructed clean Cu(111) surface have shown the existence of the so-called "rainbow peaks" which were observed experimentally. It was shown that the position of the "rainbow peak" is sensitive to the interatomic spacing, and in the case of He/Cu system it can well be described by a Born-Mayer interatomic potential $V(r) = A \exp(-br)$, where $A = 1805$ eV and $b = 4.14$ A^{-1}. The choice over the value of the pre-exponential parameter A has very little effect on the calculated position of the "rainbow peaks"; but however, it changes the shape of the simulated "rainbow peaks" where $A \approx 2000$ eV yields the narrowest "rainbow peak". Given the one-to-one correspondence between the rainbow angle and the interatomic spacing, angle-resolved fast atom scattering has potential to be developed as a technique for determination of surface structure.

APPENDIX 1

(a) The computer routine used to drive the ramp generator is as follows:

Instructions	Remarks
?αFE62=αFF	Set the User Port as an output port
?αFE60=N	Load a number, N, into the Data Register. NB: N is any integer between 0 and 255 inclusive.

The corresponding voltage outputs from the DAC and the ramp is shown below:

N	DAC's output (V)	Ramp's output (V)
0	0	−30
255	2.5	+30

(b) The K602/BBC interface converts output of either polarity from K602 to a positive voltage. The corresponding ADVAL numbers is as follows:

K602's output	Input to ADVAL Port	ADVAL number
-1 V	0.4 V	14560
0 V	0.9 V	32760
+1 V	1.4 V	50960

(c) This is a complete routine which will drive the ramp generator from pre-determined voltage V1 to voltage V2 (which correspond to N=N1 to N=N2) in (N2-N1) equal step voltages. Each step voltage is kept for 3 seconds and the output's ADVAL number is recorded every 2.8 seconds.

Instructions	Remarks
10 ?&FE62=&FF	Set User Port as output
20 FOR N=N1 TO N2	Set ramp voltage equivalent
25 ?&FE60=N	to N
30 TIME=0	Instruct the computer to hold
35 IF TIME<280 THEN 35	the ramp voltage for 2.8 s
40 X=ADVAL(1)-32760	Record the ADVAL value corresponding to K602's output
50 TIME=0	To hold the ramp voltage for
55 IF TIME<20 then 55	a further 0.2 s
60 NEXT	Move to the next step voltage

APPENDIX 2

BBC BASIC program to obtain and plot retarding potential curve for the ejected electrons. The retarding potential is ramped between ≈ 6V to ≈ −25V.

```
 10 DIM E(156),y(156)
 20 ?&FE62=&FF
 30 ?&FE60=0:INPUT "Enter voltage reading ",VF
 40 ?&FE60=155:INPUT "Enter voltage reading ",VI
 50 PRINT:PRINT "WAIT FOR K602 TO SETTLE... AND THEN"
 60 PRINT "Press S to start data collection"
 70 IF GET=83 THEN 80 ELSE 70
 80 MODE 0
 90 PROCaxis
100 FOR N=155 TO 0 STEP -1
110 ?&FE60=N
120 E(155-N)=VI*(155-N)*(VF-VI)/155
130 x=(155-N)*6
140 TIME=0
150 IF TIME<280 THEN 180
160 y(155-N)=(ADVAL(1)-32760)/16
170 TIME=0
180 IF TIME<20 THEN 180
190 PLOT 69,x+100,y(155-N)+200
200 NEXT
210 SOUND 1,-15,87,10
220 PRINT TAB(0,30);"Do you want a printout (y/N)"
230 IF GET=121 THEN PROCprint ELSE PROCsave
240 END
250 DEF PROCaxis
260 MOVE 100,200:DRAW 1030,200
270 FOR V=5 TO -25 STEP -5
280 n=INT((V-VF)*155/(VI-VF)+0.5)
290 x=(155-n)*6
300 X=INT(79*(x+100)/1279+0.5)
310 PLOT 69,x+100,196:PLOT 69,x+100,192
320 IF V=0 THEN MOVE x+100,50 ELSE 400
330 DRAW x+100,800
340 FOR Y=-1 TO 5
350 IF Y=0 THEN NEXT ELSE 360
360 PLOT 69,x+92,200+Y*120:PLOT 69,x+96,200+Y*120
370 PRINT TAB(X-3,INT(0.5+31*(1-(200+Y*120)/1023)));Y
380 NEXT Y
390 PRINT TAB(X-6,5);"Collector output (arb. units)"
400 IF V=0 THEN PRINT TAB(X+1,26);V ELSE PRINT TAB(X,26);V
410 NEXT V
420 PRINT TAB(45,29);"Retard potential (V)"
430 ENDPROC
440 DEF PROCprint
450 PROCdelete
460 *GDUMP 0,0,1,1,20
470 PROCsave
```

```
480 ENDPROC
490 DEF PROCsave
500 PRINT TAB(0,30);"Do you want to save the data (Y/N)"
510 IF GET=89 THEN PROCdelete ELSE ENDPROC
520 INPUT TAB(0,30);"Enter filename "F$
530 A=OPENOUT F$:PROCdelete
540 INPUT TAB(0,30);"Enter gas type "G$
550 PRINT#A,G$:PROCdelete
560 INPUT TAB(0,30);"Enter gun pressure (torr) "GP
570 PRINT#A,GP:PROCdelete
580 INPUT TAB(0,30);"Enter plasma current (mA) "PC
590 PRINT#A,PC:PROCdelete
600 INPUT TAB(0,30);"Enter anode voltage "V
610 PRINT#A,V:PROCdelete
620 INPUT TAB(0,30);"Enter Date "D$
630 PRINT#A,D$:PROCdelete
640 PRINT#A,VI,VF
650 FOR J=0 TO 155:PRINT#A,E(J),y(J):NEXT
660 CLOSE#A
670 PRINT TAB(0,30);"Your data was saved in file ";F$
680 ENDPROC
690 DEF PROCdelete
700 for N=0 TO 50:PRINT TAB(N,30);" ";:NEXT N
710 ENDPROC
```

APPENDIX 3

BBC BASIC program to smooth the retarding potential curve using a weighted averaging technique.

```
 10 DIM E(156),r(156),y(156)
 20 INPUT "FILENAME "F$
 30 MODE 0
 40 A=OPENIN F$
 50 INPUT#A,G$,GP,PC,V,D$,VI,VF
 60 FOR K=0 TO 155
 70 INPUT#A,E(K),r(K)
 80 y(K)=r(K)
 90 PLOT 69,100+K*6,200+r(K)
100 NEXT K
110 CLOSE#A
120 PROCaxis
130 I=10
140 FOR i=1 TO I
150 FOR N=1 TO 154
160 IF N=1 OR 154 THEN PROCwe ELSE PROCwm
170 y(N)=(W1*y(N-1)+W2*y(N)+W3*y(N+1))/totw
180 NEXT N
190 PROCendpoint
200 NEXT i
210 REM Graphics to display EDC
220 MOVE 100,200+y(N)
230 FOR N=0 TO 155
240 DRAW 100+N*6,200+y(N)
250 NEXT N
260 MOVE 100,200-300*(y(1)-y(0))/6
270 GMIN=0:LMAX=0
280 FOR L=0 TO 154
290 G=(y(L+1)-y(L))/6
300 IF G<GMIN OR G=GMIN THEN GMIN=G ELSE 320
310 LMAX=L
320 DRAW 100+L*6,200-100*G
330 NEXT
340 PRINT TAB(45,10);"Date :";D$
350 PRINT TAB(45,11);"File :";F$
360 PRINT TAB(45,12);"Gas :";G$
370 PRINT TAB(45,13);"Anode Voltage :";V;" V"
380 PRINT TAB(45,15);"Max Intensity at :";-E(LMAX);" eV"
390 PRINT TAB(0,30);"  "
400 END
410 DEF PROCwe
420 IF N=1 THEN 430 ELSE 450
430 W1=0:W2=2:W3=1:totw=3
440 ENDPROC
450 W1=1:W2=2:W3=0:totw=3
460 ENDPROC
470 DEF PROCwm
480 W1=1:W2=2:W3=1:totw=4
490 ENDPROC
500 DEF PROCaxis
```

```
510 MOVE 100,200:DRAW 1030,200
520 FOR V=5 TO -25 STEP -5
530 n=INT((V-VF)*155/(VI-VF)+0.5)
540 x=(155-n)*6
550 X=INT(79*(x+100)/1279+0.5)
560 PLOT 69,x+100,196:PLOT 69,x+100,192
570 IF V=0 THEN MOVE x+100,50 ELSE 650
580 DRAW x+100,800
590 FOR Y=-1 TO 5
600 IF Y=0 THEN NEXT ELSE 610
610 PLOT 69,x+92,200+Y*120:PLOT 69,x+96,200+Y*120
620 PRINT TAB(X-3,INT(0.5+31*(1-(200+Y*120)/1023)));Y
630 NEXT Y
640 PRINT TAB(X-6,5);"Collector output (arb. units)"
650 IF V=0 THEN PRINT TAB(X+1,26);V ELSE PRINT TAB(X,26);V
660 NEXT V
670 PRINT TAB(45,29);"Retard potential (V)"
680 ENDPROC
690 DEF PROCendpoint
700 y(0)=2*y(1)-y(2)
710 y(155)=2*y(154)-y(153)
720 ENDPROC
```

APPENDIX 4

BBC BASIC program to simulate rainbow scattering of fast He atoms from a two atom copper surface.

```
 10 MODE 0
 20 DIM C(2),R(2)A(2),AX(2),AY(2),SA(90),P(90)
 30 FOR J=0 TO 90:SA(J)=0:NEXT J
 40 AB=0:BS=0
 50 REM Insert value of Born-Mayer parameters
 60 A=1805:b=3.867
 70 INPUT "Enter He beam direction (<110> or <121>) ",D$
 80 IF D$="<110>" THEN SPRN=2.56:L=110.85
 90 IF D$="<121>" THEN SPRN=4.43:L=64
100 S=SPRN*50
110 FOR ATOM=1 TO 2
120 C(ATOM)=640+(2*ATOM-1)*S/2-S
130 PLOT 69,C(ATOM)-2,702
140 PLOT 69,C(ATOM)+2,702
150 PLOT 69,C(ATOM)+2,698
160 PLOT 69,C(ATOM)-2,698
170 NEXT ATOM
180 INPUT "Enter angle of incidence wrt normal ",ANGLE
190 INPUT "Enter fast atom energy ",E
200 V=SQR(2*E*1.6E-19/6.7E-27)*5E11
210 VX=V*SIN(RAD(ANGLE)):VY=V*COS(RAD(ANGLE))
220 SPX=C(1)-300*TAN(RAD(ANGLE)):SPY=400
230 NFA=1000
240 FOR K=0 TO S STEP S/NFA
250 T=0
260 REPEAT
270 T=T+1
280 X=VX*T*1.4E-16+SPX+K:Y=VY*T*1.4E-16+SPY
290 PLOT 69,X,Y
300 UNTIL ABS(Y-700)<100
310 REPEAT
320 AX=0:AY=0
330 FOR ATOM=1 TO 2
340 R(ATOM)=SQR((X-C(ATOM)^2+(Y-700^2)
350 IF R(ATOM)<144 THEN GOTO 360 ELSE GOTO 400
360 A(ATOM)=1.19E29*A*b*EXP(-(b/50)*R(ATOM))
370 AX(ATOM)=A(ATOM*(X-C(ATOM))/R(ATOM)
380 AY(ATOM)=A(ATOM)*(Y-700)/R(ATOM)
390 AX=AX+AX(ATOM):AY=AY+AY(ATOM)
400 NEXT ATOM
410 RC=SQR((X-640)^2+(Y-700)^2)
420 RE=SQR(RC^2+L^2)
430 AE=1.194E29*A*b*EXP(-(b/50)*RE)
440 AEX=2*AE*(X-640)/RE:AEY=2*AE*(Y-700)/RE
450 AX=AX+AEX:AY=AY+AEY
460 DX=VX*5.7E-17+0.5*AX*5.7E-17^2
470 DY=VY*5.7E-17+0.5*AY*5.7E-17^2
480 X=X+DX:Y=Y+DY
490 PLOT 69,X,Y
500 VX=VX+AX*5.7E-17:VY=VY+AY*5.7E-17
```

```
510 UNTIL ABS(Y-700)>100
520 T=0
530 REPEAT
540 T=T+1
550 X=X+VX*T*1.4E-16:Y=Y+VY*T*1.4E-16
560 R=SQR((X-640)^2+(Y-700)^2)
570 PLOT 69,X,Y
580 UNTIL R>200
590 IF VY>0 THEN AB=AB+1:GOTO 640
600 IF VY<0 THEN SCAG=DEG(ATN(VX/ABS(VY)))
610 Q=INT(SCAG)
620 IF Q<0 THEN BS:BS+1
630 IF Q>0 THEN SA(Q)=SA(Q)+1:P(Q)=SA(Q)*10/NFA
640 VX=V*SIN(RAD(ANGLE)):VY=V*COS(RAD(ANGLE))
650 VY=V*COS(RAD(ANGLE))
660 NEXT K
670 REM Graphics to display scattering yield
680 CLS
690 PRINT TAB(0,4);"He-Cu{111} Scattering"
700 PRINT
710 PRINT TAB(10,10);"Angle of incidence = ";ANGLE
720 PRINT TAB(10,11);"Energy = ";E;" eV"
730 PRINT TAB(10,12);"Spacing = ";SPRN;" A along ";D$
740 MOVE 100,700
750 DRAW 100,200
760 MOVE 953,200
770 DRAW 100,200
780 FOR M=0 TO 9
790 PLOT 69,100+(853/9)*M,196
800 PLOT 69,96,200+50*(M+1)
810 PRINT TAB(2,10);"100"
820 PRINT TAB(3,18);"50"
830 PRINT TAB(5.88*(M+1),26);10*M
840 PRINT TAB(23,27);"Polar angle (degrees)"
850 PRINT TAB(0,7);"Scattered Intensity"
860 PRINT TAB(0,8);"(arb. units)"
870 NEXT M
880 MOVE 100,200
890 REM Routine to find position of rainbow angle
900 MAX=0
910 FOR XA=0 TO 90
920 DRAW XA*(853/90)+100,200+500*P(XA)
930 IF P(XA)=MAX THEN TR=XA:MAX=P(XA)
940 IF P(XA)>MAX THEN TR=XA:MAX=P(XA)
950 IF P(XA)<MAX THEN MAX=MAX
960 NEXT XA
970 PRINT TAB(0,29);"Rainbow angle = ";TR
980 END
```

TITLE THE INTERACTION OF FAST NEUTRAL ATOMS WITH METAL SURFACES

AUTHOR MOHD NOR BIN MD YUSUF

UNIVERSITY University of Warwick, 1989